FCTUC DEPARTAMENTO DE ENGENHARIA CIVIL
FACULDADE DE CIÊNCIAS E TECNOLOGIA
UNIVERSIDADE DE COIMBRA

Design of Concrete-Steel Transitions in a Hybrid Wind Turbine Tower

Dissertação apresentada para a obtenção do grau de Mestre em Engenharia Civil na Especialidade de Mecânica Estrutural

Autor

Pedro Miguel Rodrigues Pires

Orientador

Carlos Alberto da Silva Rebelo

Rui António Duarte Simões

Coimbra, Julho, 2013

ACKNOWLEDGEMENTS

I would like to thank my advisors Prof. Dr. Carlos Rebelo and Prof. Dr. Rui Simões for making this opportunity possible. For their guidance, corrections and knowledge provided not only in this project but throughout my entire college studies.

I want to express my gratitude to Eng. Wayne White for the guidance in every step of this project, for the motivation, for the knowledge and explanations provided. I would like to express that without his contribution this thesis would not be possible.

I also want to thank ENERCON for accepting me and providing me with all the information and resources needed for this thesis. A special acknowledgement has to be made to all colleagues in the towers and foundations department for always making me feel welcome.

My gratitude to the Civil Engineering Department of the University of Coimbra for the tools and knowledge provided during the last five years allowing me to feel ready to embrace new challenges. To my friends for the company, the help during the long work hours and for the good moments.

I want to thank my family for their unconditional support throughout my studies, their encouragement in taking this opportunity and their love.

Last but not least, I want to thank my girlfriend, Cátia Ferreira, for being my companion, for always supporting me and understanding, for your love and above all for making me happy.

ABSTRACT

In recent years, the Earth has witnessed an exponential population growth demanding for more resources and energy. As a response to this need wind energy presents itself as an intelligent choice, a never ending source of energy with limited environmental impact, with its goal to preserve the earth's depleting resources.

Wind energy is the world´s fastest growing energy source increasing at an annual rate of 20%. The increasing generators capacity demands for higher towers with new solutions, new materials and new construction processes. Pre-fabricated concrete sections appeared as a good alternative to steel and hybrid solutions aim to take advantage of both materials leading to cheaper and better performing wind turbine towers.

One current problem with high concrete towers is the weight of the segments. The top concrete segments have to be built as a single section, creating quite massive elements. The main objective of this work is to design and compare different solutions for concrete-steel transitions in a 122 m externally prestressed hybrid tower. Two different geometries for the top concrete segment were studied and compared with aspects such as weight of the segments, dimensions, production requirements, reinforcement amounts or fatigue damage taken into account. The first concrete segment variation is shorter than the typical ENERCON segments and the second is a thinner one, aiming at reducing the weight of the transition element.

The design first steps consisted of the definition of the flange connection configuration and definition of the prestress tendons position. An extensive calculation of the prestress was performed with repercussions in every other element. The reinforcement of the segments was determined taking special focus to the effects of shear and torsion, early-age thermal crack width and the radial forces from the deviation points. The effects of fatigue damage on the structure were also taken into account.

RESUMO

O crescimento exponencial da população mundial tem acentuado a necessidade de recursos disponíveis e o consumo energético. Como forma de responder a essa crescente procura e com o objectivo de preservar os recursos naturais existentes, a energia eólica apresenta-se como uma solução eficaz.

A energia eólica é a fonte de energia com a maior taxa de crescimento, situando-se em cerca de 20% ao ano. O aumento da potência dos aerogeradores exige torres de maiores dimensões levando ao repensar de soluções e a procura de alternativas. Os elementos pré-fabricados de betão surgem como uma alternativa relativamente às torres metálicas. Soluções hibridas permitem aproveitar as vantagens de ambos os materiais conduzindo a soluções promissoras para grandes alturas.

O peso dos segmentos de betão é cada vez mais um problema em torres de grandes dimensões. Estes elementos são construídos em apenas uma peça o que leva a soluções pesadas, de grandes dimensões e difícil transporte. O objectivo principal deste trabalho consiste no dimensionamento e comparação de diferentes soluções para os segmentos de transição numa torre híbrida de 122 metros com um sistema de pré-esforço pelo exterior. Foram estudadas e comparadas duas variações da transição tendo em conta aspectos como peso, dimensões, necessidades construtivas, armaduras e resistência a acções de fadiga. A primeira alternativa estudada consiste num segmento mais curto e a segunda num elemento mais esbelto sempre com o objectivo de reduzir o peso do elemento de transição.

Inicialmente foi necessário definir completamente a geometria da flange, a posição e traçado dos cabos de pré-esforço. Foi realizado um cálculo detalhado das necessidades de pré-esforço e respectivas perdas. As quantidades de armaduras foram dimensionadas tendo em conta situações criticas tais como os efeitos de esforço transverso e torsão, controlo da fendilhação em betões jovens e os efeitos de forças radiais devido aos pontos de desvio do pré-esforço, foram também tidos em conta os efeitos das acções de fadiga.

TABLE OF CONTENTS

LIST OF FIGURES

LIST OF TABLES

LIST OF SYMBOLS

A_P − Prestress tendon nominal cross section area;
E_P − E-modulus of prestress steel;
f_{cd} − Design value of the concrete compressive strength;
f_{cm} − Mean value of a concrete cylinder compressive strength;
f_{pk} − Tensile strength of prestress steel;
$f_{p0,1k}$ − Yield strength of prestress steel;
G − Self-weight;
K_c − Coefficient that takes into account stress distribution within a section prior to cracking;
K − Coefficient which allows for the effect of non-uniform and self-equilibrating stress which leads to a reduction in restraint forces;
l_{sl} − Tendon length;
M_{xy} − Tower bending moment;
M_z − Tower torsion moment;
n_{Si} – Number of acting stress cycles at a given stress level and stress range;
n_{Ri} – Number of cycles causing failure at the same stress level and stress range;
n_p – Number of prestress tendons;
P_{max} − Prestress force after friction losses;
P'_{m0} − Prestress force after wedge slip losses;
Q − Shear force;
γ_{Sd} – Load safety factor taking into account uncertainties in the calculation;
$\varepsilon_{p,l}$ − Prestressing tendon strain;
$\varepsilon_{c,l}$ − Concrete compressive strain;
σ_c − Compression stresses due to self-weight;
$|\sigma_{c1}|$ – Lower value of the compressive stress within a distance of 300 mm from the surface;
$|\sigma_{c2}|$ – Larger value of the compressive stress;
$\sigma_{c,Pmo}$ – Average compressive stress after jack removal;
$\sigma_{c,QP}$ − Compression stresses due to self-weight for quasi-permanent load combinations;
σ_s − Maximum steel tensile stress allowed in the reinforcement;
ψ_2 − Factor for quasi-permanent values.

1 INTRODUCTION

1.1 General Framework

Since ancient times Man has been using wind power for his own benefit, at first with sailing ships then with windmills to mill grain or pump water and only in more recent years to produce electricity. The ever growing concerns regarding climate change and the escalating prices of coal and oil are causing a change within the energy production sectors leading to a need for cheap, clean and infinite sources of energy. Nowadays wind energy represents one of the fastest growing energy resources with the cheapest kWh in the market when taking into account all the costs involved from construction to production.

The high demand for clean energy is leading to the construction of more powerful machines and higher towers. The increasing height of the towers is carrying the need for new and better solutions. Precast concrete sections and hybrid solutions are now at the top of the table has new and better alternatives for current and future needs. The new challenges wind energy market presents lead to the definition of the present work.

1.2 Objectives

The aim of this thesis is to study, design and compare two different transition concrete segments in a 122 m externally pre-stressed hybrid tower. ENERCON looks to standardize as much as possible the production of concrete segments aiming, by doing so, to reduce the number of different elements built leading costs reduction and a simplification of every step, from design to site assembly. The geometry of both variations has been defined according to current construction practices and future production wishes.

Being this a new ENERCON tower height and externally prestressed it is necessary to define the geometry and position of some elements like the steel flange connection, number and position of the tendons, the position of the deviators. This process needs to keep in mind decisions already taken in previous towers while, at the same time, allowing for the use in future solutions.

The steel reinforcement represents one of the most expensive components in the production of the concrete segments. One of the objectives was to reduce the amount of reinforcement

provided to the segments by more accurately quantify the amount of reinforcement needed to resist shear and torsion and study the effects of temperature in the ultimate limit states. Similar analysis is done for the verifications of the serviceability limit states, where the effects of early-age thermal cracking are critical in the design. The effects on the segments from the deviation points of the tendons also need to be taken into account and local reinforcement has to be provided.

The geometry of the flange has a great influence in the overall behavior of the tower. It is intimately related with the geometry of the top concrete segment and the prestress tendons path. In order to be able to choose from one of the variations it is necessary to check if both flange solutions are viable. The verification of the fatigue damage in the concrete is frequently a controlling verification, with the thickness of the concrete segments walls having a large influence. With the performed calculations one objective was to develop templates that would allow for similar calculations with different parameters, easily changing the geometry or concrete grades and seeing the influence in the overall connection response.

The decision of each segment to build is not an easy one to make, with repercussions throughout every process, from design to production over a long period of time. With the calculations and appreciations here performed the goal is to allow for a well based knowledge of the advantages and disadvantages of both solutions and at the same time improve the calculations for the whole tower.

1.3 Detailed Structure

This document is divided into 11 different chapters and annexes aiming for a coherent organization of the document with logical and technical descriptions of every different step conducted to achieve the proposed goals.

Chapter 1 - General introduction to the problem statement and the research objectives of this thesis. The entire structure of the thesis is outlined here.

Chapter 2 - This chapter presents a general overview of energy consumption worldwide, renewable energy market in Europe and an historical summary about wind energy production.

Chapter 3 - Description of the different loads taken into account in the tower design.

Chapter 4 - Gives a small introduction into the different tower solutions, completely defines the tower in question, the two different geometry variations and the detailed definition of the prestress tendons geometry.

Chapter 5 - Description of the externally post-tensioned system, number of tendons and the jack applied force followed by the determination of the different prestress losses.

Chapter 6 - Reinforcement calculation for both ultimate limit state and serviceability limit state for the various tower segments, with a detailed description of all the different design verifications performed. Calculation of the required reinforcement due to a radial force at the tendons deviation points.

Chapter 7 - Flange design verification using the Petersen model for the two different geometries.

Chapter 8 - Fatigue analysis of both geometries conducted for different points in the concrete segments and the pre-stress tendons.

Chapter 9 - Comparative appreciation of the two different geometries with advantages and disadvantages of both.

Chapter 10 - Important tasks yet to be performed allowing for improvements in the design of the tower and different geometries variations possible to study.

Chapter 11 - Conclusion and critical analysis of results.

In the annexes is shown the complete geometry of both variations, tables with the results of the calculations, prestress force and losses, reinforcement calculations, stresses from prestress radial force, flange design and fatigue calculations. Drawings of various designed elements are also presented.

2 STATE OF THE ART

2.1 Worldwide energy consumption and sources

Since the industrial revolution the world's population has exponentially increased and in the last two hundred years more than doubled. The planet is now home to more than 7 billion people and with every person born more resources and energy are needed (UN, 2013). The world's primary energy resources are fossil fuels. In 2011 oil still represented 33.1% of the world's leading fuel sources. Coal had a share of 30.3% and natural gas 28.4%. Together these three fossil fuels make up 90% of the world's energy resources (BP, 2013). The problem with these sources is that they are finite and responsible for a large percentage of greenhouse gases emitions. The alternative presents itself in the form of renewable energies, with particular relevance to wind energy.

2.2 Renewable energies in Europe

Since 1997 the EU has adopted policies to increase the production and usage of energy from renewable resources. In 2012 about 20% of consumed energy was from renewable resources, with wind energy representing 5.3%. Current goals aim to have 34% of the produced energy coming from renewable sources and up to 100% by the end of 2050 (American Wind Energy Association, 2011).

In Portugal there were 4302 MW of installed power produced by wind energy by the end of 2011. For every hour of consumed energy 15 minutes come from renewable energies, where wind energy is responsible for 11 minutes (APREN, 2013).

2.3 Historical development

Wind is a never ending source of energy and humans soon learnt to use it to their own benefit. It's hard to precisely say when in history it was first used, but it is known that as early as 4000 B.C. the Chinese attached sails to their primitive rafts and that during the birth of the Egyptian civilization wind propelled systems where already used to grind grain or pump water (Tong, 2010). The first reference to a windmill being used comes from the Persian-Afghan border in the year 644 A.D. with a vertical axis of rotation, used to grind grain. Later it was discovered that the Chinese also used wind wheels to pump water into the rice fields. Around the 12th century windmills were largely implemented throughout Europe and had already been

improved with the invention of the horizontal axis of rotation. The Dutch started to build dykes in the 15th century and aided by wind wheels they were able to pump large volumes of water claiming large areas of land. In the 19th century there were a total of 200,000 windmills throughout all of Europe (Hau, 2006).

The first attempts to produce electricity from wind power were conducted in America in order to try to supply rural areas. However it was in Denmark that the first large scale attempt to produce electricity from wind power was made. Poul La Cour was a pioneer of electricity generation by means of wind power. He built a wind turbine, after being asked by the Danish government, which was based on a "dynamo" and he was successful in doing so. Later on he was producing turbines with 10-35 kW. In the US the first wind farms were built between 1979 and 1980. In the beginning, these farms consisted of wind turbine units with a power of up to about 100 kW. Albert Betz played an important role in the history of wind energy. He is responsible for the modern physical principles of wind-energy conversion, postulated in 1920. His work allowed him to determine exactly how much mechanical energy could be extracted from a free airflow by an energy converter (Hau, 2006).

2.4 Wind energy converters

Since the first attempt to build a wind turbine a very large number of different solutions have been tested. Converters can be classified firstly by the aerodynamic function and secondly by their constructional design. All modern wind rotors are designed to use the effect of aerodynamic lift, with the best solution being horizontal axis propellers. The classification according to constructional design can differ in various ways with the position of the axis of the rotor being the most notable. Vertical axis rotors are usually from older designs using the drag effect only. Later it became possible to use the lift effect but the costs of production of vertical axis wind turbines are so high that they cannot compete with those of the horizontal axis.

Nowadays horizontal axis turbines are the standard design type, being based on a propeller like concept. This design brings unquestionable advantages such as: the possibility to control the pitch of the rotor blades according to the flow of the wind; the ability to protect against extreme wind speeds; constantly optimized blades and taking into account the ongoing research into aerodynamic lift even better performances are expected.

3 DESIGN LOADS

3.1 Design load situations

The definition of every load that should be taken into account for the design of a wind tower is done according to the specifications from the Deutsches Institut für Bautechnik (DIBt guideline) for towers located in Germany and the International Electrotechnical Commission (IEC) for the rest of the world. The first aspect to take into account is the classification of the wind turbines, done according to the respective reference wind speed, V_{ref}, and intensity turbulence. According to the DIBt guideline wind turbine studied in this project is classified as WZ III, housing a wind zone III, and as for the IEC classified as WTC-IIA, being these the most typical classes used. For this project, the tower and its elements were designed according to the loads determined from both guidelines. This was done in order to be able to build the tower anywhere in world without having to make any changes to the design.

3.2 Wind loads

A wind turbine should be designed in order to safely withstand the wind conditions for the selected class. The wind regime for load and safety considerations is divided into normal wind conditions (which will occur frequently during normal operation of a wind turbine) and extreme wind conditions that are defined as having a 1-year or 50-year recurrence period.

3.2.1 Normal wind conditions

The loads to which the wind turbine is subjected under "normal" operating conditions are mainly relevant to fatigue life. The basics for the definition of load cases are the characteristic wind speeds which are used in the sequence of operational states. The yearly average wind speed at hub height, v_{ave}, is to be calculated from equation (EQ 1) according to the DIBt for wind turbines classified as WZ III. The most common wind profile for normal conditions is:

- **Normal turbulence model (NTM) -** represents the wind conditions applied to the operational wind turbine.

3.2.2 Extreme wind conditions

Extreme wind conditions include wind shear events, as well as peak wind speeds due to storms and rapid changes in wind speed and direction. The most commonly models used are:

- **Extreme wind speed model (EWM) -** represents the extreme conditions applied on the structure whilst the wind turbine is non-operational. The conversion from the reference speed, V_{ref}, is done for a recurrence period of 50 years and takes into account a turbulence standard deviation.
- **Extreme operating gust (EOG) -** corresponds to the extreme situations in which the turbine is operating. It considers the different operating situations like start and stop, power generation and fault conditions. Considering a recurrence period of 50 years in these situations is considered the gust speed according to the turbine classification. For this situation the gust speed is measured based on the turbine classification.

3.3 Fatigue loads

Every rotation of the blades leads to a change in the tower stress distribution. Throughout its entire life cycle a tower experiences around $5.29*10^8$ fatigue load cycles. To accurately investigate the wind turbine behavior under fatigue loading, numerous load combinations and complex cases have to be considered in order to account for the level of uncertainty in wind loads and tower response. Fatigue loading often controls the design of towers meaning that conservative assumptions regarding fatigue loading aren't economically feasible. Therefore, no simplified methods, that determine fatigue loading for large wind turbines, have been accepted by the designers. Most fatigue investigations use published S-N curves to compare with the load range spectrum, generated from simulations, for critical components.

The fatigue loads where determined based on load collectives, measuring the load range variation in the tower for each cycle. These curves where determined by the load simulation department giving the cycle stress range for loads according to the DIBt guideline and the IEC for both normal climatic conditions and cold climate conditions. In figure 3.1 is shown the envelop results of the bending moment obtained from the load simulation at flange height.

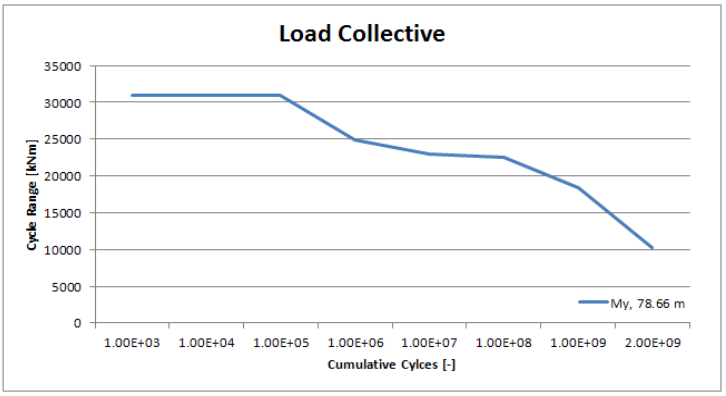

Figure 3.1 – Load collective

3.4 Temperature loads

The effects of temperature on the tower also need to be considered, determined according to the DIBt guideline. Temperature differentials throughout the tower height or uneven temperature distributions due to sunlight exposure need to be taken into account. The different temperature distributions considered are:

- A uniform temperature component around the perimeter and across the thickness, $\Delta T_{N,1} = \pm 35\ K$;
- A distribution according to a $\cos(\varphi)$ function along an arc of 180° and constant across the thickness, $\Delta T_{N,2} = \pm 15\ K$;
- A linearly varying temperature differential of $\Delta T_M = \pm 15\ K$ in the longitudinal and circumferential direction across the wall thickness.

The three different temperature situations are presented in figure 3.2.

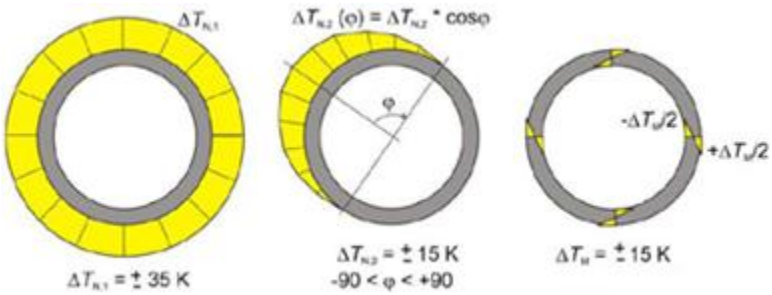

Figure 3.2 - Temperature models

For the serviceability limit state the temperature effects are considered simultaneously with the load case DLC 1.0 (IEC, 2005), characteristic combination, with a combination coefficient of $\Psi_{\text{temp}} = 0.6$ according to DIBt guideline. In the Ultimate Limit State the same coefficient is used, but this time for the extreme load case DLC 6.2 (IEC,2005).

3.5 Inertial and Gravity loads

Gravitational and inertial loads are static and dynamic loads that result from gravity, vibration, rotation and seismic activity. The gravity loads taken into account are the self-weight, the weight of every energy production component and the weight of every other additional equipment like ladders, deviators, tendons and platforms.

4 TOWERS

4.1 Wind turbine towers

Today's wind energy market is focusing its attention on more powerful machines and higher towers as a response to the society's energy demand. Wind turbines with 5 MW and more are becoming more frequent, demanding higher support structures. The most popular and current design are tubular hollow towers, being the only kind of wind turbine support structure being actually mass produced. The materials used are mainly concrete and steel or a combination of both. Steel towers still represent the vast majority of wind turbine towers. Their construction, transportation and assembly processes are relatively standardized.

As turbines become more powerful and towers grow with them, an increase in structural strength and stiffness is required to withstand the applied forces. This creates transportation issues for steel towers, bearing in mind the limitations of transportation along public highways. Researchers and manufactures are working to develop segmented designs to offset this limitation, leading to welding in the work site, where the conditions are more difficult to control reflecting on the outcome quality of the joints. Hybrid steel-concrete solutions appeared aiming to take advantage of both material advantages.

The idea behind building a concrete-steel hybrid tower is to use concrete in the wide lower part and steel in the upper part, where a conventional welded steel shell tower section may be designed without any risk of conflict with the transportation limitations. In reality, it also makes it easier to design the concrete part and to get the Eigen-frequencies right. There is generally no local buckling issues in the post-tensioned concrete tower part, frequently a critical the design situation for larger steel towers. The material cost for a large concrete steel hybrid tower is less than that for a large steel tower.

4.2 Tower in study

This thesis focuses on a 122 meter steel-concrete hybrid tower supporting an E-101 generator, a diameter of 101 meters from the blade tips. It is composed by the connection of 25 segments, of which 22 are precast concrete segments reaching a height of around 78 meters. This tower represents a new solution ENERCON wants to promote. Instead of the typical internal post-tensioned system, with bond, the tower is externally post-tensioned, meaning that the tendons are not inside the concrete segments but run close to the inside wall of the

tower. This system is composed by 28 tendons anchored at the top concrete segment and at the foundation corbel where the pre-stress force is applied. In both of these anchor points the tendons need to go through the concrete, meaning that the top transition segment has to be thick enough in order to accommodate all the anchorage components

The connection between steel and concrete is made by a 200 mm steel flange. This steel ring is welded, in a controlled environment, to the lower steel segment, and has to be wide enough in order to allow for the assembly of every component of the anchorage. The concrete tower starts with a bottom diameter of 9.7 meters and decreases to approximately 4.5 meters at the top, different in both alternatives. The lower segments are usually divided in 2 parts due to their large dimensions and weight, but as for the upper segments this is not done because of the large torsion and shear forces, that would lead to highly stressed joints, and imperfections that, even if small, are always there, leading to uncertainty about the structural behavior of the segment. The horizontal joints between concrete segments are non-reinforced. The segments rest on top of one another, being the pre-stressing force, acting as a friction force between the concrete segments, and responsible for insuring that no opening appears between the segments.

The first geometry variation for the transition consists of a shorter concrete segment. This segment is 2240 mm high, instead of ENERCON typical segments that have 3640 mm, with a thickness of 680 mm at the bottom and 630 mm at top. In table A.1 from annex A the entire geometry of the segment is shown and of the adjacent ones. The connection between concrete and steel is made with a steel ring, with a maximum thickness of 200 mm, reducing to the outside to a value around 180 mm.

The second segment variation keeps the height to 3640 mm with a bottom thickness of 674 mm and 630 mm at the top. With this geometry the intention is to slice away part of the concrete creating a taper in the segment and by doing so reducing the weight. This would mean that in the transition between the last two concrete segments the thickness variation would be gradual. The geometry of the segment and the adjacent ones is shown in table A.2. The geometry of both segments can be seen in figures 4.1 and 4.2.

As stated earlier the connection between concrete and steel is made with a thick continuous steel flange. This element is connected to the steel by a fillet weld, carried out in a controlled environment with both elements taken to the construction site already connected. The segment is lifted to the top of the concrete and connected by applying the pre-stress force. The anchoring of the tendons is done on the flange, meaning that during production holes have to be made for the tendons. In order to define the detailed geometry of the flange connection, a vast number of different factors need to be taken into account. The configuration and position of those components has to be done according to the European Technical Approval ETA-12/0150 and the DIBt guideline.

4.2.1 1st geometry variation

The steel flange rests on top of a concrete segment with a thickness of 630 mm. The width of the flange was defined with 565 mm and normally a 10 mm tolerance is left from the outside of the segment and the beginning of the flange. The angle of the cut in the flange is directly related to the position of the tendons, it is necessary to assure that the recess pipe is perpendicular to the anchor plate and that allows the tendons to run as far as the deviator without contact with other elements.

One aspect with the most influence in the structural behavior of the flange is the distance between the anchorage and the outside, with the increase of the distance leading to more bending in the flange. By taking this into account a minimal distance of 35mm from the 12 mm fillet weld to the load bearing plate was kept for constructive reasons. Because this segment is smaller a larger angle for the flange is needed. The larger the angle the more expensive the cut is and leads to more wasted material. Taking into account that the flange is cast with a maximum thickness of 200 mm, the greater the angle is the smaller the outside thickness is going to be. As a reference value it was intended to leave the outside thickness greater than 175 mm. In figure 4.1 the transition concrete segments can be seen as well as the recess pipe going through the segment and the flange.

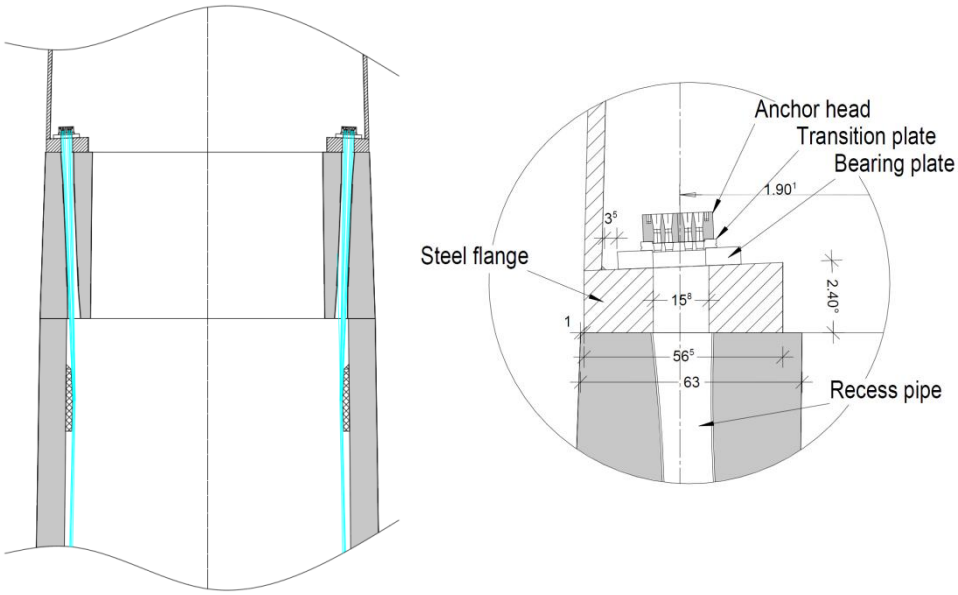

Figure 4.1 - Segment geometry and steel flange, 1st variation

In order to achieve the final geometry it was necessary to assume an angle of 2.40° degrees, leading to an outside thickness of 176 mm in the flange. It was decided to leave the deviator at one meter bellow the top of segment 5 and by taking into account that the tendons cannot touch the recess pipe, it is possible to determine the minimum deviator thickness, with this

geometry being somewhere around 90 mm. This top concrete segment weights 44.49 tons. Weights below 55 tons are within the typical ENERCON lifting range.

4.2.2 2nd geometry variation

In this second geometry the top thickness of the segment is the same, 630 mm, but with the standard ENERCON segment length, 3.64 meters. Assuming the same flange width, the same maximum thickness and distance from the outside it is possible with a smaller flange angle to define the correct connection geometry of every element. With a flange angle of 1.70° degrees, an outside thickness of 180 mm in the flange is achieved, and a minimum thickness for the deviator around 90 mm. The deviator thickness is an important aspect because of its weight, which is important to achieve a solution that allows for a small deviator thickness.

While the outside of the segment is the same as one which is already being built by ENERCON, the inside geometry is completely new. The creation of the tapper leads to a reduction of the segment weight from 67.12 to 54.36 tons. This means that the tendons (instead of coming out of the bottom of the segment) leave by the interior surface, leading to an elliptical exit hole. The configuration of the anchorage, the segment and the tendons recess pipes can be seen in figure 4.2.

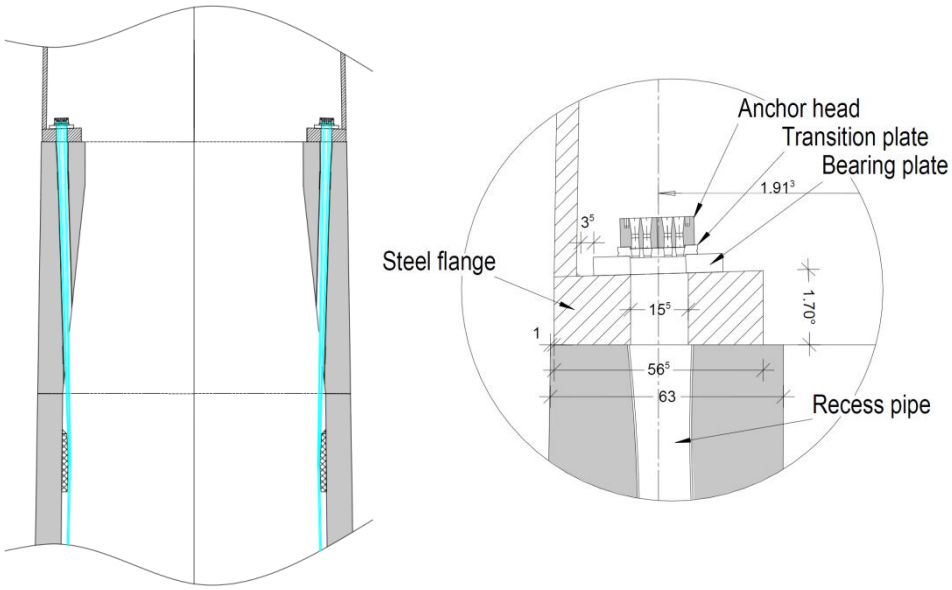

Figure 4.2 – Segment geometry and steel flange, 2nd variation

The tendons go through the concrete segments and the flange where they are later anchored. This implies the need to do holes in the steel flange. Due to limitations from the European technical approval ETA-12/0150, the hole needs to be vertical and with a diameter of 150 mm. Because the tendons do an angle with the vertical direction a larger hole needs to be made, $\tan(1.70) * 200 = 5.94$ mm, Φ=156 mm.

4.3 Deviators position

Due to the fact that this is an externally pre-stressed tower, it is necessary to carefully define the position and path of the tendons. Because of the changes in the concrete segments dimensions, the tendons cannot go straight from top to bottom. So it is necessary to have deviators in specific positions throughout the tower allowing for changes in the direction of the tendons.

The use of external pre-stress is a relatively new solution for ENERCON. Generally concrete and hybrid towers are built with internal prestress grouted BBV systems. Keeping in mind that in the future the goal is to build not only 122 m externally pre-stressed towers but also 147 m, 133 m and 97 m towers, already existing heights with internally pre-stressed systems, it is necessary to look for an optimized position for the deviators in order to have them all the same segments for the different towers. This leads to a reduction in the number of different segments that ENERCON has to build, simplifying various construction processes. For example, segment 14 was already used in a previously external pre-stressed tower, having a deviator at 1.82 m from the bottom. So the determination of the other deviators was done taking this into account.

As deviation points lead to friction losses and an increase in reinforcement, increase it is necessary to look for the solution with a minimum number of deviators possible. From the towers geometries and their swayed position under the different loads cases it was possible to estimate the number of deviators, their position and thickness. Because the contact points between the tendons and the tower is limited to the deviators a tolerance distance was used for the position determination, segments with a diameter larger than 5 meters a tolerance of 30 mm was used and for segments with a smaller diameter, 20 mm. These tolerances aim to cover imperfections in the segments. As the tower sways some tendons sway and move closer to the tower wall while at the same time others move away. In extreme conditions it could happen that the tendons cease to touch some deviators, reducing the contact points. In an extreme hypothetical situation the tendons could move to a point that their center of inertia moves to the outside the tower, leading to the need to consider the second order effects in the calculations.

At the bottom of the tower the tendons are anchored in the foundation corbel, a 1.50 m thick concrete element part of the foundation. The tendons need to be positioned near the middle of the element leading to a better structural solution. So a distance of 55.5 mm from the inside of the tower wall was kept. The thickness of the deviator is limited to ENERCON construction procedures keeping in mind the additional weight; a maximum thickness of 105 mm is used. Due to the radial force that is originated from the deviation point, which leads to an increase in the amount of needed reinforcement the best position for the deviators would be near the middle height of the segment. This was not always possible, but it was checked that it was

possible to distribute the additional needed reinforcement in the available area. The position of the deviators and their thickness is available in tables A.1 and A.2 from annex A. The second geometry variation allows for a less thick top deviator.

4.4 Position of the tendons

With the position of the deviators determined it is possible to derive on the position of the tendons throughout the tower. The ideal solution would be all the tendons equally spaced both at the bottom and at the top. This is not possible for a number of different reasons, from a clear space at the bottom for the doors, to ventilation openings or ladders. Some segments, due to their dimensions, have to be divided into two parts. This means that there would be vertical joints in the segments that need to be accessible in order to do the connection between the parts. It is necessary to leave a clear working area around the bolt box. In the figure 4.3 the tendons position can be seen in order to leave free space for the 1.36 m wide door.

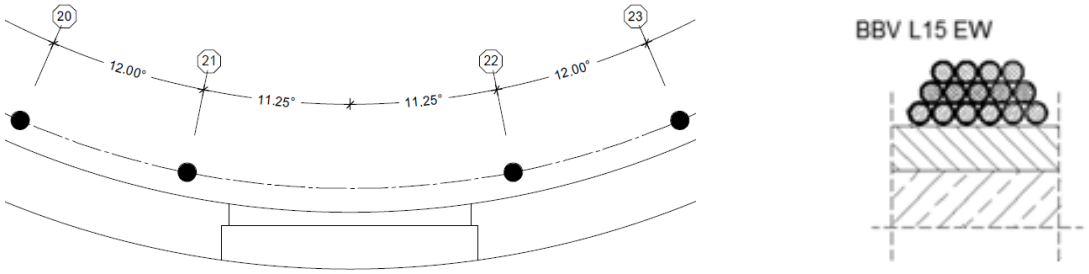

Figure 4.3 – Tendons position due to door opening and tendon configuration

Because the top of the tower needs to be accessible, it is necessary to have clear space in the wall of the segments for a 0.60 m wide ladder. At the anchor head the strands in the tendons are distributed in a circular like shape, with a certain diameter, but at the deviation points the tendon flattens and the strands assume a distribution similar to the one shown in figure 4.3, meaning that the free space needed by is greater.

In the 122 meter tower, segments 25 to 9 are built in two separate parts. This is done because due to their dimensions and weight transportation would be difficult. During construction steel joints are built in the segments allowing for them to later be bolted together. These joints, bolt boxes, are aligned vertically within the segment, each having normally six. Between consecutive segments the joints can’t be aligned because that would lead to a high stress concentration in the bolts and possibly the opening of the segments. As a current practice ENERCON usually assumes an angle of 25° degrees for the displacement between the vertical joints. The typical vertical joint is shown in figure 4.4.

Figure 4.4 – Vertical joint in a tower segment

At the top of the tower the tendons have to be equally spaced in order to allow for a constant and symmetrical stress distribution throughout the whole flange because normally the steel flange is a critical design situation. By taking into account every restriction mentioned it was possible to determine the tendons distribution at the base of the tower. These restrictions lead to constant changes in both the radius and the angle along the length of the tower. The knowledge of the correct tendons path, and their exact coordinates, is essential in order to correctly determine the losses in the pre-stress force. In the following picture is shown chart for the entire tower with the distribution of the tendons and every limitation considered.

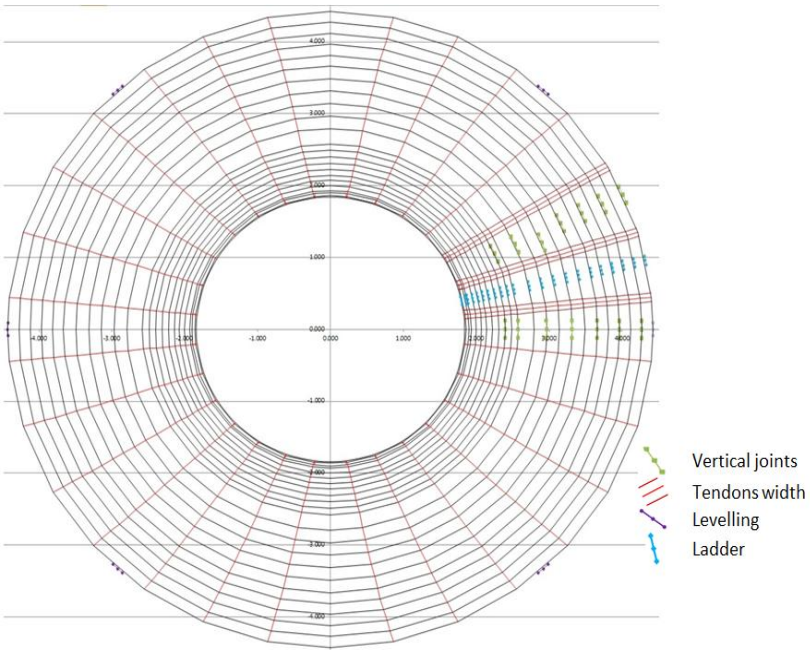

Figure 4.5 – Tendons distribution throughout the tower height

The tendons distance to the longitudinal axis of the tower is smaller at the level of the top deviator than at the flange level, meaning that the tendons change direction at that point,

bellow they were coming inwards and then head out, meaning that a contact force is applied to the structure at that point. As shown in the previous figure, the tendons closest to the openings have the larger angle difference between the bottom and the top of the tower meaning that a change in the horizontal direction also occurs. If at the deviation point the tangential component of the force is greater in one direction than the other the tendon could move. In figure 4.6 is shown how the tendon angle changes.

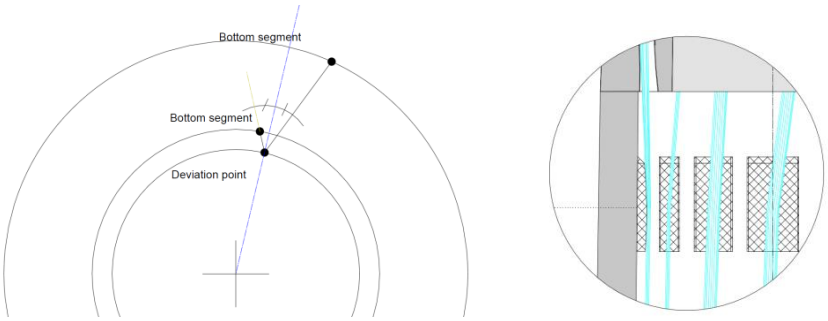

Figure 4.6 – Top view of the change in direction of a tendon near the opening

In order to a avoid problems due to a possible tendon displacement, that could lead simply occur from the sway of the tower, it has necessary to choose an angle for the deviation point that would create the same relative angle between the deviation point and the top of the tower and the deviation point and the bottom of the tower, meaning that there would be an equilibrium of forces tangential to the wall. Knowing the angles of the tendons at the base of the tower, at the top deviator and at the flange and their thickness it's possible to determine the exact coordinates of the tendons throughout the whole tower height. In figure 4.7 the tendon distribution at the base of the tower is shown. In table A.3 from annex A the tendons angles throughout the tower are shown.

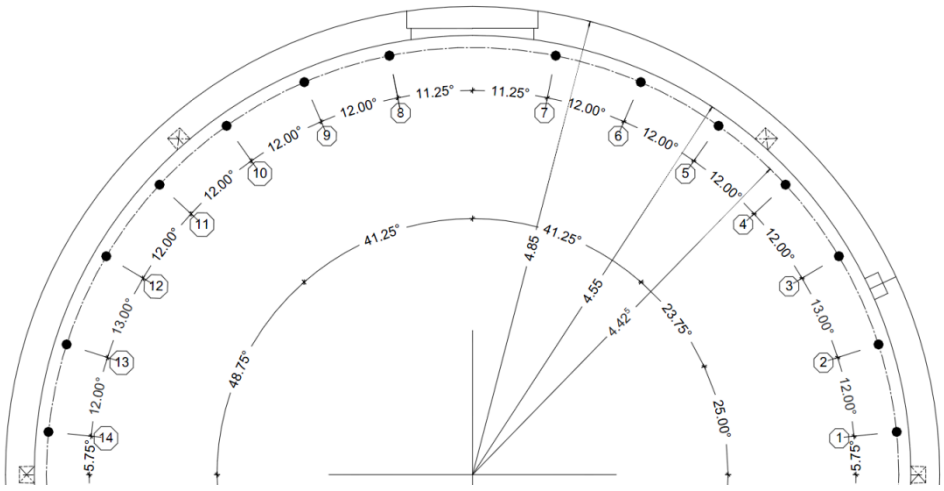

Figure 4.7 – Tendons angles at the base of the tower

5 PRESTRESS

5.1 External prestress

The concrete segments rest on top of one another, being kept in place by the applied prestress force. The prestress tendons (instead of running in ducts inside the concrete segments) are inside the tower without any bounding system. They are anchored at the top of the concrete tower and at the foundation corbel, where the prestress force is applied. In table 5.1 the characteristics of the prestress tendons according to the European technical approval are resumed.

Table 5.1 - Prestressing tendons

Manufacturer	**BBV**
Approval	ETA-12/0150
Prestr. Tendon Designation	L15 EW
No. of Strands per Anchor	15
Strand Nominal Diameter	0.62 ["]
Strand Nominal Cross-Section	150 [mm²]
Sheath	-
Prestr.Steel Grade	Y1860

One of the major advantages of a prestress system without bond is that it allows for a completely dry environment at the construction site. For example the grouting process under certain weather conditions could not be done for example. Freezing temperatures are often a problem in regions like Canada, northern Germany and Scandinavian countries. Also the water evaporation ratio is extremely dependent on the environmental conditions, making it difficult to control. By avoiding the grouting process every element is built in a controlled environment and then transported and assembled on site, without the need of additional works.

Externally prestressed tendons can be easily inspected during their entire lifetime. They can be removed and replaced if necessary, for example, where corrosion protection has deteriorated. Friction losses are greatly reduced because they are connected to the structure only at deviation and anchorage zones. This system presents some disadvantages, like being more accessible and prone to sabotage or fire exposure.

5.2 Prestress force

The horizontal joints between the concrete segments are done without the use of any linkage components or reinforcement, non-reinforced horizontal dry joint. The stresses from shear and torsion forces in the structure can lead to movement between each segment and, ultimately, the collapse of the structure. The only force keeping the segments in place is the friction developed between the segments, being directly related to the developed compression from the prestress force. The higher the prestress the higher the friction between the segments is.

One limitation from the European technical approval is the spacing between the anchor heads of the tendons. In order to assure that the compressive strength of the concrete is not achieved, due to the large compressive forces developed at the anchor head, a minimal distance between the centre distances of the tendon anchorages shall not be smaller than 382.5 mm for L15 EW tendons. The prestress force is applied by 28 tendons having to guarantee that the developed friction between the concrete segments is enough to avoid them from moving. From the loads simulation reports it is possible to verify that the maximum shear and the maximum torsion do not occur at the same time. The verification is carried for extreme loads with safety factor.

$$\begin{cases} 0.8 * M_{xy,max} + 1.0 * M_{z,max} \\ 1.0 * M_{xy,max} + 0.4 * M_{z,max} \end{cases} \quad (1)$$

Friction only occurs if the cross-section the elements is compressed, as a minimum value the prestress force has to guarantee that at least 1/3 of the wall thickness is always pressurized. The maximum and minimum stresses in the concrete are calculated by the following equation:

$$\sigma_{c,max/min} = \sigma_c + \left(\sigma_{cPm0} + \Delta\sigma_{c,P_{c+s+r}}\right) \pm \frac{M_{xy}}{w_c} * (0.8\ or\ 1.0) \quad (2)$$

For the first combination of values the entire wall cross-section is under compression being necessary to verify that shear and torsion effects are smaller than the resistant force produced by the prestress. Shear and torsion flows are determined form the following equations:

$$v_{Ed} = \frac{V_{Ed}}{\pi * r_m}(kN/m) \quad (3)$$

$$t_{Ed} = \frac{T_{Ed}}{2\pi * r_m{}^2}\ (kN/m) \quad (4)$$

The resistant force is conditioned by the type of surface finishing in the concrete segments. According to section 6.2.5 of the DIN EN 1992-1-1 the surface can be classified as very smooth, the most unfavorable situation, meaning that the friction coefficient is $\mu = 0.5$. The

compressive force is determined taking into account both the self-weight and the assumed prestress force.

$$\sigma_{Nd} = \sigma_c + \left(\sigma_{cPm0} + \Delta\sigma_{c,P_{c+s+r}}\right) \tag{5}$$

From this is possible to determine the tangential resistant stress, given that:

$$\tau_{Rd} = \min(\mu * \sigma_{Nd};\ 0.1 * f_{cd}) \Longrightarrow V_{Rd} = \tau_{Rd} * A_c \tag{6}$$

With the resistant force calculated from the tangential force multiplied by the area under compression. If the obtained value is larger than the applied, the prestress force is enough. The results for the entire tower are shown in table B.1 in annex B. The necessary prestress force applied to the tendons is 2900 kN.

The second combination of values is more critical. With the same prestress force some segments develop tensile stresses leading to a small gap. The provided prestress force has to be enough to assure that the tensile stresses do not reach 2/3 of the cross section. The critical situations occur for the joints at 29.10 m, 32.74 m and 36.38 m where small tensile forces are developed. The results are also shown in table B.1 from annex B.

5.3 Prestress losses

When the pre-stress is transferred to the concrete, immediate losses in the force occur. The difference between the pre-stressing force imposed by the jack, P_0, and the force in the steel immediately after the transfer at a particular section, P_{m0}, is the immediate loss. The gradual loss of prestress that takes place with time is called the time-dependent or deferred loss. If P_∞ is the force in the prestressing tendon after all losses, effective force, then the deferred loss is the difference between P_{m0} and P_∞.

The immediate losses are caused by elastic deformation of the concrete, taking into account deformation of the joints between precast elements as the pre-stress is transferred, friction in the tendon in a post-tensioned member, and slip at the anchorage. The time-dependent losses are caused by gradual volumetric changes in the concrete due to creep and shrinkage, and by relaxation of the steel itself. Additional losses may occur due to time-dependent deformation of the joints in segmental construction.

$$P_0 \longrightarrow P_{m0} \longrightarrow P_\infty$$

5.4 Immediate losses

5.4.1 Friction losses

When a tendon is tensioned by a jack the force produced is not constant along the length of the tendon. Usually, in post-tensioned members, the tendons are anchored at one end and stretched with jacks to the other. As the steel tendons slide through the duct, frictional resistance is developed, resulting in a different tension at the anchored end being less than the one applied at the jack. The total friction loss is the sum of the wobble friction, due to misalignment curvature friction and the intentional curvature of the tendon.

Because this tower is externally pre-stressed, the losses due to friction are very low when compared to grouted internal prestressed systems. In this tower the losses only occur due to changes in direction at the deviators. The friction losses can be determined from:

$$\Delta P_{\mu}(x) = P_0 * \left(1 - e^{-\mu(\theta + k*x)}\right) \tag{7}$$

Where μ is the friction coefficient and k the unintentional angular displacement. These parameters are given in section 2.2.3 from ETA-12/0150 approval. For externally post-tensioned systems $\mu = 0.1$ and $k = 0$. The angle θ is obtained from the tendon coordinates throughout the height of the tower. In figure 5.1 a schematic representation of a similar geometrical problem is shown.

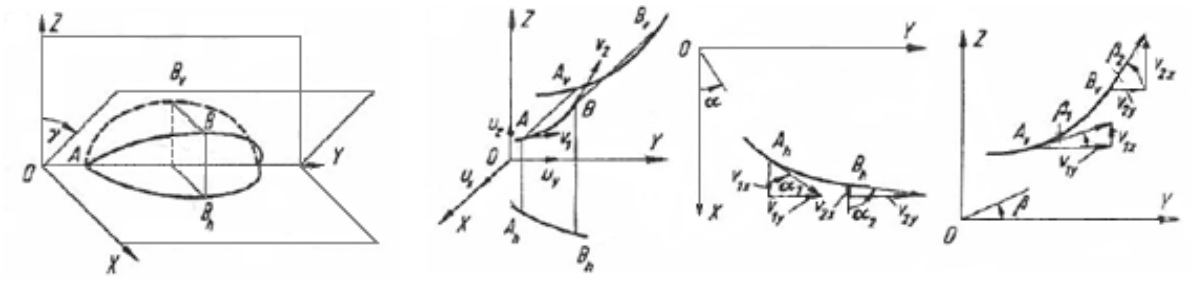

Figure 5.1 – Three dimensional representation of the coordinate's variation

The angles of the tendons are obtained from the directional change in two orthogonal planar projections. From the angles in each projection it is possible to exactly determine the angles of the tendons by using the following expression:

$$\theta = \sqrt{(\alpha_2 - \alpha_1)^2 + (\beta_2 - \beta_1)^2} = \sqrt{\theta_h^2 + \theta_v^2} \tag{8}$$

The angles at each deviation point are shown in table 5.2.

Table 5.2 – Near the door tendon coordinates

1st segment variation						2nd segment variation	
h	x	y	θ_1	θ_2	θ	h	θ
[m]	[m]	[m]	[°]	[°]	[°]	[m]	[°]
-1.525	0.883	4.404	0.000	0.000	0.000	-1.525	0.000
-0.020	0.864	4.342	0.000	0.000	0.000	-0.020	0.000
19.080	0.664	3.559	0.140	0.007	0.140	19.080	0.109
41.840	0.394	2.503	0.079	0.309	0.459	41.840	1.253
56.400	0.306	2.157	0.331	1.296	1.797	56.400	1.364
75.320	0.214	1.797	0.069	0.272	2.077	75.320	2.092
78.660	0.213	1.889	0.258	2.666	4.756	80.060	4.336

From the angle between every tendon position it is possible to exactly determine the friction losses. As shown in table 5.3, the losses due to friction are very small, corresponding at the top to less than 1% of the jack applied force.

Table 5.3 – Losses due to friction through the tower

1st segment variation				2nd segment variation	
h	P_0	$e^{-\mu (k*x+\theta)}$	P_{max}	h	P_{max}
[m]	[kN]	[-]	[kN]	[m]	[kN]
-1.525	2900	1.0000	2900.00	-1.525	2900.00
-0.020	2900	1.0000	2900.00	-0.020	2900.00
19.080	2900	0.9998	2899.29	19.080	2899.45
41.840	2900	0.9992	2897.68	41.840	2893.66
56.400	2900	0.9969	2890.92	56.400	2893.11
75.320	2900	0.9964	2889.51	75.320	2889.43
78.660	2900	0.9917	2876.03	80.060	2878.14

5.4.2 Anchorage wedge slip

Each one of the 15 strands of the tendon is kept in place by wedges at the anchor head. These elements have to be in accordance with the ETA-12/150 approval, smooth wedges type 30. Has the jacking force his released , there is a inevitably small amount of slip as the wedges seat themselves into the tendons, simultaneously a small deformation occurs at the anchor head has the force is transferred. According to ENERCON internal standards previous projects, it is known that the overall slip of the tendons is somewhere around 7 mm.

Through an iterative approach it is possible to easily determine the losses from the wedge slip. By knowing that at the level of the top deviator the total displacement would be 7mm it is possible to exactly determine the force losses from slip. By assuming an initial value for the force at the base, $P'_{mo}(x = 0)$, it allows to determine the value of the force for every other position, from that value and the variation between the losses due only to friction and the new value it allows to get the slip value. The process is done by using the following expressions:

$$P'_{mo} = P'_{mo}(x = 0) * e^{+\mu(\theta + k*x)} \quad (9)$$

$$\Delta P_m = P_{max} - P'_{mo} \quad (10)$$

$$\Delta l_{sl'} = 0.5 * \frac{\Delta P_m}{E_p * A_p} * l_{sl} \quad (11)$$

From an iterative approach the real loss value is obtained. In table 5.4 the prestress force in every position of the tower height is shown. It is possible to see that losses due to wedge slip extend throughout the tower full length.

Table 5.4 – Losses due to wedge slip

1st segment variation						2nd segment variation	
h	$e^{\mu(k*x+\theta)}$	P_{m0}'	$\Delta P_\mu(x)$	$\Delta l_{sl}'$	l_{sl}	h	P_{m0}'
[m]	[-]	[kN]	[kN]	[mm]	[m]	[m]	[kN]
-1.525	1.000	2852.60	47.40	0.00	---	-1.525	2852.10
-0.020	1.000	2852.60	47.40	0.16	---	-0.020	2852.10
19.080	1.000	2853.30	45.99	2.20	---	19.080	2852.64
41.840	1.000	2854.89	42.79	4.50	---	41.840	2858.34
56.400	1.000	2861.56	29.36	5.69	---	56.400	2858.89
75.320	1.000	2862.96	26.54	6.90	---	75.320	2862.53
78.660	1.000	2876.00	0.00	7.00	**80.185**	80.060	2873.76

In figure 5.2, for the first segment variation, the theoretical value of the prestress force taking into account friction losses and as well the real value of the force after the after the wedge slip losses, P_{m0} is shown.

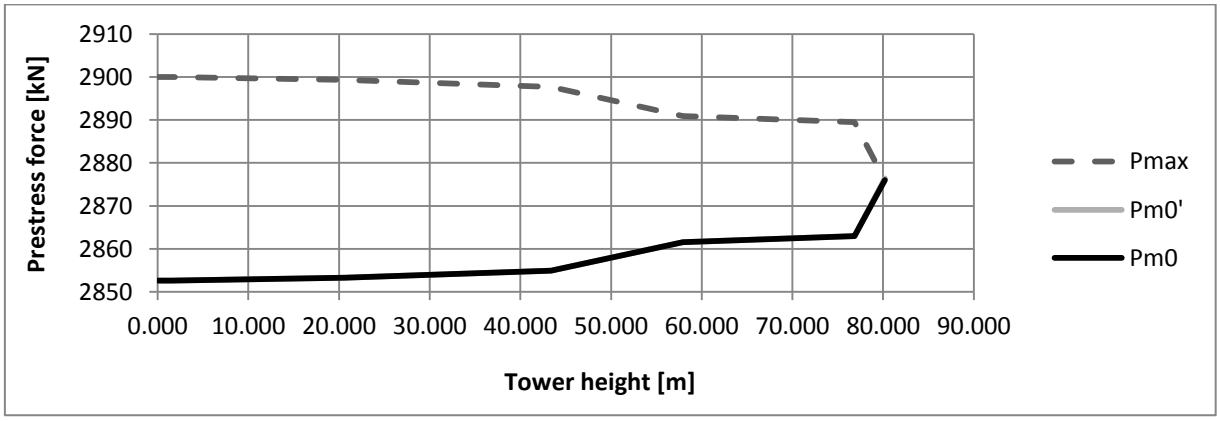

Figure 5.2 – Prestress force after immediate losses

The prestress force applied to the concrete after the immediate losses should not exceed $P_{m0,max}$ according to 5.10.3 in DIN EN 1992-1-1:

$$P_{m0,max} = A_p * \sigma_{Pmo} \tag{12}$$

Where σ_{Pmo} is given in the EN 1992-1-1 as $min\{0.75 \times f_{pk}; 0.85 \times f_{p0,1k}\}$.

$$P_{max} = \min(3139; 3137) = 3137\ kN \tag{13}$$

This value is greater than the value of the prestress force after the losses, $P_{m0,max} = 2871.59\ kN$ verifying the condition.

5.4.3 Elastic shortening of the concrete and tendons elongation

The post-tensioning force is applied at the foundation corbel where the 28 tendons are anchored. All 15 strands are tensioned at once by the jack with the force always applied in opposing tendons. Because the force is applied to the tendons the concrete will inevitably deform. This elastic shortening leads to losses in the prestress force. Another process that happens at the same time as the jack force is being applied is the elongation of the tendons.

In order to guarantee that the determined prestress force is applied to the structure it is necessary to exactly determine the elongations of both concrete and tendons. The concrete compressive strain and consequent concrete elongation are calculated by:

$$\varepsilon_{c,l} = \frac{\sigma_{c,Pmo}}{E_{cm}} \Longrightarrow \Delta l_c = l * \varepsilon_{c,l} \tag{14}$$

The overall elastic shortening is achieved right after all the tendons are stressed, corresponding to the sum of each tendons applied force. At this time the friction and wedge slip loses have already occurred being the force used in the calculation P'_{mo}. The values of the concrete shortening can be seen in table B.2 in annex B. The tendon elongation occurs while the jacking force is being applied, meaning that only friction losses have occurred at this point:

$$\varepsilon_{p,l} = \frac{\sigma_{P0}}{E_p} \Longrightarrow \Delta l_p = l * \varepsilon_{p,l} \tag{15}$$

In annex B table B.3 is shown the determination of the tendons elongation. The jacking force applied to each tendon is different, decreasing from the first tensioned tendon to the last has the concrete shortening occurs. The overall elongation is the sum of both the tendons elongation and the concrete shortening. At the time of the tensioning of the first tendon the concrete still has not started to deform, so this tendon is going to experience the greatest loss. The highest tensioning force has to be applied to this one. In Annex B table B4 the necessary prestress forces for each tendon are shown. Both segment variations lead to very similar

results. The force is obtained from the difference between the tendon elongation that normally would occur and compressive shortening of the concrete.

The determined prestress force, applied by the jack, has to be smaller than the maximum value determined according to section 5.10.2 of the DIN EN 1992-1-1:

$$\sigma_{p,max} = min\{0.8 \times f_{pk}; 0.9 \times f_{p0,1k}\} \Longrightarrow P_{0,max} = A_p * \sigma_{p,max} \quad (16)$$

With A_p being the cross section area of the prestress tendons, $A_p = 22.5\ cm^2$ and $\sigma_{p,max}$ given in the same document. The maximum allowable value for the jack applied force is $P_{0,max} = 3321\ kN$, which is larger than the maximum applied to tendon number one, $P_0 = 3042\ kN$. This verification limits the possible increase of the force meaning that is not possible to increase the jack force indefinably in order to ensure that the cross section is always compressed.

5.5 Time dependent losses

Time differed losses are mainly caused by stress reduction from creep, shrinkage and reinforcement relaxation. The determination of creep and shrinkage parameters is done according to annex B from DIN EN 1992-1-1.

5.5.1 Creep

Creep causes many materials to continuously deform over considerable periods of time under constant stress or loads. At first, the strain increase is very quick, leading to elastic shortening of the concrete, but decreases with time until a constant value is achieved. The creep coefficient $\varphi(t, t_0)$ is obtained from section B.1:

$$\varphi(t, t_0) = \varphi_0 * \beta_c(t, t_0) \quad (17)$$

Where φ_0 is the notional creep coefficient and $\beta_c(t, t_0)$ the coefficient to describe the development of creep with time after loading. These values are very much related to the relative humidity of the ambient environment, RH, the age of the concrete, t, and the age of first loading, t_0. The calculations were done assuming $RH = 80\%$ taken from the national annex for eurocode 2 - part 2, $t = 7500\ days$ and $t_0 = 20\ days$.

5.5.2 Shrinkage

Unless kept underwater or in air with 100% relative humidity, concrete losses moisture and reduces its volume. This process is known as shrinkage. Over time this variation in volume

leads to losses of the prestress force. The basic drying shrinkage strain, $\varepsilon_{cd,0}$, is given in B.2 of annex B:

$$\varepsilon_{cd,0} = 0.85 * \left[(220 + 110 * \alpha_{ds1}) * \exp\left(-\alpha_{ds2} * \frac{f_{cm}}{f_{cm0}}\right)\right] * 10^{-6} * \beta_{RH} \quad (18)$$

The relative humidity of the ambient environment and the class of cement are critical parameters. Cement class R was used.

5.5.3 Steel relaxation

Prestressing tendons are held stressed for the entire lifetime of the structure. Over time there will be a gradual reduction of stress in the steel under these conditions resulting from relaxation, even though the length is almost constantly maintained. The amount of relaxation depends largely on the steel stress force and time.

From DIN EN 1992-1-1 section 5.10.6 it is shown that the stress variation in the tendons, $\Delta\sigma_{pr}$, can be determined from the initial stress calculated for quasi-permanents actions:

$$\sigma_p = \sigma_p * (G + P_{m0} + \psi_2 * Q) \quad (19)$$

Having the creep and shrinkage coefficients determined and also the losses due to steel tendons relaxation, it is possible to evaluate the losses to every position throughout the tower, ΔP_{c+s+r}. From section 5.10.6 (2) the following formula is given:

$$\Delta P_{c+s+r} = A_p * \Delta\sigma_{p,c+s+r} = A_p * \frac{\varepsilon_{cs} * E_p + 0.8 * \Delta\sigma_{pr} + \frac{E_p}{E_{cm}} * \varphi(t,t_0) * \sigma_{c,QP}}{1 + \frac{E_p}{E_{cm}} * \frac{A_p}{A_c} * \left(1 + \frac{A_c}{I_c} * Z_{cp}^2\right) * [1 + 0.8 * \varphi(t,t_0)]} \quad (20)$$

The effect of steel relaxation depends largely on the concrete deformation due to creep and shrinkage. The interaction between these effects is taken into account by using a 0.8 reduction factor as seen in the previous equation. The calculation of the time dependent losses is show in table B.5 from annex B.

5.6 Imperfections and second order effects

Second order effects are especially influential in structures prone to instabilities, where the displacements are large enough to amplify the loads applied to the structure. In particular, second order effects have an important influence in structures with a great free span length since large displacements may occur at free end. In the specific case of a wind tower the higher the prestress force is the smaller the influence of the second order effects are, because the smaller displacements are going to be.

From a detailed calculation of the second order effects on the tower it was possible to obtain curves with the relation between bending moments and tower curvature. From this calculation and taking into account the prestress force provided to the structure it was possible to verify that the entire tower height is within the linear elastic range of behavior. In figure 5.3 is shown the m-k line for a height of 72.68 meters.

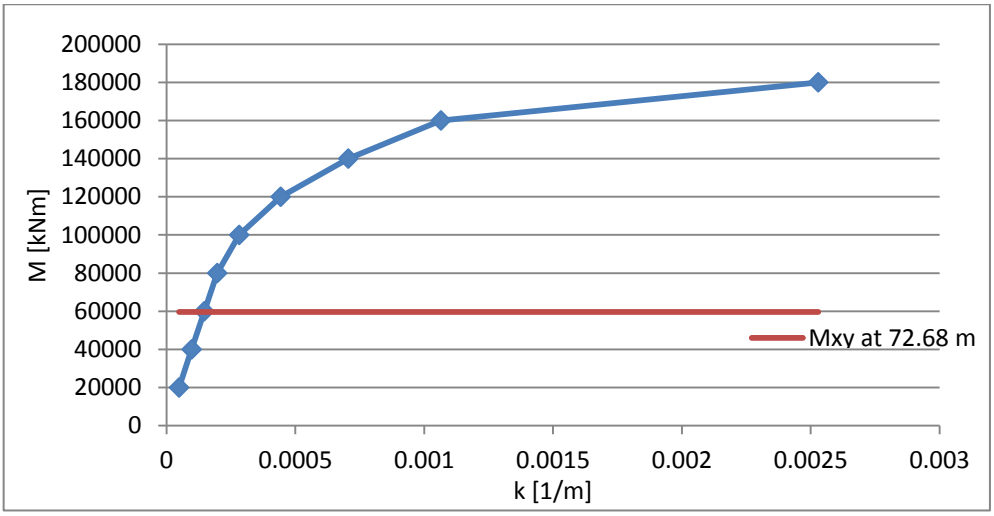

Figure 5.3 – M-k line for the height of 72.68 meters

In the previous figure it is possible to see the transition from a linear elastic behavior to non-linear. The values of the bending moments are always small enough to be in the linear elastic range (linear part of the curve), meaning that second order effects have a small influence on the structure. Unintentional misalignments have to be taken into account in the design leading to an additional moment. According to the DIBt guideline a 5 mm/m misalignment has to be considered to cover for manufacturing and erection tolerances and as a result of possible differential settlement of the soil a 3 mm/m deviation should be considered. The moment increase is obtained for every height of the tower, from simply knowing the vertical force at each point and the swayed position. This displacement is obtained by considering the 8 mm/m due to misalignments and the swayed position due to wind loads.

6 REINFORCEMENT CALCULATION

6.1 Ultimate limit state

The reinforcement design is done taking into account the contribution of wind loads that lead to bending, shear, torsion and the effects of both self-weight and pre-stress force. In a cylindrical shaped structure failure due to bending is not a critical design situation. For the determination of reinforcement the critical situations in the tower design would be the interaction between shear and torsion and the effects of temperature differentials.

6.1.1 Shear force and torsion

Flexural shear and torsion are critical verifications in the tower design. For prestressed members subjected to shear and torsion, tests show that the ultimate torsional strength can be expressed as the sum of strengths contributed by the concrete and the web reinforcement, just as for non-prestressed members. The effect of the prestress is to increase the contribution of the concrete to the ultimate torsional strength, while the contribution of reinforcement remains unchanged. Diagonal tension stress in the concrete produced by shear and torsion represents a very important factor to look at during the design. Inevitably these stresses will lead to diagonal cracking in the structure.

A crack will form in the concrete when the principal tensile stress at a specific location reaches the cracking strength of the concrete. Assuming, for example, a small element in a reinforced concrete beam subjected to positive shear stresses distribution, as shown in figure 6.1, from the construction of a Mohr’s circle it is possible to see that the principal tension acts at a 45° degree angle with the longitudinal axis of the element. Equal principal compression acts in the perpendicular direction. If cracking were to occur it would be perpendicular to the principal tensile direction.

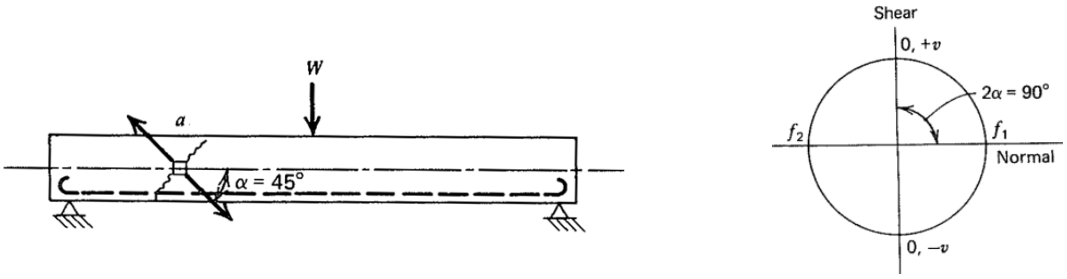

Figure 6.1 – Reinforced concrete beam

Considering the same beam and loading but adding a prestress force leads to a large compressive force in the longitudinal axis direction changing the stress distribution in the element. As seen in figure 6.2, the resulting tensile force is now smaller and occurs at a greater angle with the longitudinal axis. This can easily be verified looking at the different vectors representing the acting forces. On the other this means, that if a diagonal crack where to appear it would be at a flatter angle with the longitudinal axis.

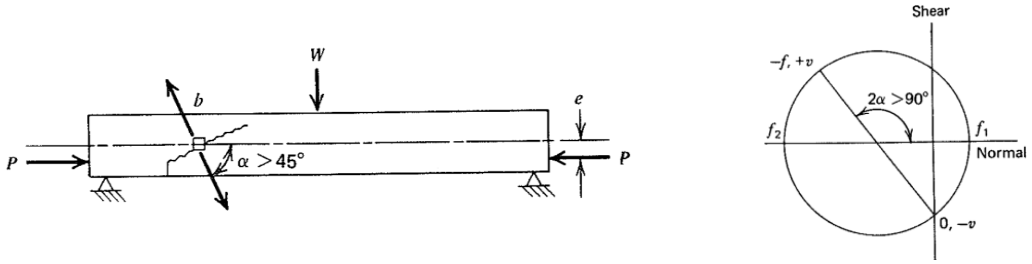

Figure 6.2 – Prestressed concrete beam

After cracking tensile stresses have to be carried out by the reinforcement. In case of existing shear reinforcement, in form of vertical stirrups, this would mean that a larger amount of reinforcement would cross the diagonal crack, and in this way, improving its effectiveness. The ideal solution would be to create the reinforcement perpendicular to cracking, creating a helicoidal reinforcement web. This solution would be harder to build and only works for forces in one direction, if the load direction were to change it would be necessary to provide reinforcement according to the new direction. So, in practical terms, it is more effective and easy to build a segment with simply horizontal and longitudinal reinforcement.

The loads applied to the tower lead to a constant torsional force distribution around the cross-section of the segment. Shear induced by the wind is only resisted by part of the segment leading to an asymmetrical distribution of stresses, effective area. Throughout the tower height wind loads lead to bending of the tower, resulting in the appearance of tensile and compressive stresses. The prestress forces and the self-weight are constant across the segment wall. The stress distribution from every load can be seen in figure 5.3:

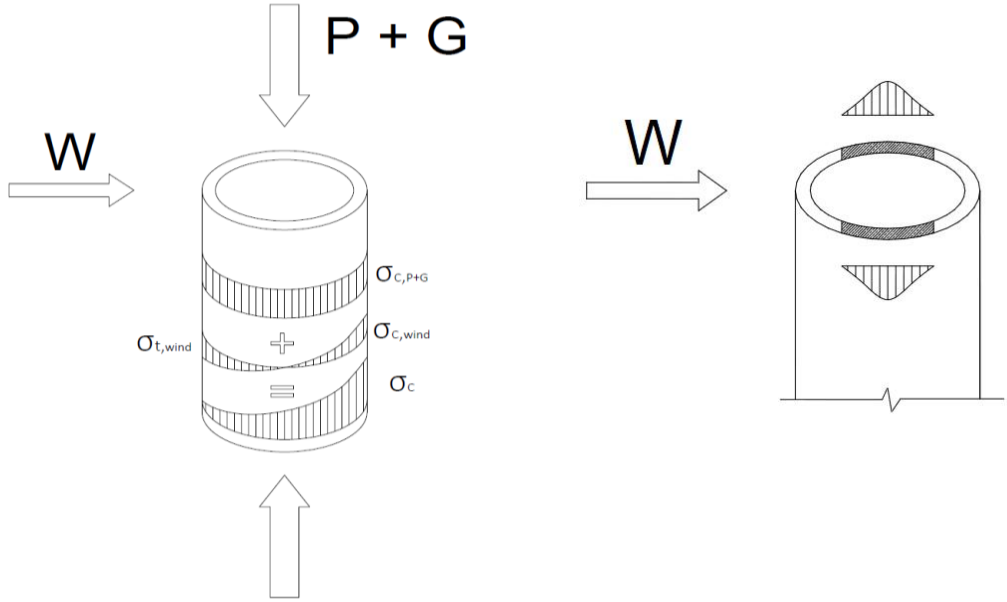

Figure 6.3 – Stress distribution due to prestress, self-weight and wind, effective section resistant to shear

In the figure previously shown it can be seen that there are some critical situations worth considering. The simultaneous effects of shear and torsion on the element cross-section mean that in the longitudinal direction there is no influence from tensile stresses due to wind. Another critical situation may occur when looking to a point of the cross-section under the effects of torsion only. At this point there is no contribution from prestress compressive forces because of the wind tensile forces. Because the prestress force was chosen in order to leave the segments cross-section always under compression, this last situation is less important.

According to sections 6.2.3(3) and 6.3.2(3) from DIN EN 1992-1-1 the reinforcement in both horizontal and longitudinal directions can be determined from the following expressions for the design under shear and torsion. The same amount of reinforcement is given to the entire segment with the calculations done per meter.

$$a_{sw} = \frac{(v_{Ed}+t_{Ed})}{f_{yd}*\cot\theta} \tag{21}$$

The horizontal reinforcement is determined taking into account the effects of both shear force and torsion. The entire segment resists to torsion but only a portion of the section resists to the shear forces at each time, as shown in the previous figure. The critical situation is when shear and torsion occur simultaneously. As for the longitudinal reinforcement:

$$a_{sl} = \frac{t_{Ed}}{f_{yd}*\tan\theta} \tag{22}$$

In the case of the longitudinal reinforcement, the pre-stress force was chosen in order to guarantee that the segments are always under compression. From the prestress calculations it can be seen that even the outside of the segments are always under compression under the action of wind loads. This means that the tension force from the wind loads is always smaller than the compressive forces from pre-stress and self-weight. Keeping this in mind, only torsion is considered for the calculation of the vertical reinforcement.

The value of θ (angle between the longitudinal axis of the tower and the compressive strut) used in the calculations was 45° degrees, leading to the same contribution from the two reinforcement directions. According to the German national annex for the DIN EN 1992-2 has to be chosen within a range of values:

$$1.0 \leq \cot\theta \leq 1.75 \tag{23}$$

It is always necessary to guarantee the structural safety of the element, with the maximum resistance to shear and torsion stresses being limited to the satisfaction of the following expression according to DIN 1045-1:

$$\frac{t_{Ed}}{t_{Rd,max}} + \frac{v_{Ed}}{v_{Rd,max}} \leq 1.0 \tag{24}$$

With $t_{Rd,max}$ and $v_{Rd,max}$ obtained from expressions (76) and (93) in the same document, for the same element with unitary dimensions:

$$T_{Rd,max} = \frac{\alpha_{c,red} * f_{cd} * 2}{\cot\theta + \tan\theta} \tag{25}$$

$$V_{Rd,max} = \frac{\alpha_c * f_{cd}}{\cot\theta + \tan\theta} \tag{26}$$

There is also the need to assure that the principal tension is smaller than f_{cd}, avoiding cracking in the segments. The stress can be calculated from:

$$\sigma_z = \frac{\sigma_1}{2} + \sqrt{\frac{{\sigma_1}^2}{2} + {\tau_1}^2} \leq f_{cd} \tag{27}$$

In tables C.1 and C.2 from annex C the amount of reinforcement necessary for the entire tower is shown. In table 6.1 is shown the amounts of reinforcement in both directions for the two different concrete segments.

Table 6.1 – Required reinforcement for both geometries

	1st segment variation		2nd segment variation	
Segment No.	*Horizontal reinforcement* a_{sw}	*Longitudinal reinforcement* a_{sl}	*Horizontal reinforcement* a_{sw}	*Longitudinal reinforcement* a_{sl}
	[cm²/m]	[cm²/m]	[cm²/m]	[cm²/m]
4	7.55	5.06	7.11	4.72

6.1.2 Reinforcement due to temperature

The temperature loads are determined according to the DIBt guideline where the differential temperature variations are critical, leading to large bending moments which the reinforcement has to resist. Across the tower wall a 15 °C temperature variation is considered according to the guideline, and for the lower segment a variation of 20 °C was considered in order to take into account the effects of the machines inside the tower located at this height. The bending moment can be determined from:

$$M_{Ed} = \left(\alpha_T * \Delta T * \frac{EI}{t}\right) * \gamma_{F,Temp} \tag{28}$$

Where α_T represents the thermal coefficient of reinforced concrete give as $\alpha_T = 0.00001\ k^{-1}$. $\gamma_{F,Temp} = 1.35$, represents a safety factor give in section 9.2 of the DIBt guideline. The amount of reinforcement is calculated from the following flexural design expressions:

$$\mu_{Eds} = \frac{M_{Eds}}{b*d^2*f_{cd}} \tag{29}$$

$$a_{s,temp,erf} = \frac{\omega*b*d*f_{cd}}{f_{yd}} \tag{30}$$

The coefficient ω is taken from flexural design tables provided. The amount of reinforcement obtained is to be applied in both horizontal and longitudinal direction. In table C.3 from annex C the required amount of reinforcement due to temperature loads is shown.

6.2 Serviceability limit state

In the serviceability limit state it is not the collapse of the structure that is under examination but the usage conditions and visual aspects of the elements. This part of the design needs to guarantee a satisfactory outcome of the following verifications: determination of the minimum reinforcement, control of crack width and the verification of the reinforcement for the critical combinations under unfactored loads. The limitation of deformation, according to

the DIBt guideline, can be avoided as long as no special requirements for the turbine operation are specified. The amounts of reinforcement provided in order to control early-age thermal cracking are usually high, and are in certain circumstances the controlling design situation.

6.2.1 Early-age thermal cracking

Cracking is not a defect but a normal phenomenon in reinforced concrete structures. Assessing the acceptable crack distribution is a critical state of the design process where a rigorous approach to the prediction of the crack-inducing strain, requiring knowledge of the concrete to be used, may lead to considerable savings in the provided reinforcement. Cracks can be assessed according to the influence in a structure, ranging from cracks which lead to durability problems and consequently a reduction in structural capacity, to cracks leading to a loss of serviceability in the structure or simply by being aesthetically unacceptable.

Under serviceability conditions, crack widths may only be excessive if the minimum reinforcement area $A_{s,min}$ is not achieved and the steel yields. The maximum crack width has to be, according to the DIBt guideline section 10.2.5, smaller than 0.2 mm. The determination of the amount of reinforcement provided sufficient to control early-age cracking, while also being adequate for controlling cracks that may develop due to long-term deformations caused by temperature change and shrinkage, is not a simple process. According to DIN EN 1992-3 when conditions during the construction phase are considered to be relevant, the heat evolution should be measured by carrying out tests. The actual heat evolution should be determined taking into account the expected conditions during the early life of the member such as curing and ambient conditions. The maximum temperature rise and the time of occurrence after casting should be established from the mix design, the nature of the formwork, environmental and boundary conditions.

Early-age thermal cracking is associated with heat release from the hydration process of the binder. As cement hydrates it generates heat, initially at a greater rate than the heat loss to the environment leading to an increase in the temperature of the concrete. The rate of heat generation decreases with time, leading to cooling and contraction of the concrete. In an unrestrained concrete segment and without temperature differentials, concrete would expand and contract without creating any stresses. This is not a realistic situation because concrete elements are always under some degree of restraint leading to the development of stresses. The elastic modulus of concrete changes considerably during the first few days after casting: it is relatively low during the heating period compared to the value as it cools down. For a given magnitude of restrained thermal strain, the compressive stress generated during heating is lower than the tensile stress generated during cooling, resulting in a residual tensile stress at the end of the heat cycle (Bamforth, 2007).

Concrete structures have always some degree of restrain, either external or internal. External restrain comes, for example, from adjacent structures or formworks. In the case of ENERCON's concrete segment they experience almost no external restrain being removed from the shutters a short period of time after concreting and kept in supports that allow movement enabling the concrete to expand and contract without causing resistance. Internal restraint, on the other hand, comes from the changes in differential temperature throughout the thickness of segments wall leading to both superficial and internal cracking. In figure 6.4 the process of crack development over time from internal restraint is shown.

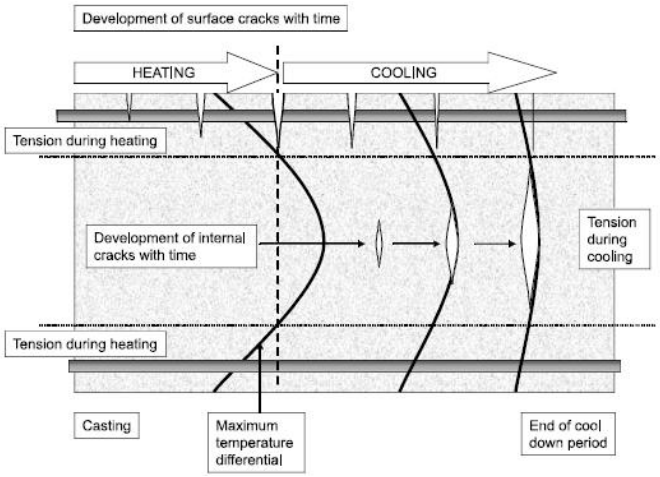

Figure 6.4 – Crack development due to internal restraint (Bamforth, 2007)

During the heating phase the surface is under tensile stresses that lead to crack openings as the centre core expands with temperatures rising. In the early stages and with high temperatures, creep is prevalent and part of the generated stresses are relived (Bamforth, 2007). In the cooling phase, tension stresses start to develop in the centre of the segment leading to a decrease in the surface crack widths. These tensile stresses that start to develop in the core part of the element, could lead to the formation of internal cracks that cannot be seen with a simple eye inspection from the outside.

6.2.2 Minimum reinforcement requirement

According to DIN EN 1992-1-1 in order to safely control the crack spacing and crack width a minimum reinforcement area can be obtained from the following equation:

$$A_{s,min} = K_c * K * f_{ct,eff} * A_{ct}/\sigma_s \tag{31}$$

Coefficients K_c, K and A_{ct} are influenced by the nature of the restraint conditions. When internal restraint is dominant like it is for the tower segments, the stress distribution can be

assumed to have the same shape as the temperature variation (Bamforth, 2007). This temperature profile is shown in figure 6.5:

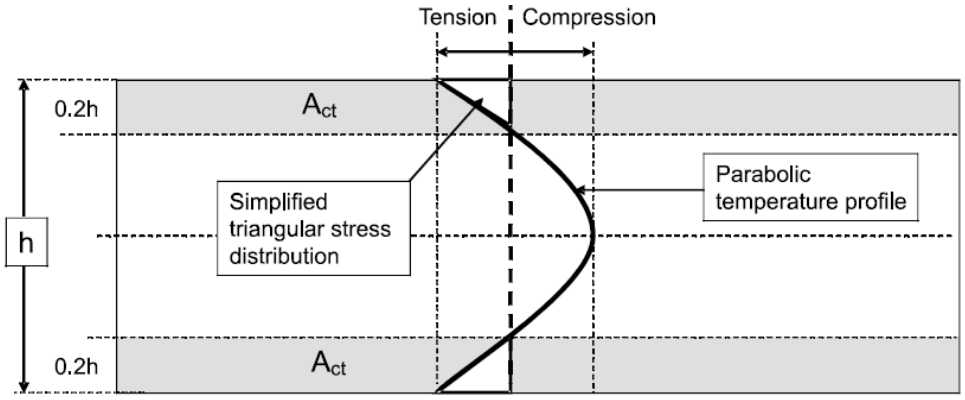

Figure 6.5 – Temperature profile in an element under internal restraint (Bamforth, 2007)

The stress distribution, as shown in the previous figure, has a triangular shape consisting of approximately 20% of the thickness of the element at the tensile zone near the surface. The value of K_c may be assumed as 0.5, by taking into account that the segments are largely influenced by internal restraint. As a conservative assumption the K value should be equal to 1.0 as the value of K_c is already taking into account the self-equilibrating-stresses. The coefficient values for both, external and internal restraint were determined according to (Bamforth, 2007). The value of $f_{ct,eff}$ may be taken as the mean value of the tensile strength of the concrete effective at the time when the first crack is expected to occur, normally $f_{ct,eff} = f_{cm}(t)$.

The evolution of the concrete tensile strength with time is intimately related to the used mix and the curing and drying conditions. The concrete mixes used by ENERCON in their production facilities have particularities that lead to a different behaviour when comparing with same grade standard concretes. The lower segments of the tower use a C55/67 concrete grade. From table 3.1 of the DIN EN 1992-1-1 and the expressions taken from section 3.1.2 (6), the compressive strength of a standard C55/67 concrete for different ages, with an average temperature of 20°C and curing conditions in accordance to EN 12390, can be estimated from:

$$f_{ctm}(t) = 2.12 * \ln\left[1 + \left(\frac{f_{cm}(t)}{10}\right)\right] \quad (32)$$

With $f_{cm}(t)$ given by:

$$f_{cm}(t) = \beta_{cc}(t) * f_{cm} \quad (33)$$

$$\beta_{cc}(t) = \exp\left\{s\left[1 - \left(\frac{28}{t}\right)^{1/2}\right]\right\} \tag{34}$$

Assuming class R has the cement strength, $s = 0.20$ and $f_{cm} = 63\ MPa$ taken from table 3.1 of the DIN EN 1992-1-1. The same calculations for the compressive strength for a concrete of the grade but produced by ENERCON show very different behavior. The development of the concrete strength for the two different concretes is shown in figure 6.6.

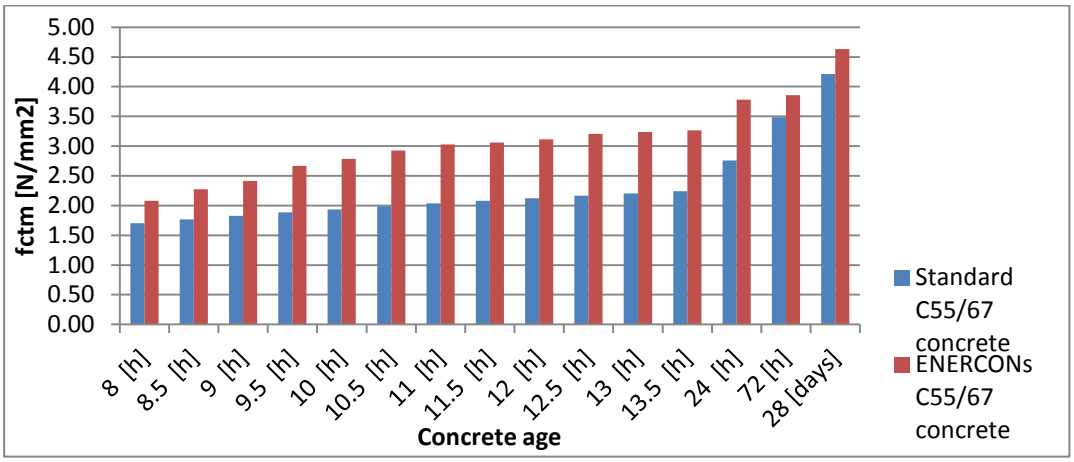

Figure 6.6 - Compressive strength for a C55/67 concrete grade

The concrete used in the segments shows always a higher compressive strength than the standard one. Over time that difference becomes less significant, but for early-age, the resistance is very large.

The value of the concrete tensile strength used for early-age thermal cracking is normally taken 3 days after concreting. In the case of the used concrete, the value of the compressive strength is $f_{ctm}(t) = 3.86\ N/mm^2$ representing already 90% of the strength for a standard concrete with 28 days.

The maximum steel tensile stress allowed in the reinforcement is determined taking into account the limitation of the crack width. The value of σ_s is chosen in order to assure that the limit of $w_k = 0.2\ mm$ for the crack width is verified. According to DIN EN 1992-2, the limitations in crack width are provided in section 7.3.3, with the steel stress being given by:

$$\sigma_s = \sqrt{w_k * \frac{3.48 * 10^6}{\phi_s^*}} \tag{35}$$

The value of the adjusted maximum bar diameter, ϕ_s^* is determined considering that the section is under bending.

$$\phi_s = \phi_s^* * \frac{K_c * K * h_{cr}}{4 * (h-d)} * \frac{f_{ct,eff}}{2.9} \geq \phi_s^* * \frac{f_{ct,eff}}{2.9} \quad (36)$$

The value of h_{cr} represents the depth of the tensile zone prior to cracking, corresponding to 20% of the overall depth of the element, as shown before. The table C.4 from annex C shows the required reinforcement for the whole tower.

6.2.3 Shear and torsion

Shear and torsion reinforcement in serviceability limit states follows the same calculation procedures as shown for the ultimate limit states. The loads taken into account in the calculations are now without safety factors. The calculation of the reinforcement is shown in table C.5 in annex C.

6.2.4 Reinforcement due to temperature

In the serviceability limit states the entire cross section of every segment is always under compression. This means that in the longitudinal direction the temperature effects are unable to create tensile stresses, so no reinforcement is necessary to provide due to temperature. In the horizontal direction, the temperature differential creates tensile stresses, which means that reinforcement is required. The calculation procedure is the same as used for ULS. The results are shown in tables C.6 and C.7 from annex C.

6.3 Required reinforcement

The reinforcement required by the segments results from the maximum value between ULS and SLS. In both situations the results are given from the critical case between the isolated effects of shear and torsion, temperature or both combined with safety factors, 0.6 according to the DIBt guideline.

The amount of provided reinforcement must always be larger than a minimum value, for constructive reasons. For ULS it was assumed that the DIN EN 1992-1-1 specifications for the minimum amount of longitudinal reinforcement for walls were adequate. So the provided reinforcement to the tower concrete segments as to be larger than:

$$A_{s,min} = 0.002 * A_c \quad (37)$$

The reinforcement of the combination of the different actions is determined as the critical situation of the two:

$$a_s = \begin{cases} a_{s,Q+T} + 0.6 * a_{s,temp} \\ 0.6 * a_{s,Q+T} + a_{s,temp} \end{cases} \quad (38)$$

The reinforcement provided to the segments corresponds to the maximum between the ultimate limit states and serviceability limit states. In tables C.8 and C.9 from annex C the determination of the required reinforcement amounts for the whole tower is shown. The reinforcement requirements for both variations are shown in table 6.2.

Table 6.2 – Required reinforcement amounts for both segment variations

1st segment variation			
Kn.	Height h	Required horizontal reinforcement a_{sw}	Required vertical reinforcement a_{sl}
	[m]	[cm²/m]	[cm²/m]
-1			
26	76.420	11.64	10.79
27	78.660	11.55	10.03

2nd segment variation			
Kn.	Height h	Required horizontal reinforcement a_{sw}	Required vertical reinforcement a_{sl}
	[m]	[cm²/m]	[cm²/m]
-1			
26	76.420	7.94	6.60
27	80.060	11.54	10.03

6.4 Reinforcement due to radial force

Throughout the tower, as the tendons change direction at the deviators, an additional force is applied to the concrete segments. At the top deviator this situation assumes a critical point because the tendons are very close to each other meaning a larger force per meter. This force can be determined by knowing the prestress force before and after a deviation point and the tendon coordinates. The critical situation occurs a short period of time after pre-stress force is applied, before the time dependent losses have occurred, representing the situation when the concrete segments experience the maximum applied loads. In table 6.3 the pre-stress force values after immediate losses and tendons angles are shown, considering the first segment variation.

Table 6.3 – Prestress force and tendon angles

Height h [m]	*Calculated Prestressing Force* P0 [kN]	*Tendon angle* θ [°]
-1.525	2852.603	0.000
-0.020	2852.603	0.000
19.080	2853.301	0.140
41.840	2854.891	0.459
56.400	2861.562	1.797
75.320	2862.963	2.077
78.660	2876.029	4.756

From the presented values it is possible to determine the value of the radial force, P.

$$P = \frac{28*P_{m0}(h=75.32)*\sin(\theta_{h=75.32})+28*P_{m0}(h=78.66)*\sin(\theta_{h=78.66})}{2*\pi*a} = 342.21kN/m \quad (39)$$

The radius a corresponds to distance between the longitudinal axis and the deviator. The calculations for the determination of the stresses due to the radial force are based on shell element theory, where the curvature of the element has a greater contribution in the overall behavior of the element. To study this problem, three segments where considered: segment 5 where the radial force is applied and the adjacent ones, 4 and 6. It was assumed that the stress distribution from the radial force had an influence over these segments. In figure 6.7 a schematic representation of the problem is shown.

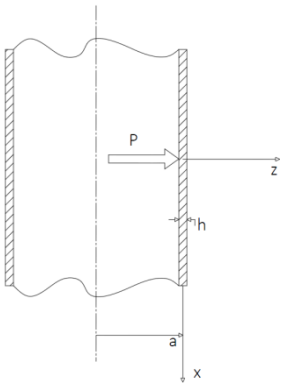

Figure 6.7 – Schematic representation of the radial force in a cylinder

The first step is to insure that the considered cylinder can be considered as a long cylinder. As the thickness varies over the different segments, an average value was used. The geometric parameter λ, according to (Meskouris, 2012) is given by:

$$\lambda = \frac{\sqrt[4]{3*(1-\mu^2)}}{\sqrt{a*h}} \tag{40}$$

Where μ is the Poisson's ration, a the radius of the cylinder and h the thickness of the wall. A cylinder is considered long, or semi-infinite, as long as the following expression is proven:

$$\lambda * l \geq 4 \tag{41}$$

For both different geometries this criteria is confirmed. According to (Meskouris, 2012) is possible to consider a simplified problem and apply the displacement method. The bending moment due to the radial force can be determined assuming the following simplified problem:

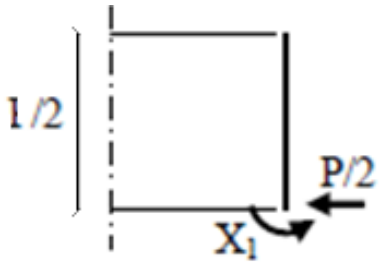

Figure 6.8 – Simplified cylinder calculation

The rotation due to a unitary bending moment is:

$$\delta_{11} = W_u' = \frac{M}{k*\lambda} \tag{42}$$

And the rotation from the external force is given by:

$$\delta_{10} = W_u' = \frac{R}{2*k*\lambda^2} \tag{43}$$

From the necessary force equilibrium it is possible to determine the value of the maximum moment:

$$\delta_{11} * X_1 = \delta_{10} \Rightarrow X_1 = \frac{R}{2*\lambda} \tag{44}$$

The value of X_1 corresponds in the previous figure to M_φ. The stress distribution throughout the height of the cylinder is obtained from:

$$M_{\varphi}(x) = \frac{R}{\lambda} * \eta'(\xi) + M_{\varphi} * \eta(\xi) \quad (45)$$

From the previous equation it is possible to see that the vast majority of the force is applied in a small area; approximately 1 m. The additional reinforcement due to radial force is applied only in that same zone. In figure 6.9 the stress distribution throughout the cylinder height from where the amount of vertical reinforcement is determined is shown.

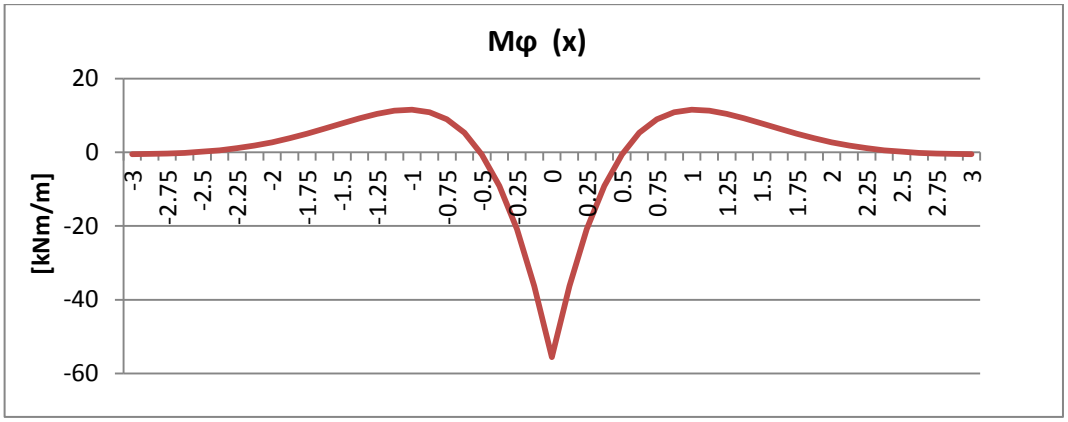

Figure 6.9 – Meridional bending moment throughout the segment

The bending moment along the perimeter of the cylinder and the forces in the tangential direction are shown in table 19 from (Meskouris, 2012):

$$M_{\vartheta} = 0.3 * M_{\varphi} \quad (46)$$

$$N_{\vartheta} = 2 * a * R * \eta'''(\xi) * a + 2 * a * M_{\varphi} * \lambda^2 * \eta''(\xi) \quad (47)$$

The tangential force variation along the height of the cylinder is shown in figure 6.10.

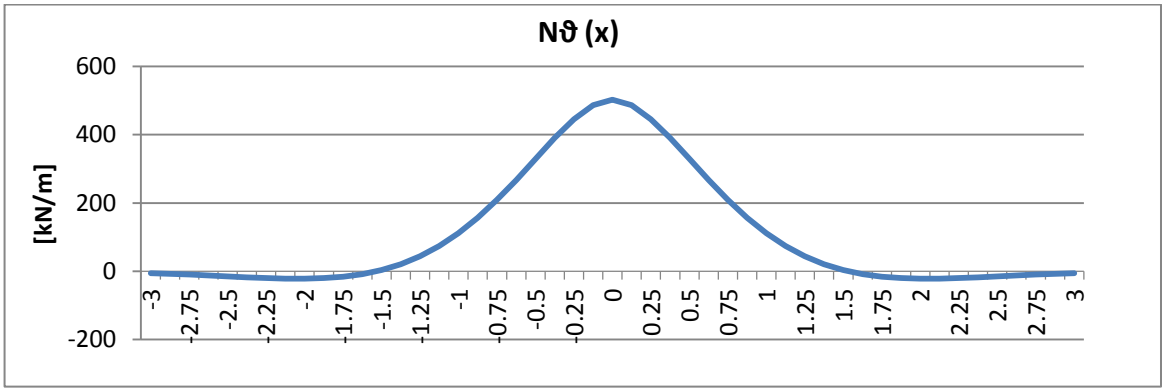

Figure 6.10 – Tangential force throughout the segment

The total amount of reinforcement necessary to provide can be determined from the stresses presented before. The horizontal reinforcement is given by:

$$A_{sw} = \frac{\frac{N_\vartheta}{f_{yd}} * \left(\frac{t}{2} - \left(c - \frac{\phi}{2}\right)\right) + \frac{M_\vartheta}{f_{yd}}}{t - 2 * \left(c + \frac{\phi}{2}\right)} \tag{48}$$

The vertical reinforcement is determined from the bending moment:

$$A_{sl} = \frac{\frac{M_\varphi}{f_{yd}}}{0.9 * \left(t - \left(c + \phi + \frac{\phi}{2}\right)\right)} \tag{49}$$

The calculations are shown in tables C.8, C.9 and C.10 in annex C. In table 6.4 the amounts of reinforcement due to the deviation force for both geometries are shown.

Table 6.4 – Reinforcement amounts for both segment geometries

	1st segment variation		2nd segment variation	
Segment No.	*Horizontal reinforcement* a_{sw}	*Longitudinal reinforcement* a_{sl}	*Horizontal reinforcement* a_{sw}	*Longitudinal reinforcement* a_{sl}
	[cm²/m]	[cm²/m]	[cm²/m]	[cm²/m]
5	6.88	4.02	6.47	3.78

7 STEEL FLANGE DESIGN

The flange geometry for both variations was defined based on geometrical and constructive limitations from the approvals being necessary to check the structural safety of the design. The flange is one of the most complex elements in the tower, representing the transition between concrete and steel as well as the anchorage of the tendons.

The flange design verification is done with the Petersen model. This model allows for the consideration of all elements involved in the connection, steel segment wall, concrete segments and prestress tendons. The model considers only the most stressed tendon, being necessary, in order to use this model, to have all the tendons equally spaced. The method reduces the analysis of the entire flange connection into a simple numerical model, considering only the tendon and section under the highest actions, only 1/28 of the area is considered. This simplification allows for small calculation efforts while still giving very accurate results.

The Petersen model can be described as beam model, allowing the determination of multiple springs that simulate the behavior of every element. These springs are determined from the geometry of the elements and the tensile stresses applied both at the steel section and the prestress tendons. The geometry of the flange and steel section is taken into account in the model shown in figure 7.1.

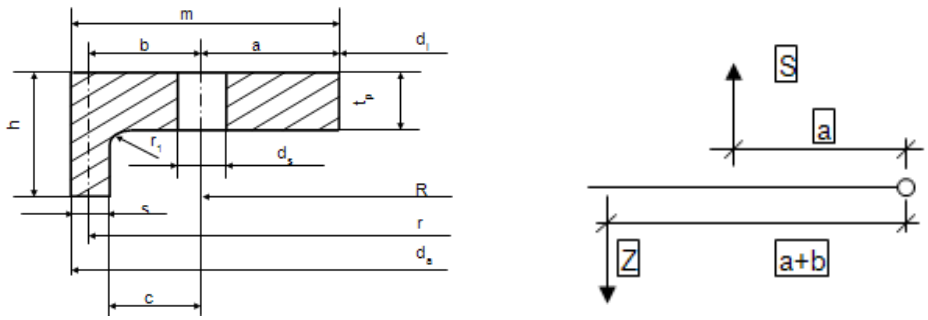

Figure 7.1- Flange geometry and working structure of the Petersen model

Due to the eccentricity between the tendons axis and the axis of the steel shell wall, the tendon force is significantly influenced by the opening of the ring flange gap under increasing loads, both for extreme and unfactored loads. The force Z represents the actions on the steel section, tensile stress determined from the loads. The prestress force is obtained from bending

moment equilibrium, as shown in the previous figure, for the inside point of the flange, $S = Z * (a + b)/a$, increasing linearly with the tensile force, range 1. As the tensile forces in the steel tower wall increase, a gap between the flange and the concrete segment starts to appear leading to a non-linear relation between the forces, range 2. As the force increases the gap grows with it, leading to an increase in the tendons force. In range 3, only the inner part of the flange and the tendons can carry the tensile loads. If the force increases and reaches the tensile strength of the connection, it plasticizes leading to failure, range 4. The range distribution can be seen in figure 7.2.

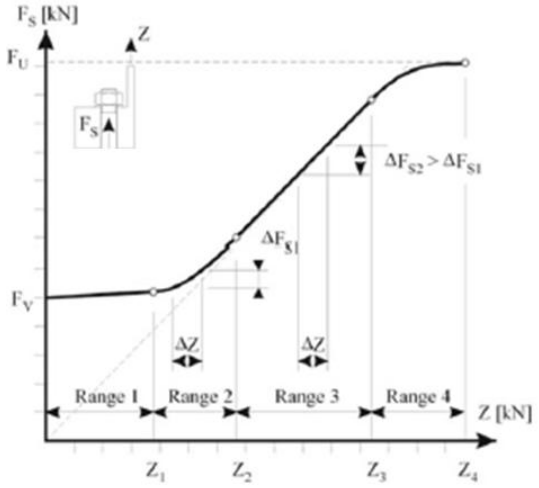

Figure 7.2 – Force variation in the flange connection (Banitopoulos, 2011)

The first step, in the Petersen model, consists of the determination of whether or not the flange is fully pressurized, and therefore, within the linear elastic region. If this situation is verified, the next steps reside in the verification that the stresses in the steel section wall, in the tendon and in the flange are smaller than the allowable resistant stresses, according to DIN EN 1993-1-1.

In the event that the flange is not fully pressurized, the connection behaves in the plasto-static region. It is necessary to check that failure does not occur from: failure of the tendon, plasticisation of a hinge in the flange neck or plasticisation of a hinge in the flange core. The outcome of the verification is shown in table 7.1.

Table 7.1 – Steel flange design verification

Plasto-Static Limiting Force:

	Extremlastfall with safety factor	frequent loads	DLC 1.0
1st segment variation	**0.83**	**0.40**	**0.18**
2nd segment variation	**0.82**	**0.41**	**0.18**

8 FATIGUE ANALYSIS

8.1 Concrete Fatigue analysis

Wind turbine towers experience throughout their lifetime changes in the applied loads, from changing wind profiles to the rotation of the blades. These never-ending changes lead to constant variations in the stress distribution of the tower. As a result of operational loading in a 20-year-design life period, a tower experiences approximately 5.29 x 10^8 fatigue load cycles (LaNier & Berger/ABAM, 2005). Accurate assessment of the fatigue loads and consequent damage is very important. Conservative assumptions lead to expensive designs when fatigue loading is often the governing loading action.

The fatigue safety verification is done according to both the DIBt guideline and the IEC specifications, aiming for a minimum 20-year life period, based on load collectives determined by ENERCONs load simulation department. Wind towers experience various load cycles with different amplitudes leading to changes in damage over time. The DIBt guideline refers to the Palmgren-Miner hypothesis in order to access the damage. It assumes that the fatigue damage from each load range is accumulative, and that the incremental fatigue damage equals the ratio of the number of cycles where the load range occurs to the total number of cycles allowed. The time-dependent losses as a result of creep, shrinkage and relaxation are to be considered according to section 3.1.4 from DIN EN 1992-1-1. The accumulative damage, D, can be determined from:

$$D = \sum_{i=1}^{j} \frac{n_{Si}}{N_{Ri}} \tag{50}$$

The first complete method for the verification of the concrete fatigue damage specified in the standard codes was in the Model Code 1990. The detailed calculation is applicable to more than 10^8 load cycles. Using this method the limit state is reached when the accumulated damage exceeds 1.0. The steps for the calculation are as follow:

$$log\, N_1 = \left(12 + 16 * S_{cd,min} + 8 * S_{cd,min}^2\right)\left(1 - S_{cd,max}\right) \tag{51}$$

$$log\, N_2 = 0.2 * LogN_1 * (logN_1 - 1) \tag{52}$$

$$log\, N_3 = LogN_2(0.3 - \frac{3}{8} s_{sd,min})/\Delta S_{cd} \tag{53}$$

$$If\ log\ N1\ \leq 6, then\ logN = logN_1 \quad (54)$$

$$If\ log\ N1 > 6\ and\ \Delta s_{cd} \geq \left(0.3 - \frac{3}{8}s_{cd,min}\right), then \log N = logN_2 \quad (55)$$

$$If\ log\ N1 > 6\ and\ \Delta s_{cd} < \left(0.3 - \frac{3}{8}s_{cd,min}\right), then \log N = logN_3 \quad (56)$$

$$S_{cd,max} = \gamma_{Sd}\sigma_{c,max}\eta_c/f_{cd,fat} \quad (57)$$

$$S_{cd,min} = \gamma_{Sd}\sigma_{c,min}\eta_c/f_{cd,fat} \quad (58)$$

$$\Delta S_{cd} = S_{cd,max} - S_{cd,min} \quad (59)$$

With:

$$\eta_c = \frac{1}{1.5 - 0.5(|\sigma_{c1}|/|\sigma_{c2}|)} \quad (60)$$

The partial safety factors shall be equal to 1.0 for all the design calculations. The fatigue reference compressive strength, taking into account the increasing fatigue sensitivity of the concrete with the increasing compressive strength, is given by:

$$f_{cd,fat} = \frac{0.85 * \beta_{cc(t)}}{\gamma_c} * \left[f_{ck}\left(1 - \frac{f_{ck}}{25 f_{ck0}}\right)\right] \quad (61)$$

This parameter is directly related to the age of the concrete at the time of the first loading. A value of 40 days was used, the sooner the concrete is loaded the lower this value is going to be. Taking into account that the sooner the concrete is loaded the lower its resistance will be.

8.1.1 Analysis at the top edge of the concrete transition segment

The influence of the fatigue damage in the concrete is critical to the design of the transition segments. At the top concrete segment, the sections close to the steel flange experience the most stress variations being necessary to make sure that the design takes into consideration the effects of the forces from the steel segment tower wall and the anchoring of the prestress tendons. In order to exactly know how the stresses from the fatigue loads are distributed along the concrete segment wall thickness, a beam model was built using STAAD.Pro. This model represents a generic cut of the cross section near the top of the concrete segment taking into account the pre-stress cable holes, in order to represent the correct load distribution throughout the thickness of the segment. Only one tendon is taken into consideration for the calculation. From the stresses distribution across the segment wall it is possible to determine the damage for both geometries. The results are shown in table 8.1. In annex E table E.1 the detailed calculation is shown.

Table 8.1 – Fatigue damage for the top edge of the concrete transition segments

	1st segment variation	2nd segment variation
Tendons fatigue damage	*4.75E-02*	*2.82E-02*

8.1.2 Analysis at the bottom edge of the concrete transition segment

The transition between the top two concrete segments is also a critical area of the design where fatigue loads have a large influence. In the case of the 1st geometry variation an abrupt change in thickness occurs. This change leads to a non-linear stress distribution in the transition zone. In order to exactly know how the load transfer occurs between the two segments a simple FE model was built has shown in figure 8.1.

Figure 8.1 – FE model for the top two concrete segments

The concrete segments were modeled using rectangular shell elements. The top concrete segment was built with 14 horizontal elements and in the vertical direction, the lower one with 8 horizontally and 65 vertically and an average thickness corresponding to the influence area of one tendon in the perimeter at discontinuity level. The loads considered in the model were applied as nodal loads, the effects of prestress, the load range from the fatigue variations and of the vertical forces from the upper part of the tower were all considered in the model.

A template was built allowing the use of the same model with different geometries. Allowing, for example, to easily calculate fatigue damage for different concrete wall thicknesses. The production of concrete segments always involves errors meaning that due to imperfections the contact area between two segments could be smaller than those used in the calculations. Keeping this in mind a 10 mm deviation between the two segments was also considered in the fatigue calculation. The initial wall thickness of the segment 5, 380 mm, had to be changed due to limitations from the definition of the flange geometry. These templates enabled the studying of the effects of different thicknesses on the fatigue damage.

The stresses obtained from the model are shown in figure 8.2. The fatigue calculations are done considering the element where the stress concentration occurs and another one 300 mm towards the outside.

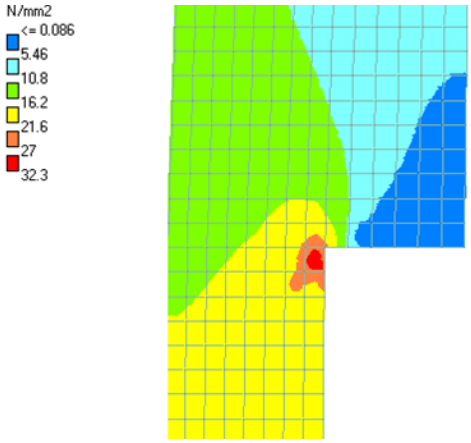

Figure 8.2 – Stress distribution across the discontinuity zone

For the second geometry the thickness variation is gradual and so no high stress concentration is expected to occur. The stress variation will change linearly with the area of the cross section. By using the following expression, it was possible to determine the stresses for both the inside point, and the 300 mm point to the outside:

$$\sigma = \frac{M}{I} * y + \frac{N}{A} \tag{62}$$

The same calculation was performed. In annex E table E.2 the detailed calculation is shown. The results for both solutions are shown in table 8.2.

Table 8.2 - Fatigue damage for the bottom edge of the concrete transition segments

	1st segment variation	2nd segment variation
Tendons fatigue damage	*6.98E-04*	*1.85E-03*

8.2 Tendons fatigue analysis

The fatigue damage in the prestress tendons is determined accordingly to Palmgren-Miner rule. In order to determine the forces in the tendons due the fatigue loads the Schmidt/Neuper method is used. This is similar to the Petersen method, taking into account the non-linear behavior of the flange connection. When a detailed calculation over time is not carried out, the fatigue verifications in prestressing steel structures are to be carried out both for the

prestressing force immediately after removal of the stressing jack, and for the prestressing force following creep, shrinkage and steel relaxation. Normally fatigue damage in the prestress tendons is not a critical design condition; nonetheless, it is necessary to guarantee the safety of the verification. The fatigue calculation follows the same procedure described in the Model Code 1990, which is similar to the one used for the concrete segments. Taking into account the fatigue loads already shown it is possible to determine the consequent tensile and compressive forces.

$$D = \sum_{i=1}^{j} \frac{n_i}{N_i} \leq 1.0 \tag{63}$$

The number of cycles causing failure at the same stress level and stress range is given by:

$$N_i = \left[\frac{\frac{\Delta\sigma_{R,sk}}{\gamma_M}}{\Delta\sigma_p'} \right]^{\max(k_1;k_2)} \tag{64}$$

From table 6.7.2 of the Model Code 1990 for prestress steel, it is possible to take the value of the slopes for an S-N curve. For post-tensioned systems with mechanical connectors the following slopes are assumed $k_1 = 3, k_2 = 5$ and with the characteristic fatigue strength as $\Delta\sigma_{R,sk} = 80\ Mpa$. S-N stress curve assume typically the configuration shown in figure 8.3.

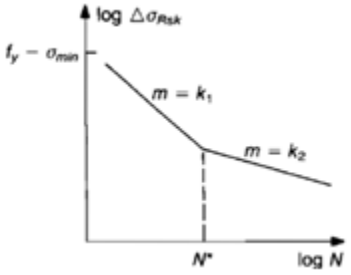

Figure 8.3 – S-N curve for fatigue loads

The fatigue damage in the tendons is very low, even when conservatively considering high safety factors. In annex E tables E.3 E.4 and E.5 the detailed calculation is shown.The results for both variations are shown in table 8.3.

Table 8.3 – Fatigue damage at the tendons

	1st segment variation	2nd segment variation
Tendons fatigue damage	*2.02E-08*	*2.71E-09*

9 COMPARATIVE ANALYSIS

One of the objectives of this project was to study and compare the advantages and disadvantages of two different concrete segment geometries. The first variation of the transition segment creates the necessity to build two new shutters because all the dimensions are completely new. On the other hand, the second variation has the same geometry as a previously existing segment, meaning that only a new inside shutter has to be built. The fabrication costs of each shutter are around 50 000 € euros. The building process of the second variation requires special attention due to the oval shape of the tendon holes in the segments meaning an addition to construction time.

Considering transportation and lifting processes weight of the elements and dimensions are a critical factor. As stated before one of the objectives with the study of both variations, was to try to keep the segments with least weight as possible. The first segment weighs 44.49 tons versus the second one with 55.02 tons. Both solutions meet ENERCON requirements, with lifts of around 50 tons being current. The segment dimensions were defined in accordance to transportation requirements in public roads. The shorter segment is clearly the easiest one to work with.

The flange connection is very similar in both variations. The first solution needs a larger angle at the top surface leading to a larger amount of wasted material and longer production times. The larger angle leads to a thinner element with a worse structural behavior. Both flange solutions, as shown is chapter 7, satisfy the design criteria, but it has proven the second variation to be better. Due to the angle of the flange different thicknesses for the top deviator would have to be used. Also has both solutions have different losses in prestress the amounts of reinforcement that are needed due to deviation forces are different. Smaller losses in prestress in the first variation mean higher reinforcement.

The reinforcement required by the segments has great a influence on the overall cost of the tower and results in many production hours and work force. The first variation, because of the thicker segment walls, requires a larger amount of reinforcement per meter. Thicker segments are most influenced by early-age thermal cracking, requiring greater amounts of reinforcement in order to avoid this.

The fatigue damage for the top part of first segment variation is larger mainly due to the smaller flange thickness. At the bottom of the segments, the second variation reveals higher

fatigue damage. Neither situation is critical to design, partially because of the high concrete grades used. If concrete grade C70/85 was used, fatigue damage would be much greater. This situation would lead to an accumulated damage larger than 1.0 in the second variation. Fatigue damage in the tendons is not an issue, as it is very low in both solutions. It is only slightly higher in the first variation mainly due to the smaller flange thickness.

In table 9.1 the results for the studied design aspects of both geometries is shown.

Table 9.1 – Comparative factors between segment variations

	1st segment variation	2nd segment variation
height of the segments	2.24 [m]	3.64 [m]
weight of the segments	41.22 [tons]	54.36 [tons]
thickness of top deviator	100 mm	90 mm
Flange angle	2.4°	1.7°
Building processes	new internal and external shutter approx. cost 50 000 €	new internal shutter approx. cost 25 000 €
Prestress losses	$\Delta P_{p,immediate}$ 23.97 [kN]	$\Delta P_{p,immediate}$ 26.24 [kN]
	$\Delta P_{p,c+s+r}$ 344.45 [kN]	$\Delta P_{p,c+s+r}$ 346.93 [kN]
Required reinforcement (transition segment)	a_{sw} 11.60 [cm2/m]	a_{sw} 9.74 [cm2/m]
	a_{sl} 10.41 [cm2/m]	a_{sl} 9.32 [cm2/m]
Required reinforcement due to deviation force	a_{sw} 6.88 [cm2/m]	a_{sw} 6.47 [cm2/m]
	a_{sl} 4.02 [cm2/m]	a_{sl} 3.78 [cm2/m]
Concrete fatigue damage	top edge 4.75E-02	top edge 2.82E-02
	bottom edge 6.98E-04	bottom edge 1.80E-03
Tendons fatigue damage	2.02E-08	2.71E-09

10 CONCLUSION

The main objective of this work was to compare two different concrete segments geometries. In order to achieve this objective a detailed design of the tower concrete segments was performed, were aspects like the reinforcement amounts and the prestress force determination have a great influence in the final solution outcome.

The tower is externally prestressed meaning that there are only a few contact points between the tendons and the tower. This leads to small immediate losses, representing less than 2%, in the prestress force. The prestress force applied to the structure is very high in order to guarantee that the joints between segments are always compressed. The verification allows the tower to resist the shear and torsion and to control the bending effects.

The reinforcement is one of the most expensive aspects in the tower construction processes, taking many hours of manual work. For the ultimate limit states shear and torsion are critical design situations. One objective was to reduce the amounts of reinforcement usually provided to the segments by taking into account the beneficial effects of the compression developed by the prestress force. This allowed reducing, to a certain amount, the reinforcement provided in the longitudinal direction.

Early-age thermal cracking has a great influence in the reinforcement outcome. An accurate assessment of the segment restraint conditions at early-age and knowledge of the concrete compressive strength at the time of the first loading have a large influence in crack width control. Early-age thermal cracking is the controlling design verification from segments 16 to 23. At the deviation points radial forces are developed leading to the need for providing local reinforcement to withstand them.

11 FURTHER WORK

In every project there is always room for improvements. The detailed study of certain aspects may allow for a reduction of construction times, material quantities or costs. Some aspects that were not extensively analyzed in this project but that are thought to be important to look at in the future are:

- For this project it would be interesting to compare the results presented with the ones from detailed FE models. As the construction of an accurate FE model is a time consuming task it is impossible to do it for every tower built. A comparison between results would allow detecting discrepancies in the presented calculations.
- Reduction of the prestress force applied to the structure by increasing the friction coefficient between the segments. This could be done, for example, with steel pins connecting both elements. With a reduction of the prestress force the consideration of a non-linear analysis would become more important. It would be interesting to study the behavior and determine the increase in the structure loading due to the consideration of second order effects.
- The evolution of the concrete compressive strength over time was only performed for a C55/65 concrete grade and a similar behavior was assumed for the other grades. It would be important to evaluate for every grade the strength development. The environmental conditions during the production of the concrete segments where not taken into account. They are different in every production facility and change throughout the year. A more rigorous quantification of these parameters could be made.
- Estimation of the degree of restraint, both internal and external, based on measurements of the segments in the production facilities. This could lead to changes in k_C and k parameters meanings changes in the required reinforcement amounts. For the top concrete segment a reduction of 0.1 in k_C would mean less 4 cm^2/m of reinforcement.

REFERENCES

American Wind Energy Association, T. (2011). “Recommended Practice for Compliance of Large Land-based wind Turbine Support Structures”. USA.

Associação Portuguesa de Energias Renováveis – APREN: www.apren.pt (accessed in March, 2013)

Banitopoulos, C., Borri, C., & Stathoupolos, T. (2011). “Environmental Wind Engineering and Design of Wind Energy Structures”. Springer Wein, New York.

BP: www.bp.com/statisticalreview (accessed in March, 2013).

Bramforth, P. B. (2007) “Early-age thermal crack control in concrete”. CIRIA Project Steering Group, London.

Bramforth, P. B. (1982) “Early-age thermal cracking in concrete”. Institute of concrete technology, Technical Note TN/2, Slough.

Burton, T., Sharpe, D., Jenkins, N., & Bossanyi, E. (2001). “Wind Energy Handbook”. Wiley, England.

CEB-FIP (1993) “MODEL CODE 1990”. Comité Euro-International du Béton (CEB) and Internation Federation for Prestressing (FIP) , Thomas Telford Services Ltd, Lausanne.

Collins, Michael P. & Mitchell, Dennis (1997) “Prestressed Concrete Structures”. Response Publications, Canada.

Daniels, L., Johnson, S., & Slaymaker, W. (2004). “Harvest the Wind: A Wind Energy Handbook for Illinois”. Illinois Institute for Rural affairs, USA.

DIBt (2005) "Richtlinie für Windenergieanlagen - Einwirkungen und Standsicherheitsnachweise für Turn und Gründung". Deutches Institut für Bautechnik.

DIN 1045-1, “Concrete, reinforced and prestressed concrete structures – Part 1: Design”, Deutsches Institut für Normung, July 2011.

DIN EN 1992-1-1:2004, “Eurocode 2 – Design of concrete structures - Part 1-1: General rules and rules for buildings”, European Committee for Standardization, 2010.

DIN EN 1992-2:1996, “Eurocode 2 – Design of concrete structures - Part 2: Concrete bridges - Design and detailing rules”, European Committee for Standardization, 2005.

DIN EN 1992-2/NA, German National Annex – National determined parameters - "Eurocode 2 – Design of concrete structures - Part 2: Concrete bridges – Design and detailing rules", European Committee for Standardization, April 2013.

DIN EN 1992-2:1998, "Eurocode 2 – Design of concrete structures - Part 3: Liquid Retaining and containment", European Committee for Standardization, 2006.

DIN EN 1993-1-1:2005, "Eurocode 3 – Design of steel structures - Part 1-1: General rules and rules for buildings", European Committee for Standardization, 2010.

DIN EN 1993-1-9:2005, "Eurocode 3 – Design of steel structures - Part 1-9: Fatigue", European Committee for Standardization, 2010.

Hau, E. (2006). "Wind Turbines - Fundamentals, Technologies, Applications, Economics. Krailling", Springer-Verlag, Germany.

IEC, (2005). IEC61400-1: "Wind Turbines - Part 1: Design Requirements" 3rd, International Electrothecnical Comission, Geneva,

LaNier, M. W., & Berger/ABAM, E. I. (2005). LWST Phase I Project Conceptual Design and Construction Approaches for Economical Hybrid Steel/Concrete Wind Turbine Towers. Colorado, USA: subcontractor report NREL/SR-500-36777.

Meskouris, K., Butenweg, C., Holler, S. (2012) "Baustatik in Beispielen". Springer-Verlag, Berlin.

Nilson, Arthur H. (1987) "Design of Prestressed Concrete". John Wileys & Sons, Inc., New York.

REN21. (2012). Renewables 2012 Global Status Report. REN21 Secretariat, Paris.

Rombach, G. (2005). "Spannbetonbau". Ernst & Sohn Verlag, Hamburg Germany.

Sétra (2012). "BBV Post-tensioning System type L 7 EW to L 15 EW", BBV Post-Tensioning System for 7 to 15 strands for external or internal unbounded prestressing, European Technical Approval ETA-12/0150, Germany.

Tong, W. (2010). "Wind Power Generation and Wind Turbine Design". WIT Press, Boston.

United Nations – UN: www.un.pt (accessed in March, 2013).

Veljkovic, M. [et al.], (2011) HISTWIN – High-Strength Steel Tower for Wind Turbine, Grant agreement n° RFSR-CT-2006-00031, RFCS Publications, European Commission, Brussels.

Ventsel, E., Krauthammer, T. (2001) "Thin Plates and Shells – Theory, Analysis and Applications". Marcel Dekker, Inc., New York.

APPENDIX

A. Tower Geometry

B. Prestress

C. Reinforcement

D. Steel Flange

E. Fatigue Analysis

A. TOWER GEOMETRY

Table A.1 – Tower geometry, 1st variation

Seg. Nr. [-]	Seg. h [mm]	Plate h [mm]	Fl. h [mm]	Kn. [-]	h [mm]	d_a [mm]	d_i [mm]	t [mm]	Mat. [-]	E [N/mm²]	s [mm/m]	Masses $m_{Tow.}$ [to]	Masses $m_{Fl.}$ [to]	Deviators Position Distance from the bottom [mm]	Deviator thickness [mm]
			211	1	122170	3218	3148	35					2.700		
				2	119295	3291	3221	35	S355	210000					
				3	119295	3291	3243	24							
				4	116535	3367	3319	24	S355	210000					
				5	116535	3367	3323	22							
				6	108735	3580	3536	22	S355	210000					
				7	108735	3580	3536	22							
1	20505	20154	140	8	101665	3770	3726	22	S355	210000	13.69	41.94	1.219		
			140	9	101665	3770	3726	22					1.219		
				10	98745	3845	3801	22	S355	210000					
				11	98745	3845	3797	24							
				12	91365	4043	3995	24	S355	210000					
				13	91365	4043	3991	26							
2	20005	19710	155	14	81660	4300	4248	26	S355	210000	13.44	49.15	1.710		
			155	15	81660	4300	4248	26					1.710		
				16	80660	4315	4263	26	S355	210000					
				17	80660	4315	4215	50							
3	3000	2645	200	18	78660	4346	4246	50	S355	210000	8.70	12.05	8.814		
				19	78660	4366	3106	630							
4	2240			20	76420	4518	3158	680	C80/95	42000	33.93	44.49			
				21	76420	4518	3798	360							
5	3640			22	72780	4630	3870	380	C80/95	42000	15.38	45.33		2540	100
				23	72780	4630	3870	380							
6	3640			24	69140	4748	4028	360	C70/85	41000	16.21	46.56			
				25	69140	4748	4028	360							
7	3640			26	65500	4874	4154	360	C70/85	41000	17.31	46.70			
				27	65500	4874	4154	360							
8	3640			28	61860	5007	4287	360	C70/85	41000	18.27	48.05			
				29	61860	5007	4287	360							
9	3640			30	58220	5150	4470	340	C70/85	41000	19.64	48.22			
				31	58220	5150	4470	340							
10	3640			32	54580	5304	4624	340	C70/85	41000	21.15	48.42		1820	95
				33	54580	5304	4624	340							
11	3640			34	50940	5472	4792	340	C55/67	38000	23.08	50.02			
				35	50940	5472	4792	340							
12	3640			36	47300	5654	4974	340	C55/67	38000	25.00	51.75			
				37	47300	5654	4974	340							
13	3640			38	43660	5851	5171	340	C55/67	38000	27.06	53.63			
				39	43660	5851	5171	340							
14	3640			40	40020	6064	5384	340	C55/67	38000	29.26	55.66		1820	105
				41	40020	6064	5384	340							
15	3640			42	36380	6293	5613	340	C55/67	38000	31.46	57.85			
				43	36380	6293	5613	340							
16	3640			44	32740	6539	5859	340	C55/67	38000	33.79	60.20			
				45	32740	6539	5859	340							
17	3640			46	29100	6802	6122	340	C55/67	38000	36.13	62.72			
				47	29100	6802	6122	340							
18	3640			48	25460	7084	6484	300	C55/67	38000	38.74	61.73			
				49	25460	7084	6484	300							
19	3640			50	21820	7386	6786	300	C55/67	38000	41.48	60.63			
				51	21820	7386	6786	300							
20	3640			52	18180	7711	7111	300	C55/67	38000	44.64	63.37		900	105
				53	18180	7711	7111	300							
21	3640			54	14540	8058	7458	300	C55/67	38000	47.66	66.31			
				55	14540	8058	7458	300							
22	3640			56	10900	8429	7829	300	C55/67	38000	50.96	69.45			
				57	10900	8429	7829	300							
23	3640			58	7260	8825	8225	300	C55/67	38000	54.40	72.80			
				59	7260	8825	8225	300							
24	3640			60	3620	9248	8648	300	C55/67	38000	58.10	76.38			
				61	3620	9248	8648	300							
25	3640			62	-20	9703	9103	300	C55/67	38000	62.50	80.22			

Table A.2 – Tower geometry, 2nd variation

Seg.		Plate	Fl.								s	Masses		Deviators Position	Deviator thickness
Nr.	h	h	h	Kn.	h	d_a	d_i	t	Mat.	E		$m_{Tow.}$	$m_{Fl.}$	Distance from the bottom [mm]	[mm]
[-]	[mm]	[mm]	[mm]	[-]	[mm]	[mm]	[mm]	[mm]	[-]	[N/mm²]	[mm/m]	[to]	[to]		
			155	15	83060	4300	4248	26					1.710		
				16	82060	4315	4263	26	S355	210000					
				17	82060	4315	4215	50							
3	3000	2645	200	18	80060	4390	4290	50	S355	210000	15.00	12.05	8.801		
				19	80060	4410	3150	630							
4	3640			20	76420	4518	3158	680	C80/95	42000	14.84	55.02			
				21	76420	4518	3798	360						2640	90
5	3640			22	72780	4630	3870	380	C80/95	42000	15.38	45.33			

Table A.3 – Tendons angles, both geometries

					1st segment variation				2nd segment variation			
Height	h	[m]	-0.020		75.320		78.660		75.420		80.060	
Radius of the Segment	R_a	[m]	4.427		1.810		1.901		1.814		1.913	
			relative angle	absolute angle	relative angle	absolute angle	relative angle	absolute angle	Winkel vor	Winkel absolut	Winkel vor	Winkel absolut
			0.00	0.00	0.00	0.00	0.00	0.00	0.00	0.00	0.00	0.00
Tendon Pos.	1	[°]	5.75	5.75	6.43	6.43	6.43	6.43	6.43	6.43	6.43	6.43
Tendon Pos.	2	[°]	12.00	17.75	12.86	19.29	12.86	19.29	12.86	19.29	12.86	19.29
Tendon Pos.	3	[°]	13.00	30.75	12.86	32.14	12.86	32.14	12.86	32.14	12.86	32.14
Tendon Pos.	4	[°]	12.00	42.75	12.86	45.00	12.86	45.00	12.86	45.00	12.86	45.00
Tendon Pos.	5	[°]	12.00	54.75	12.86	57.86	12.86	57.86	12.86	57.86	12.86	57.86
Tendon Pos.	6	[°]	12.00	66.75	12.86	70.71	12.86	70.71	12.86	70.71	12.86	70.71
Tendon Pos.	7	[°]	12.00	78.75	12.49	83.21	12.86	83.57	12.48	83.20	12.86	83.57
			11.25	90.00	6.79	90.00	6.43	90.00	6.80	90.00	6.43	90.00
Tendon Pos.	8	[°]	11.25	101.25	6.79	96.79	6.43	96.43	6.80	96.80	6.43	96.43
Tendon Pos.	9	[°]	12.00	113.25	12.49	109.29	12.86	109.29	12.48	109.29	12.86	109.29
Tendon Pos.	10	[°]	12.00	125.25	12.86	122.14	12.86	122.14	12.86	122.14	12.86	122.14
Tendon Pos.	11	[°]	12.00	137.25	12.86	135.00	12.86	135.00	12.86	135.00	12.86	135.00
Tendon Pos.	12	[°]	12.00	149.25	12.86	147.86	12.86	147.86	12.86	147.86	12.86	147.86
Tendon Pos.	13	[°]	13.00	162.25	12.86	160.71	12.86	160.71	12.86	160.71	12.86	160.71
Tendon Pos.	14	[°]	12.00	174.25	12.86	173.57	12.86	173.57	12.86	173.57	12.86	173.57
			5.75	180.00	6.43	180.00	6.43	180.00	6.43	180.00	6.43	180.00
Tendon Pos.	15	[°]	5.75	185.75	6.43	186.43	6.43	186.43	6.43	186.43	6.43	186.43
Tendon Pos.	16	[°]	12.00	197.75	12.86	199.29	12.86	199.29	12.86	199.29	12.86	199.29
Tendon Pos.	17	[°]	13.00	210.75	12.86	212.15	12.86	212.14	12.86	212.15	12.86	212.14
Tendon Pos.	18	[°]	12.00	222.75	12.86	225.00	12.86	225.00	12.86	225.00	12.86	225.00
Tendon Pos.	19	[°]	12.00	234.75	12.86	237.86	12.86	237.86	12.86	237.86	12.86	237.86
Tendon Pos.	20	[°]	12.00	246.75	12.86	250.72	12.86	250.71	12.86	250.72	12.86	250.71
Tendon Pos.	21	[°]	12.00	258.75	12.49	263.21	12.86	263.57	12.48	263.20	12.86	263.57
			11.25	270.00	6.79	270.00	6.43	270.00	6.80	270.00	6.43	270.00
Tendon Pos.	22	[°]	11.25	281.25	6.79	276.79	6.43	276.43	6.80	276.80	6.43	276.43
Tendon Pos.	23	[°]	12.00	293.25	12.49	289.29	12.86	289.29	12.48	289.29	12.86	289.29
Tendon Pos.	24	[°]	12.00	305.25	12.86	302.15	12.86	302.14	12.86	302.15	12.86	302.14
Tendon Pos.	25	[°]	12.00	317.25	12.86	315.00	12.86	315.00	12.86	315.00	12.86	315.00
Tendon Pos.	26	[°]	12.00	329.25	12.86	327.86	12.86	327.86	12.86	327.86	12.86	327.86
Tendon Pos.	27	[°]	13.00	342.25	12.86	340.72	12.86	340.71	12.86	340.72	12.86	340.71
Tendon Pos.	28	[°]	12.00	354.25	12.86	353.57	12.86	353.57	12.86	353.57	12.86	353.57
			5.75	360.00	6.43	360.00	6.43	360.00	6.43	360.00	6.43	360.00

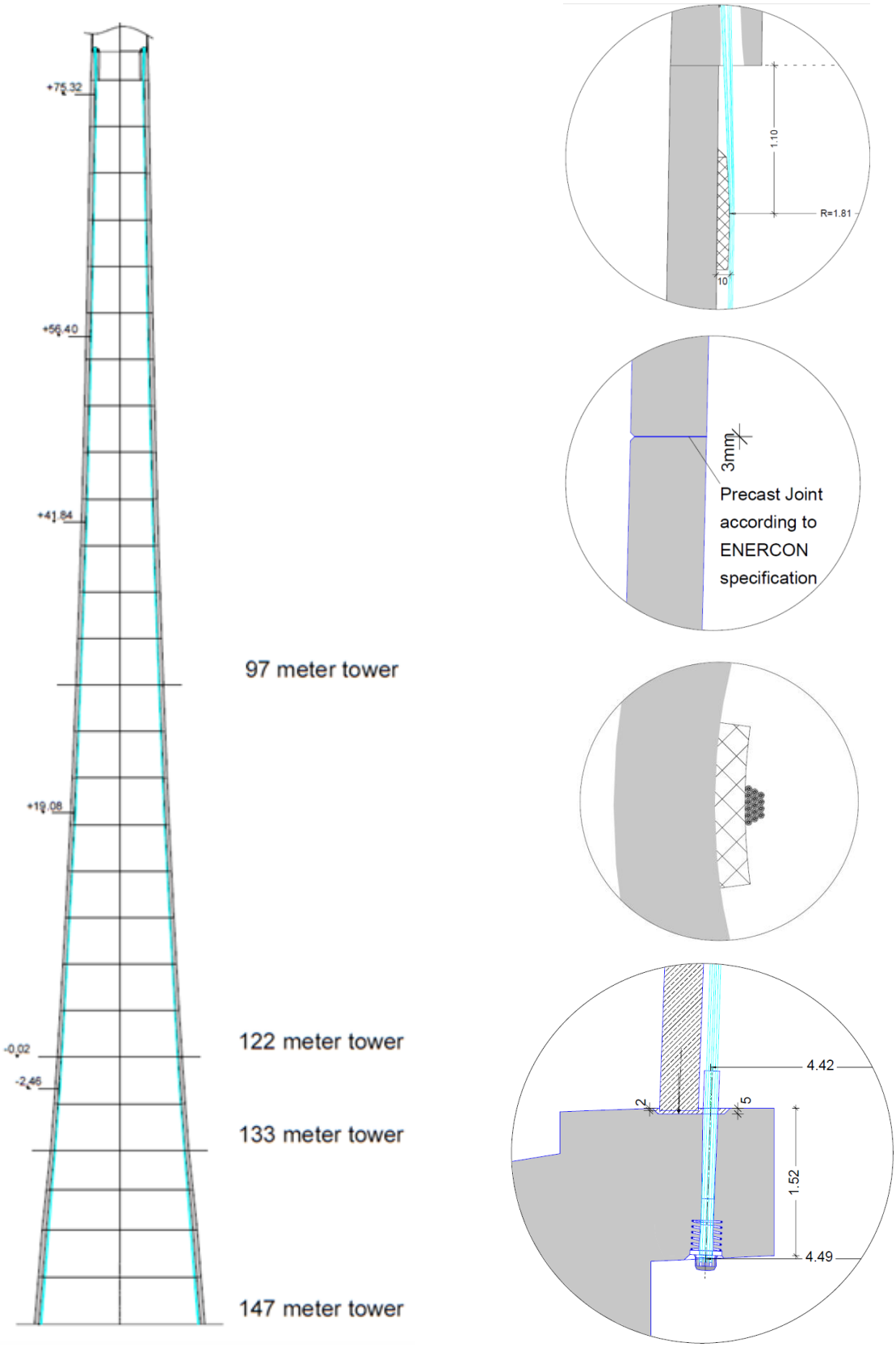

Figure A.1 – Externally prestressed towers and constructive details

B. PRESTRESS

Table B.1 – Verification of the minimum compressed thickness from the prestress force

$0.8 * M_{xy,max} + 1.0 * M_{z,max}$

Verification Concept 1: Pressurised Joint

No.	h	Tension stresses sc,max	Compressive stresses sc,min	If < 0 - Tension in the segment X - Da	Compressed length X	Compressed thickness res t		Minimum thickness under compression 1/3 × t	Shear Force F_{XY}	Torsion M_Z	Shear flow v_{Ed}	torsion flow t_{Ed}	shear + torsion $v_{Ed} + t_{Ed}$	Compressive stresses σ_{Nd}	Tangential resistant stress $\tau_{Rdj} \leq 0.1 \times f_{cd}$	Shear Resistance v_{Rdi}	$\frac{v_{Ed} + t_{Ed}}{v_{Rdi}}$
	[m]	[N/mm²]	[N/mm²]	[m]	[m]	[m]		[m]	[kN]	[kNm]	[kN/m]	[kN/m]	[kN/m]	[N/mm²]	[N/mm²]	[kN/m]	[-]
-1																	
1	-0.02	-2.987	-17.898	1.938	11.611	0.280	>	0.093	1994	-10192	135	74	209	-10.44	3.46	970	**0.22**
2	3.62	-2.936	-18.811	1.705	10.923	0.280	>	0.093	1959	-10192	140	81	221	-10.87	3.46	970	**0.23**
3	7.26	-2.892	-19.734	1.510	10.305	0.280	>	0.093	1924	-10192	144	89	233	-11.31	3.46	970	**0.24**
4	10.90	-2.856	-20.673	1.346	9.745	0.280	>	0.093	1889	-10192	148	98	247	-11.76	3.46	970	**0.25**
5	14.54	-2.832	-21.622	1.210	9.238	0.280	>	0.093	1854	-10192	152	108	260	-12.23	3.46	970	**0.27**
6	18.18	-2.822	-22.578	1.097	8.778	0.280	>	0.093	1815	-10192	156	118	275	-12.70	3.46	970	**0.28**
7	21.82	-2.832	-23.534	1.006	8.362	0.280	>	0.093	1777	-10192	160	130	289	-13.18	3.46	970	**0.30**
8	25.46	-2.870	-24.470	0.937	7.991	0.280	>	0.093	1738	-10192	163	141	305	-13.67	3.46	970	**0.31**
9	29.10	-2.467	-22.462	0.836	7.608	0.320	>	0.107	1699	-10192	168	156	324	-12.46	3.46	1108	**0.29**
10	32.74	-2.536	-23.253	0.797	7.306	0.320	>	0.107	1646	-10192	169	169	339	-12.89	3.46	1108	**0.31**
11	36.38	-2.642	-24.016	0.774	7.037	0.320	>	0.107	1593	-10192	171	184	354	-13.33	3.46	1108	**0.32**
12	40.02	-2.793	-24.735	0.768	6.802	0.320	>	0.107	1541	-10192	172	199	370	-13.76	3.46	1108	**0.33**
13	40.02	-2.793	-24.735	0.768	6.802	0.320	>	0.107	1541	-10192	172	199	370	-13.76	4.41	1410	**0.26**
14	43.66	-2.994	-25.400	0.778	6.599	0.320	>	0.107	1488	-10192	172	214	387	-14.20	4.41	1410	**0.27**
15	47.30	-3.255	-25.996	0.805	6.429	0.320	>	0.107	1435	-10192	172	231	403	-14.63	4.41	1410	**0.29**
16	50.94	-3.473	-26.619	0.817	6.259	0.320	>	0.107	1418	-10192	176	247	424	-15.05	4.41	1410	**0.30**
17	54.58	-3.747	-27.167	0.844	6.118	0.320	>	0.107	1400	-10192	180	264	444	-15.46	4.41	1410	**0.32**
18	54.58	-3.747	-27.167	0.844	6.118	0.320	>	0.107	1400	-10192	180	264	444	-15.46	4.41	1410	**0.32**
19	58.22	-4.082	-27.625	0.888	6.008	0.320	>	0.107	1383	-10193	183	282	465	-15.85	4.41	1410	**0.33**
20	61.86	-4.142	-26.556	0.920	5.897	0.340	>	0.113	1365	-10193	187	302	489	-15.35	4.41	1499	**0.33**
21	65.50	-4.572	-26.836	0.995	5.839	0.340	>	0.113	1348	-10193	191	320	510	-15.70	4.41	1499	**0.34**
22	69.14	-4.928	-27.186	1.045	5.763	0.340	>	0.113	1334	-10193	194	339	533	-16.06	4.41	1499	**0.36**
23	72.78	-4.970	-26.155	1.079	5.679	0.360	>	0.120	1320	-10193	198	361	559	-15.56	4.41	1587	**0.35**
24	72.78	-4.970	-26.155	1.079	5.679	0.360	>	0.120	1320	-10193	198	361	559	-15.56	5.04	1813	**0.31**
25	76.42	-5.934	-26.668	1.316	5.916	0.340	>	0.113	1307	-10193	195	358	553	-16.30	5.04	1713	**0.32**
26	76.42	-2.471	-15.687	0.860	5.460	0.660	>	0.220	1307	-10193	211	418	629	-9.08	3.63	2397	**0.26**
27	78.66	-2.993	-19.919	0.767	5.103	0.610	>	0.203	1298	-10193	222	467	689	-11.46	4.58	2795	**0.25**

$1.0 * M_{xy,max} + 0.4 * M_{z,max}$

Verification Concept 1: Pressurised Joint

No.	h	Tension stresses sc,max	Compressive stresses sc,min	If < 0 - Tension in the segment X - Da	Compressed length X	Compressed thickness res t		Minimum thickness under compression 1/3 × t	Shear Force F_{XY}	Torsion M_Z	Shear flow v_{Ed}	torsion flow t_{Ed}	shear + torsion $v_{Ed} + t_{Ed}$	Compressive stresses σ_{Nd}	Tangential resistant stress $\tau_{Rdj} \leq 0.1 \times f_{cd}$	Shear Resistance v_{Rdi}	$\frac{v_{Ed} + t_{Ed}}{v_{Rdi}}$
	[m]	[N/mm²]	[N/mm²]	[m]	[m]	[m]		[m]	[kN]	[kNm]	[kN/m]	[kN/m]	[kN/m]	[N/mm²]	[N/mm²]	[kN/m]	[-]
-1																	
1	-0.02	-1.123	-19.762	0.583	10.256	0.280	>	0.093	1994	-4077	135	29	165	-10.44	3.46	970	**0.17**
2	3.62	-0.952	-20.795	0.442	9.660	0.280	>	0.093	1959	-4077	140	32	172	-10.87	3.46	970	**0.18**
3	7.26	-0.787	-21.839	0.329	9.124	0.280	>	0.093	1924	-4077	144	36	180	-11.31	3.46	970	**0.19**
4	10.90	-0.629	-22.900	0.237	8.636	0.280	>	0.093	1889	-4077	148	39	187	-11.76	3.46	970	**0.19**
5	14.54	-0.483	-23.971	0.165	8.193	0.280	>	0.093	1854	-4077	152	43	196	-12.23	3.46	970	**0.20**
6	18.18	-0.352	-25.048	0.110	7.791	0.280	>	0.093	1815	-4077	156	47	204	-12.70	3.46	970	**0.21**
7	21.82	-0.244	-26.122	0.069	7.425	0.280	>	0.093	1777	-4077	160	52	212	-13.18	3.46	970	**0.22**
8	25.46	-0.170	-27.170	0.044	7.098	0.280	>	0.093	1738	-4077	163	57	220	-13.67	3.46	970	**0.23**
9	**29.10**	**0.032**	**-24.961**	**-0.009**	**6.763**	**0.311**	**>**	**0.107**	1699	-4077	168	63	230	-12.46	3.46	1078	0.21
10	**32.74**	**0.053**	**-25.843**	**-0.013**	**6.496**	**0.307**	**>**	**0.107**	1646	-4077	170	68	238	-12.89	3.46	1062	0.22
11	**36.38**	**0.029**	**-26.688**	**-0.007**	**6.256**	**0.313**	**>**	**0.107**	1593	-4077	171	74	245	-13.33	3.46	1084	0.23
12	40.02	-0.050	-27.478	0.011	6.045	0.320	>	0.107	1541	-4077	172	79	251	-13.76	3.46	1108	**0.23**
13	40.02	-0.050	-27.478	0.011	6.045	0.320	>	0.107	1541	-4077	172	79	251	-13.76	4.41	1410	**0.18**
14	43.66	-0.194	-28.201	0.040	5.861	0.320	>	0.107	1488	-4077	172	86	258	-14.20	4.41	1410	**0.18**
15	47.30	-0.412	-28.839	0.082	5.706	0.320	>	0.107	1435	-4077	172	92	264	-14.63	4.41	1410	**0.19**
16	50.94	-0.580	-29.512	0.109	5.551	0.320	>	0.107	1418	-4077	176	99	275	-15.05	4.41	1410	**0.20**
17	54.58	-0.819	-30.094	0.148	5.422	0.320	>	0.107	1400	-4077	180	106	286	-15.46	4.41	1410	**0.20**
18	54.58	-0.819	-30.094	0.148	5.422	0.320	>	0.107	1400	-4077	180	106	286	-15.46	4.41	1410	**0.20**
19	58.22	-1.139	-30.568	0.198	5.318	0.320	>	0.107	1383	-4077	183	113	296	-15.85	4.41	1410	**0.21**
20	61.86	-1.340	-29.358	0.238	5.215	0.340	>	0.113	1365	-4077	187	121	308	-15.35	4.41	1499	**0.21**
21	65.50	-1.789	-29.619	0.311	5.155	0.340	>	0.113	1348	-4077	191	128	318	-15.70	4.41	1499	**0.21**
22	69.14	-2.146	-29.968	0.364	5.082	0.340	>	0.113	1334	-4077	194	135	329	-16.06	4.41	1499	**0.22**
23	72.78	-2.322	-28.803	0.403	5.003	0.360	>	0.120	1320	-4077	198	144	343	-15.56	4.41	1587	**0.22**
24	72.78	-2.322	-28.803	0.403	5.003	0.360	>	0.120	1320	-4077	198	144	343	-15.56	5.04	1813	**0.19**
25	76.42	-3.342	-29.259	0.593	5.193	0.340	>	0.113	1307	-4077	195	143	338	-16.30	5.04	1713	**0.20**
26	76.42	-0.819	-17.339	0.228	4.828	0.660	>	0.220	1307	-4077	211	167	378	-9.08	3.63	2397	**0.16**
27	78.66	-0.878	-22.034	0.180	4.516	0.610	>	0.203	1298	-4077	222	187	409	-11.46	4.58	2795	**0.15**

Table B.2 – Concrete compressive strain, elastic shortening of the concrete segments

No.	Height	Average Concrete Stress imm. after	E-Modulus Concrete Secant Modulus	Concrete Compressive Strain per Segment	Concrete Elongation per Segment	Sum of Concrete Elongation per Segment	Sum of Concrete Elongation per Prestressing Tendon
	h	σ_{cpm0}	E_{cm}	$\varepsilon_{c,i}$	$\Delta l_{c,np,i}$	$\Delta l_{c,np}$	Δl_c
	[m]	[N/mm²]	[N/mm²]	[-]	[mm]	[mm]	[mm]
-1							
1	-0.020	-8.980	38000.000				
2	3.620	-9.437	38000.000	-2.42E-04	-0.882	-0.882	-0.032
3	7.260	-9.905	38000.000	-2.54E-04	-0.926	-1.808	-0.065
4	10.900	-10.387	38000.000	-2.67E-04	-0.972	-2.780	-0.099
5	14.540	-10.884	38000.000	-2.80E-04	-1.019	-3.799	-0.136
6	18.180	-11.394	38000.000	-2.93E-04	-1.067	-4.866	-0.174
7	21.820	-11.916	38000.000	-3.07E-04	-1.116	-5.982	-0.214
8	25.460	-12.447	38000.000	-3.21E-04	-1.167	-7.149	-0.255
9	29.100	-11.530	38000.000	-3.15E-04	-1.148	-8.298	-0.296
10	32.740	-12.019	38000.000	-3.10E-04	-1.128	-9.425	-0.337
11	36.380	-12.515	38000.000	-3.23E-04	-1.175	-10.601	-0.379
12	40.020	-13.016	38000.000	-3.36E-04	-1.223	-11.823	-0.422
13	40.020	-13.016	41000.000	0.00E+00	0.000	-11.823	-0.422
14	43.660	-13.519	41000.000	-3.24E-04	-1.178	-13.001	-0.464
15	47.300	-14.020	41000.000	-3.36E-04	-1.222	-14.224	-0.508
16	50.940	-14.517	41000.000	-3.48E-04	-1.267	-15.491	-0.553
17	54.580	-15.009	41000.000	-3.60E-04	-1.311	-16.801	-0.600
18	54.580	-15.009	41000.000	0.00E+00	0.000	-16.801	-0.600
19	58.220	-15.489	41000.000	-3.72E-04	-1.354	-18.155	-0.648
20	61.860	-15.142	41000.000	-3.74E-04	-1.360	-19.515	-0.697
21	65.500	-15.588	41000.000	-3.75E-04	-1.364	-20.879	-0.746
22	69.140	-16.035	41000.000	-3.86E-04	-1.404	-22.283	-0.796
23	72.780	-15.684	41000.000	-3.87E-04	-1.408	-23.691	-0.846
24	72.780	-15.684	42000.000	0.00E+00	0.000	-23.691	-0.846
25	76.420	-16.478	42000.000	-3.83E-04	-1.394	-25.084	-0.896
26	76.420	-9.430	42000.000	0.00E+00	0.000	-25.084	-0.896
27	78.660	-11.896	42000.000	-2.54E-04	-0.569	-25.653	-0.916

Table B.3 – Prestress tendon strain, losses due to tendon elongation

Height	Prestressing Tendon Stress after removing Jack	Partial Length of Prestressing Tendon	Prestressing Tendon Length	Prestressing Tendon Strain per Segment	Prestressing Tendon Elongation per Segment	Sum of Prestressing Tendon Elongation per Prestressing Tendon
h	σ_{p0}	lp,i	λ_p	$\varepsilon_{p,i}$	$\Delta\lambda_{p,i}$	$\Delta\lambda_p$
[m]	[N/mm²]	[m]	[m]	[-]	[mm]	[mm]
-0.020	1288.889	0.000	0.000		0.000	0.000
19.080	1288.574	20.605	20.605	6.61E-03	136.193	136.193
41.840	1287.856	22.760	43.365	6.61E-03	150.400	286.592
56.400	1284.854	14.560	57.925	6.60E-03	96.160	382.752
75.320	1284.225	18.920	76.845	6.59E-03	124.664	507.416
78.660	1278.235	3.340	80.185	6.59E-03	21.996	529.412

Table B.4 – Prestress force applied to each tendon

Prestressing Sequence	*Prestressing Tendon*	*Prestressing Tendon Length*	*Prestressing Tendon Elongation*	*Calculated Prestressing Tendon Elongation incl. Wedge Slip*	*Concrete Compression Proportion per Prestressing Tendon*	*Concrete Compression before Prestressing*	***Necessary Elongation Length***	*Calculated Prestressing Force*	***Prestressing Force per Tendon***	***Prestressing Force per Tendon - 2nd Variation***
	Nr.	l_p	Δl_p	$\Delta l_{p,cal}$	Δl_c	$\Delta l_{c,ges}$	**Δl_{erf}**	P_0	**$P_{0,erf}$**	**$P_{0,erf}$**
[-]	[-]	[m]	[mm]	[mm]	[mm]	[mm]	**[mm]**	[kN]	**[kN]**	**[kN]**
1	1	80.373	530.64	523.64	-0.92	**-25.65**	**549.3**	2900	**3042**	**3043**
2	15	80.373	530.64	523.64	-0.92	-24.74	**548.4**	2900	**3037**	**3038**
3	2	80.373	530.64	523.64	-0.92	-23.82	**547.5**	2900	**3032**	**3033**
4	16	80.373	530.64	523.64	-0.92	-22.90	**546.5**	2900	**3027**	**3028**
5	3	80.373	530.64	523.64	-0.92	-21.99	**545.6**	2900	**3022**	**3023**
6	17	80.373	530.64	523.64	-0.92	-21.07	**544.7**	2900	**3017**	**3018**
7	4	80.373	530.64	523.64	-0.92	-20.16	**543.8**	2900	**3012**	**3013**
8	18	80.373	530.64	523.64	-0.92	-19.24	**542.9**	2900	**3007**	**3007**
9	5	80.373	530.64	523.64	-0.92	-18.32	**542.0**	2900	**3001**	**3002**
10	19	80.373	530.64	523.64	-0.92	-17.41	**541.1**	2900	**2996**	**2997**
11	6	80.373	530.64	523.64	-0.92	-16.49	**540.1**	2900	**2991**	**2992**
12	20	80.373	530.64	523.64	-0.92	-15.58	**539.2**	2900	**2986**	**2987**
13	7	80.373	530.64	523.64	-0.92	-14.66	**538.3**	2900	**2981**	**2982**
14	21	80.373	530.64	523.64	-0.92	-13.74	**537.4**	2900	**2976**	**2977**
15	8	80.373	530.64	523.64	-0.92	-12.83	**536.5**	2900	**2971**	**2972**
16	22	80.373	530.64	523.64	-0.92	-11.91	**535.6**	2900	**2966**	**2966**
17	9	80.373	530.64	523.64	-0.92	-10.99	**534.6**	2900	**2961**	**2961**
18	23	80.373	530.64	523.64	-0.92	-10.08	**533.7**	2900	**2956**	**2956**
19	10	80.373	530.64	523.64	-0.92	-9.16	**532.8**	2900	**2951**	**2951**
20	24	80.373	530.64	523.64	-0.92	-8.25	**531.9**	2900	**2946**	**2946**
21	11	80.373	530.64	523.64	-0.92	-7.33	**531.0**	2900	**2941**	**2941**
22	25	80.373	530.64	523.64	-0.92	-6.41	**530.1**	2900	**2936**	**2936**
23	12	80.373	530.64	523.64	-0.92	-5.50	**529.1**	2900	**2930**	**2931**
24	26	80.373	530.64	523.64	-0.92	-4.58	**528.2**	2900	**2925**	**2926**
25	13	80.373	530.64	523.64	-0.92	-3.66	**527.3**	2900	**2920**	**2920**
26	27	80.373	530.64	523.64	-0.92	-2.75	**526.4**	2900	**2915**	**2915**
27	14	80.373	530.64	523.64	-0.92	-1.83	**525.5**	2900	**2910**	**2910**
28	28	80.373	530.64	523.64	-0.92	-0.92	**524.6**	2900	**2905**	**2905**

Table B.5 – Prestress time-dependent losses

No.	*Height*	*Creep Coefficient*	*Average Shrinkage Strain*	*Losses due to Creep Shrinkage and relaxation*	*Losses due to Creep Shrinkage and relaxation per tendon*	*Losses due to Creep Shrinkage and relaxation per tendon - 2nd variation*
	h	$\varphi(t, t_0)$	$\varepsilon_{cs}(t)$	$\Delta P_{p,c+s+r}$	$\Delta P_{p,c+s+r}$	$\Delta P_{p,c+s+r}$
	[m]	[-]	[-]	[kN]	[kN]	[kN]
-1						
1	-0.020	1.068	2.068E+00	9644.7	344.5	346.9
2	3.620	1.068	3.068E+00	9644.7	344.5	346.9
3	7.260	1.068	4.068E+00	9644.7	344.5	346.9
4	10.900	1.068	5.068E+00	9644.7	344.5	346.9
5	14.540	1.068	6.068E+00	9644.7	344.5	346.9
6	18.180	1.068	7.068E+00	9644.7	344.5	346.9
7	21.820	1.068	8.068E+00	9644.7	344.5	346.9
8	25.460	1.068	9.068E+00	9644.7	344.5	346.9
9	29.100	1.060	1.006E+01	9644.7	344.5	346.9
10	32.740	1.060	1.106E+01	9644.7	344.5	346.9
11	36.380	1.060	1.206E+01	9644.7	344.5	346.9
12	40.020	1.060	1.306E+01	9644.7	344.5	346.9
13	40.020	0.897	1.390E+01	9644.7	344.5	346.9
14	43.660	0.897	1.490E+01	9644.7	344.5	346.9
15	47.300	0.897	1.590E+01	9644.7	344.5	346.9
16	50.940	0.897	1.690E+01	9644.7	344.5	346.9
17	54.580	0.898	1.790E+01	9644.7	344.5	346.9
18	54.580	0.898	1.890E+01	9644.7	344.5	346.9
19	58.220	0.898	1.990E+01	9644.7	344.5	346.9
20	61.860	0.895	2.090E+01	9644.7	344.5	346.9
21	65.500	0.895	2.190E+01	9644.7	344.5	346.9
22	69.140	0.895	2.290E+01	9644.7	344.5	346.9
23	72.780	0.894	2.389E+01	9644.7	344.5	346.9
24	72.780	0.814	2.481E+01	9644.7	344.5	346.9
25	76.420	0.816	2.582E+01	9644.7	344.5	346.9
26	76.420	0.798	2.680E+01	9644.7	344.5	346.9
27	78.660	0.803	2.780E+01	9644.7	344.5	346.9

C. REINFORCEMENT

Table C.1 – Reinforcement due to shear and torsion, 1st segment variation

No.	Height h	Shear flow vEd	Torsion flow tEd	Angle of compressive strut - horizontal direction cot θ	Angle of compressive strut - Longitudinal direction cot θ	Horizontal reinforcement a_{sw}	Longitudinal reinforcement a_{sl}	Shear and torsion Resistance vRd,max = tRd,max	(tEd+vEd)/vRd,max,t+v
	[m]	[kN/m]	[kN/m]	[-]	[-]	[cm²/m]	[cm²/m]	[kN/m]	[-]
-1									
1	-0.020	135.0	73.4	1.00	1.00	2.40	0.84	3895.83	0.05
2	3.620	139.4	81.0	1.00	1.00	2.53	0.93	3895.83	0.06
3	7.260	143.7	89.3	1.00	1.00	2.68	1.03	3895.83	0.06
4	10.900	147.9	98.2	1.00	1.00	2.83	1.13	3895.83	0.06
5	14.540	152.1	107.8	1.00	1.00	2.99	1.24	3895.83	0.07
6	18.180	155.9	118.1	1.00	1.00	3.15	1.36	3895.83	0.07
7	21.820	159.6	129.2	1.00	1.00	3.32	1.49	3895.83	0.07
8	25.460	163.1	141.0	1.00	1.00	3.50	1.62	3895.83	0.08
9	29.100	167.4	155.4	1.00	1.00	3.71	1.79	4415.28	0.07
10	32.740	169.1	168.8	1.00	1.00	3.89	1.94	4415.28	0.08
11	36.380	170.4	183.1	1.00	1.00	4.07	2.11	4415.28	0.08
12	40.020	171.3	198.0	1.00	1.00	4.25	2.28	4415.28	0.08
13	40.020	171.3	198.0	1.00	1.00	4.25	2.28	5619.44	0.07
14	43.660	171.9	213.6	1.00	1.00	4.43	2.46	5619.44	0.07
15	47.300	171.9	229.8	1.00	1.00	4.62	2.64	5619.44	0.07
16	50.940	175.9	246.4	1.00	1.00	4.86	2.83	5619.44	0.08
17	54.580	179.6	263.3	1.00	1.00	5.09	3.03	5619.44	0.08
18	54.580	179.6	263.3	1.00	1.00	5.09	3.03	5619.44	0.08
19	58.220	183.0	280.5	1.00	1.00	5.33	3.23	5619.44	0.08
20	61.860	187.1	300.5	1.00	1.00	5.61	3.46	5950.00	0.08
21	65.500	190.1	318.5	1.00	1.00	5.85	3.66	5950.00	0.09
22	69.140	193.6	337.0	1.00	1.00	6.10	3.88	5950.00	0.09
23	72.780	197.8	359.3	1.00	1.00	6.41	4.13	6280.56	0.09
24	72.780	197.8	359.3	1.00	1.00	6.41	4.13	7177.78	0.08
25	76.420	194.8	355.9	1.00	1.00	6.33	4.09	6800.00	0.08
26	76.420	210.6	415.9	1.00	1.00	7.20	4.78	12844.44	0.05
27	78.660	221.2	464.9	1.00	1.00	7.89	5.35	11900.00	0.06

Table C.2 – Reinforcement due to shear and torsion, 2nd segment variation

No.	Height h	Shear flow vEd	Torsion flow tEd	Horizontal reinforcement a_{sw}	Longitudinal reinforcement a_{sl}
	[m]	[kN/m]	[kN/m]	[cm²/m]	[cm²/m]
26	76.420	210.6	415.9	6.33	4.09
27	80.060	221.2	464.9	7.89	5.35

Table C.3 – Reinforcement due to temperature in both directions

ø 14 mm — 2nd variation

Temperature Effects							B500		B500
Kn.	*Height* h	Differential Temperature ΔT	effective section depth d	Moment along the section M_{Ed}	μ_{Eds}	ω	reinforcement amount per face $a_{s,temp,erf}$	*Height* h	reinforcement amount per face $a_{s,temp,erf}$
	[m]	[K]	[mm]	[kNm/m]	[-]	[m]	[cm²/m]	[m]	[cm²/m]
-1									
1	-0.020	20	241	46.17	0.0230	0.0233	4.48		
2	3.620	20	241	46.17	0.0230	0.0233	4.48		
3	7.260	15	241	34.63	0.0172	0.0175	3.35		
4	10.900	15	241	34.63	0.0172	0.0175	3.35		
5	14.540	15	241	34.63	0.0172	0.0175	3.35		
6	18.180	15	241	34.63	0.0172	0.0175	3.35		
7	21.820	15	241	34.63	0.0172	0.0175	3.35		
8	25.460	15	241	34.63	0.0172	0.0175	3.35		
9	29.100	15	281	44.48	0.0163	0.0165	3.69		
10	32.740	15	281	44.48	0.0163	0.0165	3.69		
11	36.380	15	281	44.48	0.0163	0.0165	3.69		
12	40.020	15	281	44.48	0.0163	0.0165	3.69		
13	40.020	15	281	47.99	0.0138	0.0140	3.98		
14	43.660	15	281	47.99	0.0138	0.0140	3.98		
15	47.300	15	281	47.99	0.0138	0.0140	3.98		
16	50.940	15	281	47.99	0.0138	0.0140	3.98		
17	54.580	15	281	47.99	0.0138	0.0140	3.98		
18	54.580	15	281	47.99	0.0138	0.0140	3.98		
19	58.220	15	281	47.99	0.0138	0.0140	3.98		
20	61.860	15	301	53.80	0.0135	0.0136	4.16		
21	65.500	15	301	53.80	0.0135	0.0136	4.16		
22	69.140	15	301	53.80	0.0135	0.0136	4.16		
23	72.780	15	321	59.94	0.0132	0.0134	4.35		
24	72.780	15	321	61.41	0.0118	0.0120	4.45		
25	76.420	15	309	55.11	0.0114	0.0116	4.14		
26	76.420	15	624	196.64	0.0100	0.0101	7.32	76.420	4.15
27	78.660	15	575	168.78	0.0101	0.0102	6.82	80.060	6.82

Table C.4 – Required reinforcement for early-age crack width control

Kn.	*Height* h	*Thickness* h	*Depth of the tensile zone* hcr	fct,eff	kc	k	*reinforcement edge distance* d1	*effective section depth* d	*reinforcement bar diameter* ϕ_S	*adjusted bar diameter* ϕ_S*	*steel stress* σ_S	*reinforcement due to crack width* $a_{s,r,erf}$	*reinforcement (per face)* $a_{s,r,erf}$	*Height* h	*reinforcement (per face)* $a_{s,r,erf}$
	[m]	[mm]	[mm]	[N/mm²]	[-]	[-]	[mm]	[mm]	[mm]	[mm]	[N/mm²]	[cm²/m]	[cm²/m]	[m]	[cm²/m]
-1															
1	-0.020	300	60	3.78	0.5	1.00	59	241	14	10.7	254.56	8.91	**4.45**		
2	3.620	300	60	3.78	0.5	1.00	59	241	14	10.7	254.56	8.91	**4.45**		
3	7.260	300	60	3.78	0.5	1.00	59	241	14	10.7	254.56	8.91	**4.45**		
4	10.900	300	60	3.78	0.5	1.00	59	241	14	10.7	254.56	8.91	**4.45**		
5	14.540	300	60	3.78	0.5	1.00	59	241	14	10.7	254.56	8.91	**4.45**		
6	18.180	300	60	3.78	0.5	1.00	59	241	14	10.7	254.56	8.91	**4.45**		
7	21.820	300	60	3.78	0.5	1.00	59	241	14	10.7	254.56	8.91	**4.45**		
8	25.460	300	60	3.78	0.5	1.00	59	241	14	10.7	254.56	8.91	**4.45**		
9	29.100	340	68	3.78	0.5	1.00	59	281	14	10.7	254.56	10.10	**5.05**		
10	32.740	340	68	3.78	0.5	1.00	59	281	14	10.7	254.56	10.10	**5.05**		
11	36.380	340	68	3.78	0.5	1.00	59	281	14	10.7	254.56	10.10	**5.05**		
12	40.020	340	68	3.78	0.5	1.00	59	281	14	10.7	254.56	10.10	**5.05**		
13	40.020	340	68	4.14	0.5	1.00	59	281	14	9.8	266.40	10.57	**5.28**		
14	43.660	340	68	4.14	0.5	1.00	59	281	14	9.8	266.40	10.57	**5.28**		
15	47.300	340	68	4.14	0.5	1.00	59	281	14	9.8	266.40	10.57	**5.28**		
16	50.940	340	68	4.14	0.5	1.00	59	281	14	9.8	266.40	10.57	**5.28**		
17	54.580	340	68	4.14	0.5	1.00	59	281	14	9.8	266.40	10.57	**5.28**		
18	54.580	340	68	4.14	0.5	1.00	59	281	14	9.8	266.40	10.57	**5.28**		
19	58.220	340	68	4.14	0.5	1.00	59	281	14	9.8	266.40	10.57	**5.28**		
20	61.860	360	72	4.14	0.5	1.00	59	301	14	9.8	266.40	11.19	**5.59**		
21	65.500	360	72	4.14	0.5	1.00	59	301	14	9.8	266.40	11.19	**5.59**		
22	69.140	360	72	4.14	0.5	1.00	59	301	14	9.8	266.40	11.19	**5.59**		
23	72.780	380	76	4.14	0.5	1.00	59	321	14	9.8	266.40	11.81	**5.91**		
24	72.780	380	76	4.32	0.5	1.00	59	321	14	9.4	272.13	12.06	**6.03**		
25	76.420	360	72	4.32	0.5	1.00	59	301	14	9.4	272.13	11.43	**5.71**		
26	76.420	680	136	4.32	0.5	1.00	59	621	14	9.4	272.13	21.59	**10.79**	76.420	**5.71**
27	78.660	630	126	4.32	0.5	1.00	59	571	14	9.4	272.13	20.00	**10.00**	80.060	**10.00**

Table C.5 – Required reinforcement for SLS, shear and torsion

Kn.	*Height* h	*Shear flow* t_{Ed}	*torsion flow* v_{Ed}	cot θ	tan θ	*Longitudinal reinforcement* $a_{sl,t}$ B500	*Horizontal Reinforcement* $a_{sw,t+v}$ B500
	[m]	[kN/m]	[kN/m]	[-]	[-]	[cm²/m]	[cm²/m]
-1							
1	-0.020	45.9	76.2	1.20	0.83	0.63	1.17
2	3.620	50.7	79.7	1.20	0.83	0.70	1.25
3	7.260	55.9	83.4	1.20	0.83	0.77	1.33
4	10.900	61.4	87.1	1.20	0.83	0.85	1.42
5	14.540	67.4	90.9	1.20	0.83	0.93	1.52
6	18.180	73.9	94.4	1.20	0.83	1.02	1.61
7	21.820	80.8	97.9	1.20	0.83	1.12	1.71
8	25.460	88.2	101.4	1.20	0.83	1.22	1.82
9	29.100	97.2	105.6	1.20	0.83	1.34	1.94
10	32.740	105.6	109.1	1.20	0.83	1.46	2.06
11	36.380	114.5	112.6	1.20	0.83	1.58	2.18
12	40.020	123.9	116.1	1.20	0.83	1.71	2.30
13	40.020	123.9	116.1	1.20	0.83	1.71	2.30
14	43.660	133.6	119.5	1.20	0.83	1.84	2.43
15	47.300	143.7	122.8	1.20	0.83	1.98	2.55
16	50.940	154.1	126.5	1.20	0.83	2.13	2.69
17	54.580	164.7	130.1	1.20	0.83	2.27	2.83
18	54.580	164.7	130.1	1.20	0.83	2.27	2.83
19	58.220	175.4	133.6	1.20	0.83	2.42	2.96
20	61.860	187.9	137.6	1.20	0.83	2.59	3.12
21	65.500	199.2	140.9	1.20	0.83	2.75	3.26
22	69.140	210.8	143.5	1.20	0.83	2.91	3.39
23	72.780	224.7	146.6	1.20	0.83	3.10	3.56
24	72.780	224.7	146.6	1.20	0.83	3.10	3.56
25	76.420	222.6	144.4	1.20	0.83	3.07	3.52
26	76.420	260.1	156.1	1.20	0.83	3.59	3.99
27	78.660	290.8	163.9	1.20	0.83	4.01	4.36

Table C.6 – Required reinforcement for SLS due to temperature, vertical direction

Kn.	*Height* h	Moment due to Temp. with γ_{Temp}=1,0 M_{Ed}	Com LF 1.5/1.11 G + P_{inf} in Wandmitte σ_{cm}	Axial force from LF 1.5/1.11 G + P N_{Ed}	lever arm distance z_{s1}	Moment along the section M_{Eds}	μ_{Eds}	ω	reinforcement from M_{xy} + Temp. a_{sl} B500
	[m]	[kNm/m]	[N/mm²]	[kN/m]	[mm]	[kNm/m]	[-]	[-]	[cm²/m]
-1									
1	-0.020	57.00	-3.398	-1019	91	150	0.0745	0.07761	0.00
2	3.620	57.00	-3.398	-1019	91	150	0.0745	0.07762	0.00
3	7.260	42.75	-3.405	-1022	91	136	0.0675	0.07010	0.00
4	10.900	42.75	-3.421	-1026	91	136	0.0677	0.07033	0.00
5	14.540	42.75	-3.449	-1035	91	137	0.0681	0.07073	0.00
6	18.180	42.75	-3.486	-1046	91	138	0.0686	0.07127	0.00
7	21.820	42.75	-3.541	-1062	91	139	0.0693	0.07207	0.00
8	25.460	42.75	-3.620	-1086	91	142	0.0704	0.07321	0.00
9	29.100	54.91	-3.258	-1108	111	178	0.0651	0.06751	0.00
10	32.740	54.91	-3.346	-1138	111	181	0.0663	0.06880	0.00
11	36.380	54.91	-3.462	-1177	111	186	0.0679	0.07052	0.00
12	40.020	54.91	-3.612	-1228	111	191	0.0699	0.07272	0.00
13	40.020	59.25	-3.612	-1228	111	196	0.0562	0.05806	0.00
14	43.660	59.25	-3.799	-1292	111	203	0.0582	0.06022	0.00
15	47.300	59.25	-4.030	-1370	111	211	0.0607	0.06288	0.00
16	50.940	59.25	-4.198	-1427	111	218	0.0625	0.06482	0.00
17	54.580	59.25	-4.402	-1497	111	225	0.0648	0.06719	0.00
18	54.580	59.25	-4.402	-1497	111	225	0.0648	0.06719	0.00
19	58.220	59.25	-4.646	-1580	111	235	0.0674	0.07003	0.00
20	61.860	66.42	-4.643	-1671	121	269	0.0673	0.06989	0.00
21	65.500	66.42	-4.950	-1782	121	282	0.0706	0.07348	0.00
22	69.140	66.42	-5.255	-1892	121	295	0.0740	0.07707	0.00
23	72.780	74.01	-5.294	-2012	131	338	0.0743	0.07748	0.00
24	72.780	75.81	-5.294	-2012	131	339	0.0654	0.06786	0.00
25	76.420	68.04	-6.050	-2178	121	332	0.0727	0.07567	0.00
26	76.420	242.76	-3.181	-2163	281	851	0.0438	0.04498	0.00
27	78.660	208.37	-3.852	-2427	256	830	0.0505	0.05205	0.00

Table C.7 – Required reinforcement for SLS due to temperature, horizontal direction

ø 14 mm

Kn.	*Height* h	Moment due to Temp. with γ_{Temp}=1,0 M_{Ed}	μ_{Eds}	ω	horizontal reinforcement a_{sw} B500
	[m]	[kNm/m]	[-]		
-1					
1	-0.020	45.60	0.0227	0.02305	4.42
2	3.620	45.60	0.0227	0.02305	4.42
3	7.260	34.20	0.0170	0.01724	3.31
4	10.900	34.20	0.0170	0.01724	3.31
5	14.540	34.20	0.0170	0.01724	3.31
6	18.180	34.20	0.0170	0.01724	3.31
7	21.820	34.20	0.0170	0.01724	3.31
8	25.460	34.20	0.0170	0.01724	3.31
9	29.100	43.93	0.0161	0.01629	3.65
10	32.740	43.93	0.0161	0.01629	3.65
11	36.380	43.93	0.0161	0.01629	3.65
12	40.020	43.93	0.0161	0.01629	3.65
13	40.020	47.40	0.0136	0.01379	3.93
14	43.660	47.40	0.0136	0.01379	3.93
15	47.300	47.40	0.0136	0.01379	3.93
16	50.940	47.40	0.0136	0.01379	3.93
17	54.580	47.40	0.0136	0.01379	3.93
18	54.580	47.40	0.0136	0.01379	3.93
19	58.220	47.40	0.0136	0.01379	3.93
20	61.860	53.14	0.0133	0.01347	4.11
21	65.500	53.14	0.0133	0.01347	4.11
22	69.140	53.14	0.0133	0.01347	4.11
23	72.780	59.20	0.0130	0.01320	4.29
24	72.780	60.65	0.0117	0.01182	4.40
25	76.420	54.43	0.0119	0.01207	4.21
26	76.420	194.21	0.0100	0.01010	7.27
27	78.660	166.70	0.0102	0.01025	6.78

Table C.8 – Required reinforcement, 2nd variation

ø 14

		ULS		SLS			
Kn.	Height h	Shear + Torsion and Temperature /per face a_{sw}	Shear + Torsion and Temperature /per face a_{sl}	Shear + Torsion and Temperature /per face a_{sw}	Shear + Torsion and Temperature /per face a_{sL}	Required horizontal reinforcement a_{sw}	Required vertical reinforcement a_{sl}
	[m]	[cm²/m]	[cm²/m]	[cm²/m]	[cm²/m]	[cm²/m]	[cm²/m]
26	76.420	7.94	6.60	6.30	5.71	7.94	6.60
27	80.060	11.54	10.03	10.00	10.00	11.54	10.03

Table C.9 – Required reinforcement for each segment, 1st variation

ø 14		ULS		SLS			
Kn.	Height h	Torsion and Temperature /per face a_{sw}	Torsion and Temperature /per face a_{sl}	Shear + Torsion and Temperature /per face a_{sw}	Shear + Torsion and Temperature /per face a_{sL}	Required horizontal reinforcement a_{sw}	Required vertical reinforcement a_{sl}
	[m]	[cm²/m]	[cm²/m]	[cm²/m]	[cm²/m]	[cm²/m]	[cm²/m]
-1							
1	-0.020	5.92	4.99	5.13	4.45	5.92	4.99
2	3.620	6.00	5.04	5.17	4.45	6.00	5.04
3	7.260	4.96	3.97	4.45	4.45	4.96	4.45
4	10.900	5.05	4.03	4.45	4.45	5.05	4.45
5	14.540	5.15	4.10	4.45	4.45	5.15	4.45
6	18.180	5.24	4.17	4.45	4.45	5.24	4.45
7	21.820	5.34	4.24	4.45	4.45	5.34	4.45
8	25.460	5.45	4.32	4.45	4.45	5.45	4.45
9	29.100	5.92	4.76	5.05	5.05	5.92	5.05
10	32.740	6.02	4.86	5.05	5.05	6.02	5.05
11	36.380	6.13	4.95	5.05	5.05	6.13	5.05
12	40.020	6.24	5.06	5.05	5.05	6.24	5.06
13	40.020	6.53	5.34	5.31	5.28	6.53	5.34
14	43.660	6.64	5.45	5.38	5.28	6.64	5.45
15	47.300	6.75	5.56	5.46	5.28	6.75	5.56
16	50.940	6.89	5.68	5.54	5.28	6.89	5.68
17	54.580	7.03	5.79	5.62	5.28	7.03	5.79
18	54.580	7.03	5.79	5.62	5.28	7.03	5.79
19	58.220	7.18	5.91	5.71	5.28	7.18	5.91
20	61.860	7.53	6.24	5.98	5.59	7.53	6.24
21	65.500	7.67	6.36	6.07	5.59	7.67	6.36
22	69.140	7.82	6.49	6.15	5.59	7.82	6.49
23	72.780	8.19	6.83	6.43	5.91	8.19	6.83
24	72.780	8.29	6.93	6.53	6.03	8.29	6.93
25	76.420	7.94	6.60	6.32	5.71	7.94	6.60
26	76.420	11.64	10.19	10.79	10.79	11.64	10.79
27	78.660	11.55	10.03	10.00	10.00	11.55	10.03

Table C.10 – Reinforcement spacing, 1st variation

		Chosen Horizontal Reinforcement Area per face					*Chosen Vertical Reinforcement Area per face*				
Kn.	Height h	diameter ϕ_s	spacing s	$a_{s,vorh}$	$a_{sw,erf} / a_{s,vorh}$	$a_{s,erf} \leq a_{s,vorh}$	diameter ϕ_s	spacing s	$a_{s,vorh}$	$a_{sl,erf} / a_{s,vorh}$	$a_{s,erf} \leq a_{s,vorh}$
	[m]	[mm]	[cm]	[cm²/m]	[-]		[mm]	[cm]	[cm²/m]	[-]	
-1											
1	-0.020	14	16.0	9.62	**0.62**	**OK**	14	20.0	7.70	**0.65**	**OK**
2	3.620	14	16.0	9.62	**0.62**	**OK**	14	20.0	7.70	**0.65**	**OK**
3	7.260	14	16.0	9.62	**0.52**	**OK**	14	20.0	7.70	**0.58**	**OK**
4	10.900	14	16.0	9.62	**0.52**	**OK**	14	20.0	7.70	**0.58**	**OK**
5	14.540	14	16.0	9.62	**0.53**	**OK**	14	20.0	7.70	**0.58**	**OK**
6	18.180	14	16.0	9.62	**0.54**	**OK**	14	20.0	7.70	**0.58**	**OK**
7	21.820	14	16.0	9.62	**0.56**	**OK**	14	20.0	7.70	**0.58**	**OK**
8	25.460	14	16.0	9.62	**0.57**	**OK**	14	20.0	7.70	**0.58**	**OK**
9	29.100	14	16.0	9.62	**0.62**	**OK**	14	20.0	7.70	**0.66**	**OK**
10	32.740	14	16.0	9.62	**0.63**	**OK**	14	20.0	7.70	**0.66**	**OK**
11	36.380	14	16.0	9.62	**0.64**	**OK**	14	20.0	7.70	**0.66**	**OK**
12	40.020	14	14.0	11.00	**0.57**	**OK**	14	20.0	7.70	**0.66**	**OK**
13	40.020	14	14.0	11.00	**0.59**	**OK**	14	20.0	7.70	**0.69**	**OK**
14	43.660	14	14.0	11.00	**0.60**	**OK**	14	20.0	7.70	**0.71**	**OK**
15	47.300	14	14.0	11.00	**0.61**	**OK**	14	20.0	7.70	**0.72**	**OK**
16	50.940	14	14.0	11.00	**0.63**	**OK**	14	20.0	7.70	**0.74**	**OK**
17	54.580	14	14.0	11.00	**0.64**	**OK**	14	20.0	7.70	**0.75**	**OK**
18	54.580	14	14.0	11.00	**0.64**	**OK**	14	20.0	7.70	**0.75**	**OK**
19	58.220	14	13.0	11.84	**0.61**	**OK**	14	20.0	7.70	**0.77**	**OK**
20	61.860	14	13.0	11.84	**0.64**	**OK**	14	18.0	8.55	**0.73**	**OK**
21	65.500	14	13.0	11.84	**0.65**	**OK**	14	18.0	8.55	**0.74**	**OK**
22	69.140	14	12.0	12.83	**0.61**	**OK**	14	18.0	8.55	**0.76**	**OK**
23	72.780	14	12.0	12.83	**0.64**	**OK**	14	18.0	8.55	**0.80**	**OK**
24	72.780	14	12.0	12.83	**0.65**	**OK**	14	16.0	9.62	**0.72**	**OK**
25	76.420	14	12.0	12.83	**0.62**	**OK**	14	16.0	9.62	**0.69**	**OK**
26	76.420	14	9.0	17.10	**0.68**	**OK**	14	10.0	15.39	**0.70**	**OK**
27	78.660	14	9.0	17.10	**0.68**	**OK**	14	10.0	15.39	**0.65**	**OK**

Table C.11 – Parameters for the reinforcement due to radial force

Geometry definition			
a =	1.910	[m]	Radius at the deviation point
h =	0.365	[m]	Average thickness of the wall
l =	3.64	[m]	Length of the segment
P =	342.206	[kN]	Radial Force
μ =	0.3		Poison ratio
λ =	1.538		
λ*l =	5.600	Long Cylindrical shell	
K =	174375.123		

Table C.12 – Rotation at the force application point

Rotation			
	moment due to the rotation		
unitary action:	M	1	[kNm]
d11 =	w'u	3.7275E-06	
	Due to the nodal force		
action:	P	171.103	[kN]
d10=	w'u	0.00020728	

Table C.13 – Resultant moments in the structure, convention

mφ	**-55.607**	**kNm/m**
mϑ	**-16.682**	**kNm/m**
nϑ	**502.760**	**kN/m**
q	**-171.103**	**kN/m**

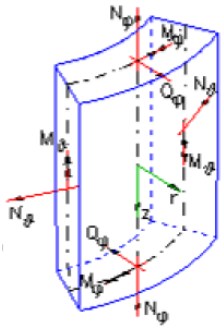

D. STEEL FLANGE

Flange Geometry:			
External Diameter	d_a	**4346**	[mm]
Internal Diameter	d_i	**3216**	[mm]
Winkel at Flange Surface	β	**2.4**	[°]
Internal Plate Thickness	$t_{p,i}$	**200**	[mm]
External Plate Thickness	$t_{p,a}$	**176.32**	[mm]
Plate Thickness	t_p	**188.16**	[mm]
Tower Plate Thickness	s	**50**	[mm]
No. of Prestr. Tendons	n_b	**28**	[-]
No. Of Strands		**15 Litzen**	
Prestr. Tendon Cross-Section	A_p	**2250**	[mm²]
Pitch Circle Radius	R	1901	[mm]
Connection Radius	r	2148	[mm]
Hole Diameter in the Flange	d_s	**157.9**	[mm]
Flange Height	h	188	[mm]
Fillet Radius	r_1	**0**	[mm]
Flange Width	m	565	[mm]
Measurement	a	293	[mm]
Measurement	b	247	[mm]
Measurement	c	**221.9**	[mm]

Materials:			
Nominal Dia. of Prestr. Tendon	d	53.52	[mm]
Steel Grade		Y1860	
Prestr. Force, without	P_{m0}	**2871.59**	[kN]
Losses from Creep a. Shrinkage			
Tendon Yield Strength	$f_{p,0.1,k}$	1640	[N/mm²]
Tednon Tensile Strength	$f_{p,k}$	1860	[N/mm²]
Youngs Modulus	E_p	195000	[N/mm²]
Anchor Head Hole Diameter	A	146	[mm]
Anchor Head External Dia.	D	200	[mm]
Anchor Head Thickness	h	82	[mm]
	A	146	[mm]
	D	215	[mm]
	h	25	[mm]
	A	150	[mm]
	D	350	[mm]
	h	50	[mm]
Clamped Length	l_K	1345	[mm]
Clamped Length over Tower Height	l_K	3340	[mm]
Flange Material		S355	
Flange Yield Strength	R_{eH}	**285**	[N/mm²]
Tower Plate Material		S355	
Tower Plate Yield Strength	R_{eH}	**335**	[N/mm²]
Youngs Modulus for Steel	E_s	210000	[N/mm²]
Concrete Grade		C80/95	
Youngs Modulus for Concrete	E_c	42000	[N/mm²]

Extreme Loading:

		Extremlastfall with safety factor	frequent loads	DLC 1.0	
Tower Plate Bending Moment	M_{XY}	**53780**	**28621**	**15692**	[kNm]
Tower Plate Normal Force	F_Z	**-4695**	**-4695**	**-4695**	[kN]

Tower Plate Cross-sectional Area	A_{Bl}	6.75E+05			[mm²]	
Tower Plate Moment of Resistance	W_{Bl}	7.17E+08			[mm³]	
Tower Plate Nominal Stress	σ_{Bl}	68.10	32.99	14.94	[N/mm²]	$\sigma_{Bl} = F_Z / A_{Bl} + M_{XY} / W_{Bl}$
Influence Angle per Prestr. Tendon	α	12.86			[°]	
Influence Width per Prestr. Tendon	c	482			[mm]	$c = 2\pi \times r / n_b$
Cross-sect. Area Segmental Part	A_T	24101			[mm²]	$A_T = c \times s$
Tower Plate Tension Force	Z	1641.28	795.03	360.15	[kN]	$Z = \sigma_{Bl} \times A_T$
Bolt Force	**S**	**1854.44**	**898.29**	**406.93**	**[kN]**	$S = Z \times r / R$
Bolt Stress	**σ_B**	**824.19**	**399.24**	**180.86**	**[N/mm²]**	$\sigma_B = S / A_p$

Determination of the Spring Values:

Tower Plate Rotational Spring					
Tower Plate Rot. Spring Constant	K	4.5422E+09	[Nmm/1]	$K = E \times c \times s^3 / (8{,}5 \times (r \times s)^{0,5})$	
Flange Compression Spring					
Subst. Cylinder Strain Stiffness	EA_D	3.7849E+09	[N]	$EA_D = E \times \pi / 4 \times ((d_2(S) + (t_p) / 10)^2 - d_1(S)^2)$	
Flange Compression Spring	C_{d2}	2.0115E+07	[N/mm]	$C_{d2} = EA_D / (t_p)$	
Anchor Head Compression String					
Anchor Head Compression String	C_{d1}	3.7581E+07	[N/mm]	$C_{d1} = E \times (d_2(S)^2 - d_1(S)^2) * \pi / 4 / h(S)$	
Concrete Compression Spring					
Subst. Cylinder Strain Stiffness	EA_C	1.1438E+10	[N]	$EA_C = E_c \times m \times c - \pi / 4 \times (d_1(S)^2)$	
Concrete Compression Spring	C_{d3}	1.1438E+07	[N/mm]	$C_{d3} = EA_c / (1000)$	
Total Compression Spring					
Compression Spring Total	C_d	**6.1069E+06**	[N/mm]	$C_d = 1 / (1 / C_{d1} + 1 / C_{d2} + 1 / C_{d3})$	
Prestr. Tendon Tensional Spring					
Prestr. Tendon Tensional Spring	C_S	**1.3136E+05**	[N/mm]	$C_S = E \times A_{Sch} / l_K$	
Total Spring					
Total Spring System	C	**6.2382E+06**	[N/mm]	$C = C_d + C_S$	

Determination of the Parameters:

Distribution Factor for Bolt	p	0.0211	[-]	$p = C_S / C$	
Distribution Factor for Flange	q	0.9789	[-]	$q = C_d / C$	
Flange Bending Stiffness	EI	5.62E+13	[Nmm²]	$EI = E \times c \times t_p^3 / 12$	
Parameter	λ	1.84237		$\lambda = (a + b) / a$	
Parameter	γ	1.18712		$\gamma = a / b$	
Parameter	δ	3.96712		$\delta = 2 \times C \times a \times b^2 / EI$	
Parameter	ε	2.00E-02		$\varepsilon = K \times b / EI$	
Parameter	β	1.7805E-03	8.6249E-04	3.9071E-04	$\beta = Z \times b^2 / EI$
Parameter	α	3.24E-03	1.57E-03	7.11E-04	$\alpha = ((1/2 + 1/\varepsilon + (1 + 1/\varepsilon + \gamma/3) \times \gamma) \times \delta) / (1 + (1 + 1/\varepsilon + \gamma/3) \times \gamma \times \delta) \times \beta$

Verifications in the Linear Elastic Region:

Bolt Force	F	2987.49	1447.14	655.56	[kN]	$F = \alpha \times EI / b^2$
Real Forces in the Bolt	F_{VS}'	2935	2902	2886	[kN]	$F_{VS}' = F_V + p \times \lambda \times Z$
Real Forces in the Compr. Cylinder	F_{VD}'	-89	1438	2222	[kN]	$F_{VD}' = F_V - q \times \lambda \times Z$
Flange pressurised:		**FAIL**	**OK**	**OK**		
Critical Tension Force	**Z_{krit}**	**1592.16**	**1592.16**	**1592.16**	**[kN]**	$Z_{krit} = F_V / (q \times \lambda)$

Calculation of the Plasto-Static Limiting Force:

Tendon Load Carrying Capacity	F_{Pl}	3321.00	[kN]	$F_{Pl} = MIN(0.9 \times f_{p0,1k}; 0{,}8 \times f_{pk}) \times A_p$	
Flange Plate	$W_{Pl,2}$	2868705	[mm³]	$W_{Pl,2} = (c-d_s) \times t_p^2 / 4$	
Flange Plate	$M_{Pl,2}$	743.26	[kNm]	$M_{Pl,2} = \sigma_{R,d} \times W_{Pl}$	
Tower Plate	$W_{Pl,3}$	301256	[mm³]	$W_{Pl,3} = c \times s^2 / 4$	
Tower Plate	$N_{Pl,3}$	7339.70	[kN]	$N_{Pl,3} = \sigma_{R,d} \times A$	
Tower Plate	$M_{Pl,3}$	91.75	[kNm]	$M_{Pl,3} = \sigma_{R,d} \times W_{Pl,3}$	
Failure Mode:					
A (Prestr. Tendon Failure)	Z_U	3321.0	[kN]	$Z_U = F_{Pl}$	
B (Pl. Hinge in Fl.-Neck)	Z_U	1972.5	[kN]	$Z_U = (F_{Pl} \times a + M_{Pl,3}) / (a + b)$	
C (Pl. Hinge in Flange)	Z_U	3381.9	[kN]	$Z_U = (M_{Pl,2} + M_{Pl,3}) / b$	
Ver. of the Limiting Force Z_U		**0.83**	**0.40**	**0.18**	
		OK	**OK**	**OK**	

E. FATIGUE ANALYSIS

Table E.1 – Fatigue damage in the top concrete edge of the transition segment

n_i	Δn_i	$\lvert\sigma_{c1}\rvert$	$\lvert\sigma_{c2}\rvert$;$\lvert\sigma_{c,max}\rvert$	$\lvert\sigma_{c,min}\rvert$	η_c	$S_{cd,max}$	$S_{cd,min}$	log N	$\Delta n_i / N_i$
-	-	N/mm²	N/mm²	N/mm²	-	-	-	-	-
1.00E+03	**1.00E+03**	**16.49**	**20.34**	**6.47**	**0.914**	**0.578**	**0.184**	**6.96**	**1.09E-04**
1.26E+03	2.59E+02	16.49	20.34	6.47	0.914	0.578	0.184	6.96	2.81E-05
1.58E+03	3.26E+02	16.49	20.34	6.47	0.914	0.578	0.184	6.96	3.54E-05
2.00E+03	4.10E+02	16.49	20.34	6.47	0.914	0.578	0.184	6.96	4.45E-05
2.51E+03	5.17E+02	16.49	20.34	6.47	0.914	0.578	0.184	6.96	5.61E-05
3.16E+03	6.50E+02	16.49	20.34	6.47	0.914	0.578	0.184	6.96	7.06E-05
3.98E+03	8.19E+02	16.49	20.34	6.47	0.914	0.578	0.184	6.96	8.89E-05
5.01E+03	1.03E+03	16.49	20.34	6.47	0.914	0.578	0.184	6.96	1.12E-04
6.31E+03	1.30E+03	16.49	20.34	6.47	0.914	0.578	0.184	6.96	1.41E-04
7.94E+03	1.63E+03	16.49	20.34	6.47	0.914	0.578	0.184	6.96	1.77E-04
1.00E+04	**2.06E+03**	**16.49**	**20.34**	**6.47**	**0.914**	**0.578**	**0.184**	**6.96**	**2.23E-04**
1.26E+04	2.59E+03	16.49	20.34	6.47	0.914	0.578	0.184	6.96	2.81E-04
1.58E+04	3.26E+03	16.49	20.34	6.47	0.914	0.578	0.184	6.96	3.54E-04
2.00E+04	4.10E+03	16.49	20.34	6.47	0.914	0.578	0.184	6.96	4.45E-04
2.51E+04	5.17E+03	16.49	20.34	6.47	0.914	0.578	0.184	6.96	5.61E-04
3.16E+04	6.50E+03	16.49	20.34	6.47	0.914	0.578	0.184	6.96	7.06E-04
3.98E+04	8.19E+03	16.49	20.34	6.47	0.914	0.578	0.184	6.96	8.89E-04
5.01E+04	1.03E+04	16.49	20.34	6.47	0.914	0.578	0.184	6.96	1.12E-03
6.31E+04	1.30E+04	16.49	20.34	6.47	0.914	0.578	0.184	6.96	1.41E-03
7.94E+04	1.63E+04	16.49	20.34	6.47	0.914	0.578	0.184	6.96	1.77E-03
1.00E+05	**2.06E+04**	**16.49**	**20.34**	**6.47**	**0.914**	**0.578**	**0.184**	**6.96**	**2.23E-03**
1.26E+05	2.59E+04	16.47	20.21	6.60	0.915	0.575	0.188	7.15	1.85E-03
1.58E+05	3.26E+04	16.44	20.07	6.74	0.917	0.572	0.192	7.33	1.52E-03
2.00E+05	4.10E+04	16.41	19.94	6.87	0.919	0.569	0.196	7.52	1.24E-03
2.51E+05	5.17E+04	16.38	19.80	7.01	0.920	0.567	0.200	7.72	9.96E-04
3.16E+05	6.50E+04	16.35	19.67	7.14	0.922	0.564	0.205	7.91	7.95E-04
3.98E+05	8.19E+04	16.32	19.53	7.28	0.924	0.561	0.209	8.12	6.28E-04
5.01E+05	1.03E+05	16.29	19.40	7.41	0.926	0.558	0.213	8.32	4.91E-04
6.31E+05	1.30E+05	16.26	19.26	7.55	0.928	0.555	0.218	8.53	3.80E-04
7.94E+05	1.63E+05	16.23	19.13	7.68	0.930	0.553	0.222	8.75	2.91E-04
1.00E+06	**2.06E+05**	**16.20**	**18.99**	**7.82**	**0.931**	**0.550**	**0.226**	**8.97**	**2.21E-04**
1.26E+06	2.59E+05	16.19	18.95	7.86	0.932	0.549	0.228	9.04	2.36E-04
1.58E+06	3.26E+05	16.18	18.91	7.90	0.933	0.548	0.229	9.11	2.51E-04
2.00E+06	4.10E+05	16.17	18.86	7.95	0.933	0.547	0.231	9.19	2.68E-04
2.51E+06	5.17E+05	16.16	18.82	7.99	0.934	0.546	0.232	9.26	2.85E-04
3.16E+06	6.50E+05	16.15	18.78	8.03	0.935	0.546	0.233	9.33	3.02E-04
3.98E+06	8.19E+05	16.14	18.73	8.08	0.935	0.545	0.235	9.41	3.21E-04
5.01E+06	1.03E+06	16.13	18.69	8.12	0.936	0.544	0.236	9.48	3.40E-04
6.31E+06	1.30E+06	16.12	18.65	8.16	0.937	0.543	0.238	9.56	3.60E-04
7.94E+06	1.63E+06	16.11	18.60	8.21	0.937	0.542	0.239	9.63	3.80E-04
1.00E+07	**2.06E+06**	**16.11**	**18.56**	**8.25**	**0.938**	**0.541**	**0.241**	**9.71**	**4.02E-04**
1.26E+07	2.59E+06	16.10	18.55	8.26	0.938	0.541	0.241	9.73	4.87E-04
1.58E+07	3.26E+06	16.10	18.54	8.27	0.938	0.541	0.241	9.74	5.90E-04
2.00E+07	4.10E+06	16.10	18.53	8.28	0.938	0.541	0.241	9.76	7.15E-04
2.51E+07	5.17E+06	16.10	18.52	8.29	0.939	0.540	0.242	9.78	8.66E-04
3.16E+07	6.50E+06	16.09	18.51	8.30	0.939	0.540	0.242	9.79	1.05E-03
3.98E+07	8.19E+06	16.09	18.50	8.31	0.939	0.540	0.242	9.81	1.27E-03
5.01E+07	1.03E+07	16.09	18.49	8.32	0.939	0.540	0.243	9.83	1.54E-03
6.31E+07	1.30E+07	16.09	18.48	8.33	0.939	0.540	0.243	9.84	1.86E-03
7.94E+07	1.63E+07	16.09	18.48	8.34	0.939	0.539	0.243	9.86	2.26E-03
1.00E+08	**2.06E+07**	**16.08**	**18.47**	**8.34**	**0.939**	**0.539**	**0.244**	**9.88**	**2.73E-03**
1.26E+08	2.59E+07	16.06	18.37	8.44	0.941	0.537	0.247	10.05	2.33E-03
1.58E+08	3.26E+07	16.04	18.28	8.53	0.942	0.535	0.250	10.22	1.97E-03
2.00E+08	4.10E+07	16.02	18.18	8.63	0.944	0.533	0.253	10.40	1.65E-03
2.51E+08	5.17E+07	16.00	18.09	8.72	0.945	0.532	0.256	10.57	1.38E-03
3.16E+08	6.50E+07	15.98	17.99	8.82	0.947	0.530	0.260	10.75	1.14E-03
3.98E+08	8.19E+07	15.96	17.90	8.91	0.949	0.528	0.263	10.94	9.43E-04
5.01E+08	1.03E+08	15.94	17.81	9.01	0.950	0.526	0.266	11.13	7.72E-04
6.31E+08	1.30E+08	15.92	17.71	9.10	0.952	0.524	0.269	11.31	6.28E-04
7.94E+08	1.63E+08	15.90	17.62	9.19	0.954	0.522	0.272	11.51	5.08E-04
1.00E+09	**2.06E+08**	**15.88**	**17.52**	**9.29**	**0.955**	**0.520**	**0.276**	**11.70**	**4.08E-04**
1.26E+09	2.59E+08	15.86	16.15	10.66	0.991	0.497	0.328	15.43	9.57E-08
1.58E+09	3.26E+08	15.84	14.78	12.03	1.037	0.476	0.388	32.53	9.70E-25
2.00E+09	**4.10E+08**	**15.82**	**13.41**	**13.41**	**1.099**	**0.458**	**0.458**	**-**	**0.00E+00**
$\Sigma \Delta n_i$:	2.00E+09							**d:**	**4.75E-02**

Table E.2 – Fatigue damage in the bottom concrete edge of the transition segment

n_i -	Δn_i -	$\lvert\sigma_{c1}\rvert$ N/mm²	$\lvert\sigma_{c2}\rvert_i \lvert\sigma_{c,max}\rvert$ N/mm²	$\lvert\sigma_{c,min}\rvert$ N/mm²	η_c -	$S_{cd,max}$ -	$S_{cd,min}$ -	log N -	$\Delta n_i / N_i$ -
1.00E+03	**1.00E+03**	**19.42**	**25.29**	**18.14**	**0.896**	**0.672**	**0.482**	**8.58**	**2.61E-06**
1.26E+03	2.59E+02	19.42	25.29	18.14	0.896	0.672	0.482	8.58	6.76E-07
1.58E+03	3.26E+02	19.42	25.29	18.14	0.896	0.672	0.482	8.58	8.49E-07
2.00E+03	4.10E+02	19.42	25.29	18.14	0.896	0.672	0.482	8.58	1.07E-06
2.51E+03	5.17E+02	19.42	25.29	18.14	0.896	0.672	0.482	8.59	1.34E-06
3.16E+03	6.50E+02	19.42	25.29	18.15	0.896	0.672	0.482	8.59	1.69E-06
3.98E+03	8.19E+02	19.42	25.29	18.15	0.896	0.672	0.482	8.59	2.12E-06
5.01E+03	1.03E+03	19.42	25.29	18.15	0.896	0.672	0.482	8.59	2.67E-06
6.31E+03	1.30E+03	19.42	25.29	18.15	0.896	0.672	0.482	8.59	3.36E-06
7.94E+03	1.63E+03	19.42	25.29	18.15	0.896	0.672	0.482	8.59	4.22E-06
1.00E+04	**2.06E+03**	**19.42**	**25.29**	**18.15**	**0.896**	**0.672**	**0.483**	**8.59**	**5.31E-06**
1.26E+04	2.59E+03	19.42	25.29	18.15	0.896	0.672	0.483	8.59	6.68E-06
1.58E+04	3.26E+03	19.42	25.29	18.15	0.896	0.672	0.483	8.59	8.41E-06
2.00E+04	4.10E+03	19.42	25.29	18.15	0.896	0.672	0.483	8.59	1.06E-05
2.51E+04	5.17E+03	19.42	25.29	18.15	0.896	0.672	0.483	8.59	1.33E-05
3.16E+04	6.50E+03	19.42	25.29	18.15	0.896	0.672	0.483	8.59	1.68E-05
3.98E+04	8.19E+03	19.42	25.29	18.15	0.896	0.672	0.483	8.59	2.11E-05
5.01E+04	1.03E+04	19.42	25.29	18.15	0.896	0.672	0.483	8.59	2.66E-05
6.31E+04	1.30E+04	19.42	25.29	18.15	0.896	0.672	0.483	8.59	3.35E-05
7.94E+04	1.63E+04	19.42	25.29	18.15	0.896	0.672	0.483	8.59	4.21E-05
1.00E+05	**2.06E+04**	**19.42**	**25.29**	**18.15**	**0.896**	**0.672**	**0.483**	**8.59**	**5.31E-05**
1.26E+05	2.59E+04	19.32	25.29	18.28	0.894	0.671	0.485	8.71	5.08E-05
1.58E+05	3.26E+04	19.23	25.29	18.41	0.893	0.670	0.488	8.83	4.85E-05
2.00E+05	4.10E+04	19.13	25.29	18.54	0.891	0.669	0.490	8.95	4.62E-05
2.51E+05	5.17E+04	19.03	25.29	18.67	0.890	0.668	0.493	9.07	4.40E-05
3.16E+05	6.50E+04	18.94	25.29	18.80	0.888	0.667	0.495	9.19	4.17E-05
3.98E+05	8.19E+04	18.84	25.29	18.92	0.887	0.665	0.498	9.32	3.95E-05
5.01E+05	1.03E+05	18.74	25.29	19.05	0.885	0.664	0.500	9.44	3.74E-05
6.31E+05	1.30E+05	18.64	25.29	19.18	0.884	0.663	0.503	9.57	3.53E-05
7.94E+05	1.63E+05	18.55	25.29	19.31	0.882	0.662	0.506	9.69	3.32E-05
1.00E+06	**2.06E+05**	**18.45**	**25.29**	**19.44**	**0.881**	**0.661**	**0.508**	**9.82**	**3.12E-05**
1.26E+06	2.59E+05	18.38	25.07	19.54	0.882	0.656	0.511	10.20	1.62E-05
1.58E+06	3.26E+05	18.30	24.84	19.64	0.884	0.651	0.515	10.60	8.19E-06
2.00E+06	4.10E+05	18.23	24.62	19.74	0.885	0.646	0.518	11.01	4.05E-06
2.51E+06	5.17E+05	18.15	24.39	19.84	0.887	0.642	0.522	11.42	1.95E-06
3.16E+06	6.50E+05	18.08	24.17	19.94	0.888	0.637	0.525	11.85	9.16E-07
3.98E+06	8.19E+05	18.00	23.94	20.03	0.890	0.632	0.529	12.29	4.20E-07
5.01E+06	1.03E+06	17.93	23.72	20.13	0.891	0.627	0.532	13.50	3.25E-08
6.31E+06	1.30E+06	17.85	23.49	20.23	0.893	0.622	0.536	15.15	9.22E-10
7.94E+06	1.63E+06	17.78	23.27	20.33	0.894	0.617	0.540	17.16	1.14E-11
1.00E+07	**2.06E+06**	**17.70**	**23.04**	**20.43**	**0.896**	**0.613**	**0.543**	**19.65**	**4.56E-14**
1.26E+07	2.59E+06	17.64	22.97	20.51	0.896	0.611	0.545	21.00	2.58E-15
1.58E+07	3.26E+06	17.59	22.89	20.58	0.896	0.609	0.547	22.52	9.83E-17
2.00E+07	4.10E+06	17.53	22.82	20.66	0.896	0.607	0.549	24.25	2.32E-18
2.51E+07	5.17E+06	17.47	22.74	20.73	0.896	0.605	0.551	26.23	3.05E-20
3.16E+07	6.50E+06	17.42	22.67	20.81	0.896	0.603	0.553	28.52	1.95E-22
3.98E+07	8.19E+06	17.36	22.60	20.88	0.896	0.601	0.555	31.21	5.00E-25
5.01E+07	1.03E+07	17.30	22.52	20.96	0.896	0.599	0.557	34.41	3.97E-28
6.31E+07	1.30E+07	17.24	22.45	21.03	0.896	0.597	0.559	38.28	6.75E-32
7.94E+07	1.63E+07	17.19	22.37	21.11	0.896	0.595	0.561	43.06	1.43E-36
1.00E+08	**2.06E+07**	**17.13**	**22.30**	**21.18**	**0.896**	**0.593**	**0.563**	**49.10**	**1.64E-42**
1.26E+08	2.59E+07	17.10	22.26	21.23	0.896	0.592	0.564	53.64	5.94E-47
1.58E+08	3.26E+07	17.06	22.21	21.27	0.896	0.591	0.566	59.06	2.84E-52
2.00E+08	4.10E+07	17.03	22.17	21.32	0.896	0.589	0.567	65.64	9.34E-59
2.51E+08	5.17E+07	16.99	22.12	21.36	0.896	0.588	0.568	73.81	8.04E-67
3.16E+08	6.50E+07	16.96	22.08	21.41	0.896	0.587	0.569	84.20	4.07E-77
3.98E+08	8.19E+07	16.93	22.03	21.46	0.896	0.586	0.571	97.89	1.05E-90
5.01E+08	1.03E+08	16.89	21.99	21.50	0.896	0.585	0.572	116.74	1.89E-109
6.31E+08	1.30E+08	16.86	21.94	21.55	0.896	0.583	0.573	144.32	6.19E-137
7.94E+08	1.63E+08	16.82	21.90	21.59	0.896	0.582	0.574	188.58	4.30E-181
1.00E+09	**2.06E+08**	**16.79**	**21.85**	**21.64**	**0.896**	**0.581**	**0.575**	**271.18**	**1.34E-263**
1.26E+09	2.59E+08	16.76	21.84	21.65	0.896	0.580	0.575	306.11	2.01E-298
1.58E+09	3.26E+08	16.72	21.83	21.67	0.895	0.580	0.576	351.01	0.00E+00
2.00E+09	**4.10E+08**	**16.69**	**21.82**	**21.68**	**0.895**	**0.579**	**0.576**	**-**	**0.00E+00**
$\Sigma \Delta n_i$:	2.00E+09							**d:**	**6.98E-04**

Table E.3 – Tendons fatigue damage

Σ N	ΔM_Y	$Z_{compression}$	$Z_{tension}$	F_{Pu}	F_{Po}	F_D	ΔF_P	$\Delta\sigma_P$
[-]	[kNm]	[kN]	[kN]	[kN]	[kN]	[kN]	[kN]	[N/mm²]
1.00E+03	30975	-492.1	549.8	2871.6	2882.4	2332.7	10.82	4.81
1.00E+04	30975	-492.1	549.8	2871.6	2882.4	2332.7	10.82	4.81
1.00E+05	30975	-492.1	549.8	2871.6	2882.4	2332.7	10.82	4.81
1.00E+06	24944	-390.7	448.3	2871.6	2880.4	2432.1	8.82	3.92
1.00E+07	23009	-358.1	415.8	2871.6	2879.8	2464.0	8.18	3.64
1.00E+08	22590	-351.1	408.7	2871.6	2879.6	2470.9	8.04	3.58
1.00E+09	18379	-280.3	337.9	2871.6	2878.2	2540.3	6.65	2.96
2.00E+09	10265	-143.8	201.5	2871.6	2875.6	2674.1	3.96	1.76
Average	5841							
$F_{Z,g}$	-4695							

Table E.4 – Accumulative damage calculation

log n_i	**n_i**	**Δn_i**	**$\Delta \sigma_p$**	**$\Delta \sigma_p'$**	**k**	**N_i**	**$\Delta n_i / N_i$**
[-]	**[-]**	**[-]**	**[N/mm²]**	**[N/mm²]**	**[-]**	**[-]**	**[-]**
3.0	**1.00E+03**	**1.00E+03**	**4.81**	**4.81**	**5**	**3.94E+11**	**2.54E-09**
3.1	1.26E+03	2.59E+02	4.81	4.81	5	3.94E+11	6.58E-10
3.2	1.58E+03	3.26E+02	4.81	4.81	5	3.94E+11	8.28E-10
3.3	2.00E+03	4.10E+02	4.81	4.81	5	3.94E+11	1.04E-09
3.4	2.51E+03	5.17E+02	4.81	4.81	5	3.94E+11	1.31E-09
3.5	3.16E+03	6.50E+02	4.81	4.81	5	3.94E+11	1.65E-09
3.6	3.98E+03	8.19E+02	4.81	4.81	5	3.94E+11	2.08E-09
3.7	5.01E+03	1.03E+03	4.81	4.81	5	3.94E+11	2.62E-09
3.8	6.31E+03	1.30E+03	4.81	4.81	5	3.94E+11	3.30E-09
3.9	7.94E+03	1.63E+03	4.81	4.81	5	3.94E+11	4.15E-09
4.0	**1.00E+04**	**2.06E+03**	**4.81**	**4.81**	**5**	**3.94E+11**	**5.23E-09**
4.1	1.26E+04	2.59E+03	4.81	4.81	5	3.94E+11	6.58E-09
4.2	1.58E+04	3.26E+03	4.81	4.81	5	3.94E+11	8.28E-09
4.3	2.00E+04	4.10E+03	4.81	4.81	5	3.94E+11	1.04E-08
4.4	2.51E+04	5.17E+03	4.81	4.81	5	3.94E+11	1.31E-08
4.5	3.16E+04	6.50E+03	4.81	4.81	5	3.94E+11	1.65E-08
4.6	3.98E+04	8.19E+03	4.81	4.81	5	3.94E+11	2.08E-08
4.7	5.01E+04	1.03E+04	4.81	4.81	5	3.94E+11	2.62E-08
4.8	6.31E+04	1.30E+04	4.81	4.81	5	3.94E+11	3.30E-08
4.9	7.94E+04	1.63E+04	4.81	4.81	5	3.94E+11	4.15E-08
5.0	**1.00E+05**	**2.06E+04**	**4.81**	**4.81**	**5**	**3.94E+11**	**5.23E-08**
5.1	1.26E+05	2.59E+04	4.72	4.76	5	4.12E+11	6.28E-08
5.2	1.58E+05	3.26E+04	4.63	4.68	5	4.53E+11	7.20E-08
5.3	2.00E+05	4.10E+04	4.54	4.59	5	4.98E+11	8.24E-08
5.4	2.51E+05	5.17E+04	4.45	4.50	5	5.49E+11	9.40E-08
5.5	3.16E+05	6.50E+04	4.36	4.41	5	6.07E+11	1.07E-07
5.6	3.98E+05	8.19E+04	4.28	4.32	5	6.72E+11	1.22E-07
5.7	5.01E+05	1.03E+05	4.19	4.23	5	7.45E+11	1.38E-07
5.8	6.31E+05	1.30E+05	4.10	4.14	5	8.29E+11	1.57E-07
5.9	7.94E+05	1.63E+05	4.01	4.05	5	9.23E+11	1.77E-07
6.0	**1.00E+06**	**2.06E+05**	**3.92**	**3.97**	**5**	**1.03E+12**	**1.99E-07**

Table E.5 – Accumulative damage calculation

log n_i [-]	n_i [-]	Δn_i [-]	$\Delta \sigma_p$ [N/mm²]	$\Delta \sigma_p'$ [N/mm²]	k [-]	N_i [-]	$\Delta n_i / N_i$ [-]
6.0	**1.00E+06**	**2.06E+05**	**3.92**	**3.97**	**5**	**1.03E+12**	**1.99E-07**
6.1	1.26E+06	2.59E+05	3.89	3.91	5	1.11E+12	2.33E-07
6.2	1.58E+06	3.26E+05	3.86	3.88	5	1.15E+12	2.83E-07
6.3	2.00E+06	4.10E+05	3.84	3.85	5	1.20E+12	3.43E-07
6.4	2.51E+06	5.17E+05	3.81	3.82	5	1.24E+12	4.16E-07
6.5	3.16E+06	6.50E+05	3.78	3.79	5	1.29E+12	5.05E-07
6.6	3.98E+06	8.19E+05	3.75	3.76	5	1.34E+12	6.12E-07
6.7	5.01E+06	1.03E+06	3.72	3.74	5	1.39E+12	7.42E-07
6.8	6.31E+06	1.30E+06	3.69	3.71	5	1.44E+12	8.99E-07
6.9	7.94E+06	1.63E+06	3.67	3.68	5	1.50E+12	1.09E-06
7.0	**1.00E+07**	**2.06E+06**	**3.64**	**3.65**	**5**	**1.56E+12**	**1.32E-06**
7.1	1.26E+07	2.59E+06	3.63	3.63	5	1.60E+12	1.62E-06
7.2	1.58E+07	3.26E+06	3.62	3.63	5	1.61E+12	2.02E-06
7.3	2.00E+07	4.10E+06	3.62	3.62	5	1.62E+12	2.53E-06
7.4	2.51E+07	5.17E+06	3.61	3.62	5	1.64E+12	3.15E-06
7.5	3.16E+07	6.50E+06	3.61	3.61	5	1.65E+12	3.94E-06
7.6	3.98E+07	8.19E+06	3.60	3.60	5	1.67E+12	4.91E-06
7.7	5.01E+07	1.03E+07	3.59	3.60	5	1.68E+12	6.13E-06
7.8	6.31E+07	1.30E+07	3.59	3.59	5	1.70E+12	7.65E-06
7.9	7.94E+07	1.63E+07	3.58	3.58	5	1.71E+12	9.55E-06
8.0	**1.00E+08**	**2.06E+07**	**3.58**	**3.58**	**5**	**1.72E+12**	**1.19E-05**
8.1	1.26E+08	2.59E+07	3.51	3.54	5	1.81E+12	1.43E-05
8.2	1.58E+08	3.26E+07	3.45	3.48	5	1.98E+12	1.65E-05
8.3	2.00E+08	4.10E+07	3.39	3.42	5	2.16E+12	1.90E-05
8.4	2.51E+08	5.17E+07	3.33	3.36	5	2.37E+12	2.18E-05
8.5	3.16E+08	6.50E+07	3.27	3.30	5	2.60E+12	2.50E-05
8.6	3.98E+08	8.19E+07	3.20	3.23	5	2.86E+12	2.86E-05
8.7	5.01E+08	1.03E+08	3.14	3.17	5	3.15E+12	3.27E-05
8.8	6.31E+08	1.30E+08	3.08	3.11	5	3.47E+12	3.74E-05
8.9	7.94E+08	1.63E+08	3.02	3.05	5	3.84E+12	4.25E-05
9.0	**1.00E+09**	**2.06E+08**	**2.96**	**2.99**	**5**	**4.26E+12**	**4.83E-05**
9.1	1.26E+09	2.59E+08	2.84	2.90	5	4.97E+12	5.21E-05
9.2	1.58E+09	3.26E+08	2.72	2.78	5	6.13E+12	5.32E-05
9.3	**2.00E+09**	**4.10E+08**	**1.76**	**2.24**	**5**	**1.80E+13**	**2.28E-05**
					d :	2.02E-08	